AD-A168 950 APPLICATION OF NONLINEAR OPTICS TO FREE ELECTRON LASER SYSTEMS(U) TRW ELECTRONICS AND DEFENSE SECTOR REDONDO BEACH CA C SHIH ET AL. 06 JUN 86 N00014-84-C-0668 1/2

UNCLASSIFIED F/G 20/5 NL

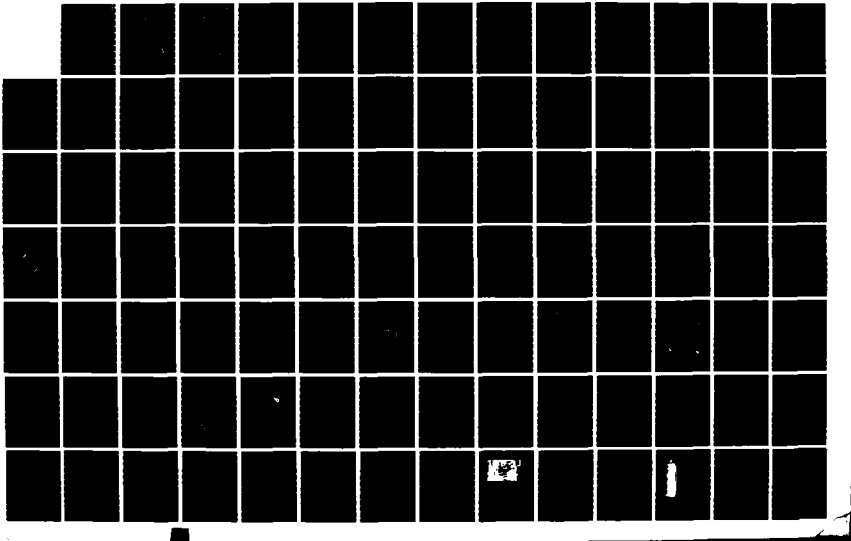

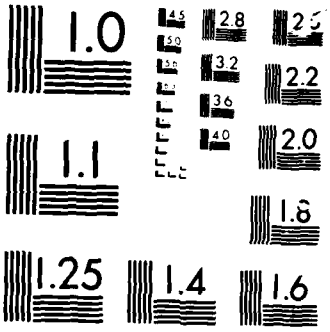
1.0
1.1
1.25
1.4
1.6
2.8
3.2
3.6
4.0
2.2
2.0
1.8

TRW

Application of Nonlinear Optics to Free Electron Laser Systems

C. C. Shih, G. R. Neil,
J. H. Menders, T. P. Yang

TRW Electronics & Defense Sector
Applied Technology Division
One Space Park
Redondo Beach, CA 90278

May 1986

Final Report for
Free Electron Laser
Resonator Development Program

Office of Naval Research
1030 East Green Street
Pasadena, CA 91106

TRW

Application of Nonlinear Optics to Free Electron Laser Systems

C. C. Shih, G. R. Neil,
J. H. Menders, T. P. Yang

TRW Electronics & Defense Sector
Applied Technology Division
One Space Park
Redondo Beach, CA 90278

May 1986

Final Report for
Free Electron Laser
Resonator Development Program

Office of Naval Research
1030 East Green Street
Pasadena, CA 91106

Unclassified

SECURITY CLASSIFICATION OF THIS PAGE

REPORT DOCUMENTATION PAGE

1a. REPORT SECURITY CLASSIFICATION: Unclassified	1b. RESTRICTIVE MARKINGS: None
2a. SECURITY CLASSIFICATION AUTHORITY	3. DISTRIBUTION/AVAILABILITY OF REPORT
2b. DECLASSIFICATION/DOWNGRADING SCHEDULE	
4. PERFORMING ORGANIZATION REPORT NUMBER(S)	5. MONITORING ORGANIZATION REPORT NUMBER(S)
6a. NAME OF PERFORMING ORGANIZATION: TRW Electronics & Defense Applied Technology Division; 6b. OFFICE SYMBOL (If applicable): 01/1070	7a. NAME OF MONITORING ORGANIZATION
6c. ADDRESS (City, State and ZIP Code): One Space Park, Redondo Beach, CA 90278	7b. ADDRESS (City, State and ZIP Code)
8a. NAME OF FUNDING/SPONSORING ORGANIZATION: Office of Naval Research; 8b. OFFICE SYMBOL (If applicable): ONR	9. PROCUREMENT INSTRUMENT IDENTIFICATION NUMBER: N00014-84-C-0668
8c. ADDRESS (City, State and ZIP Code): 1030 East Green Street, Pasadena, CA 91106	10. SOURCE OF FUNDING NOS.

PROGRAM ELEMENT NO.	PROJECT NO.	TASK NO.	WORK UNIT NO.

11. TITLE (Include Security Classification): Application of Nonlinear Optics to free electron laser Systems

12. PERSONAL AUTHOR(S): C. Shih, G. Neil, J. Menders, T. Yang

13a. TYPE OF REPORT	13b. TIME COVERED	14. DATE OF REPORT (Yr., Mo., Day)	15. PAGE COUNT
Final	FROM 12/84 TO 5/86	1986, June, 6	148

16. SUPPLEMENTARY NOTATION

17 COSATI CODES		
FIELD	GROUP	SUB GR

18. SUBJECT TERMS (Continue on reverse if necessary and identify by block number): Free electron laser; Optical resonator, nonlinear optics; Brillouin scattering, Four wave mixing, Phase conjugation

19. ABSTRACT (Continue on reverse if necessary and identify by block number):

Novel free electron laser (FEL) resonator concepts employing nonlinear optics techniques were developed in support of advanced FEL technologies. Among these concepts, three major schemes were studied for details as to their potential applications to the ground-based FEL systems: phase conjugate cavity and phase conjugate outcoupling for RF linac FEL resonators, and phase conjugate beam conversion for induction linac FEL devices. These schemes involve the utilization of some novel nonlinear optics techniques that have received very little attention before: multiple-pulse stimulated Brillouin scattering, short-pulse four wave mixing, and four-wave stimulated Brillouin scattering. Theoretical studies, modeling and proof-of-principle experiments have been performed to explore these phenomena. The analytical theory and numerical simulation showed the feasibility of these techniques to meet the system requirements and also determined parametrically the operational conditions. The experiments for short-pulse four wave mixing and four-wave stimulated Brillouin scattering were conducted in carbon-disulfide and acetone media, respectively. The results verified the scaling relations and demonstrated high conjugate reflectivities (~1000) for a weak signal.

20. DISTRIBUTION/AVAILABILITY OF ABSTRACT	21. ABSTRACT SECURITY CLASSIFICATION	
UNCLASSIFIED/UNLIMITED ☒ SAME AS RPT ☐ OTIC USERS ☐	Unclassified	
22a. NAME OF RESPONSIBLE INDIVIDUAL: Chun-Ching Shih	22b. TELEPHONE NUMBER (Include Area Code): (213) 536-4770	22c. OFFICE SYMBOL: 01/1070

DD FORM 1473, 83 APR EDITION OF 1 JAN 73 IS OBSOLETE

Unclassified

SECURITY CLASSIFICATION OF THIS PAGE

CONTENTS

CONTENTS (Continued)

CONTENTS (Continued)

Page

ILLUSTRATIONS

CONTENTS (Continued)

Page

ILLUSTRATIONS (Continued)

CONTENTS (Continued)

Page

ILLUSTRATIONS (Continued)

Page

ILLUSTRATIONS (Continued)

CONTENTS (Continued)

I. INTRODUCTION AND SUMMARY

Frec electron lasers have many attributes that makes them attractive for a variety of applications. The attributes include wavelength agility, high efficiency and scalability to high powers. The short-wavelength free electron laser device may be configurated in two major ways which are characterized by the type of electron accelerator used: radio frequency (RF) or induction linear accelerator. Both of these classes of devices have optical problems that are unique and, when approached using conventional techniques, are technologically difficult. The objective of this program was to examine nonlinear optical techniques for addressing these problems.

This report begins with a summary of the operational characteristics of induction and radio frequency driven free electron lasers and conventional approaches to the optical issues. A discussion in more details is given again in Section II. The following section describes various nonlinear optical process and delineates areas in which these can be applied. As a result of the examination of technical issues and applicability of nonlinear optics to these issues, three major areas were pursued. These techniques include the multiple-pulse stimulated Brillouin scattering, short-pulse four wave mixing and the four wave stimulated Brillouin scattering. The concepts developed using these techniques are phase conjugate resonator, phase conjugate outcoupling and phase conjugate beam conversion.

Theoretical models and laboratory experiments were performed for initial analyses and verifications of the derived concepts and the associated nonlinear optics technology. These are discussed in section III and IV of this report. As a result of this effort, it was found that the nonlinear optics technology is promising for free electron laser system applications. Some major optical issues associated with the conventional optics can be resolved using the identified nonlinear optics techniques, especially in the areas of resonator mode stabilization and atmospheric beam transmission.

1.1 FREE ELECTRON LASER SYSTEMS

Free Electron Lasers (FELs) have been studied for over a decade since the first observation of radiation at Stanford University in 1972. Experiments have progressed from the observation of oscillation with a constant wiggler[1,2] to the verification of increased gain and efficiency using a tapered wiggler.[3,4] A key feature of FEL resonators is their extremely high saturation flux in the interaction region. This leads to a number of presently unresolved issues when high power scaling is envisioned.[5-11] In particular, scaling analyses show that advances in the state of the art of resonator design will be required to achieve high output powers.[12-14] This program had the goal of performing initial measurements and verifications of approaches to deal with the issues associated with the high flux as well as the atmospheric propagation of high power FEL beams. In order to discuss these issues it is necessary to have an understanding of the components of an FEL directed energy system. The system is divided into three major subsystems: laser device, transfer optics, and beam director.

1.1.1 Laser

RF Approach

The RF linac FEL is shown schematically in Figure 1. An electron beam is produced in an injector by thermionic emission and initially accelerated to an energy of around 10 MeV. RF cavities then accelerate the beam to approximately of 100 MeV which is required for visible FEL operation. The accelerator produces a series of short micropulses 10 ns long separated by a small integral number of RF periods. Peak currents are in the several hundred ampere range, and at this low current and associated low gain it is necessary to operate the system as an oscillator. The beam passes through a several meter long wiggler where sinusoidal magnetic fields convert some fraction (10%) of the electron energy to light. The spent electron beam is sent to a beam dump or decelerated through a separate set of cavities to recover some of the energy.

In oscillator operation the FEL produces an intense beam of small divergence, so that high fluxes impinge on the mirrors. At high average

Free-Electron Laser
RF Linac

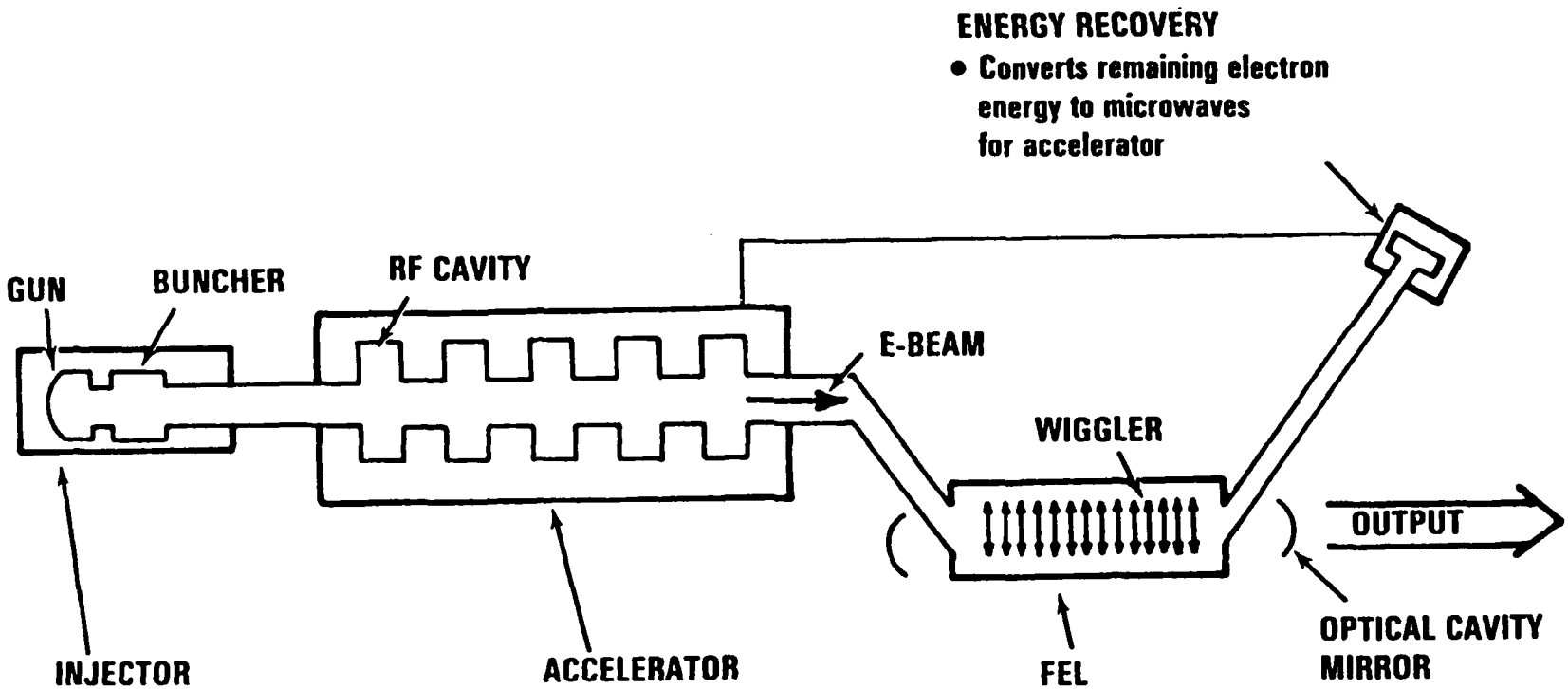

Figure 1. Schematic of RF linac FEL

powers it is necessary to utilize some advanced technique to handle such fluxes, e.g., very long cavities with exacting alignment requirements, intracavity aerolenses to magnify the beam spreading, or grazing incidence mirrors to spread the beam over a larger area. Generally, with these optical approaches it is difficult to achieve good beam quality and state-of-the-art alignment tolerances. In addition methods for outcoupling are difficult to devise and generally require the complementation of high power gratings.

Typical requirements for such systems are shown in Table 1.

Table 1. Typical RF FEL Optical System Requirements

Optical Systems	Requirements
Cavity Length	300 m
Alignment	300 nrad
Damage threshold	1 MW/cm^2
Mirror Figure	Lambda/40

In summarizing the issues associated with such systems, the following are seen to be the key issues:

- Optical damage threshold
- Alignment requirements
- Figure requirements
- Outcoupling methods
- Use of intracavity with aerolenses
- Bandwidth control
- Production of harmonics and sidebands in the FEL

Induction Linac

A schematic of an induction linac system is illustrated in Figure 2. An electron beam of several thousand amps and 50 ns duration is produced in the injector by thermionic or field emission cathodes. This beam is

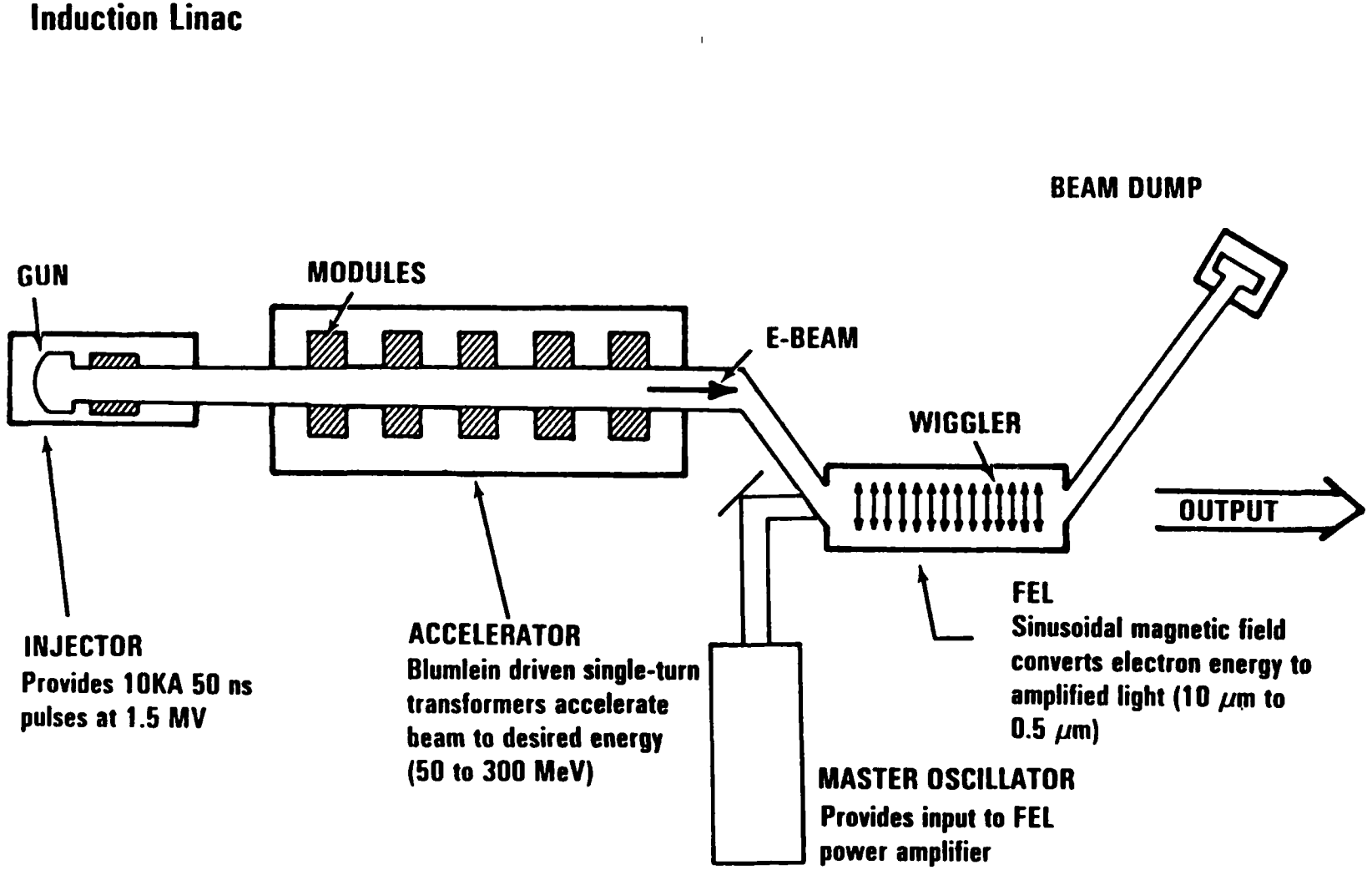

Figure 2. Schematic of induction linac FEL

accelerated to 300 MeV by a series of single turn transformers. High average power is achieved by repetitively pulsing the system hundreds or thousands of times a second. Because the length of the electron pulses are less than the oscillator length, oscillator operation is impossible but the high currents involved allow the system to have very high gain which permits amplifier operation. A master oscillator pulse, produced by a YAG system, for example, at 1 joule is amplified to several thousand joules while passing through a 100 m long wiggler. The optical pulse is essentially trapped by the electron beam much as in an optical fiber so that divergence of the optical pulse does not occur during the passage through such a long wiggler. This has the unfortunate side effect of introducing jitter to the output beam. The peak intensities involved are enormous, since the power is delivered at the end of the wiggler over a fraction of a square centimeter. The damage mechanism for the optics is the pulse energy rather than average power in this case, and distances of several kilometers are required to allow the beam to spread sufficiently so the surface breakdown of mirrors does not occur. Aerolenses could possible reduce this to a more manageable distance.

Typical requirements for such systems are shown in Table 2.

Table 2. Typical Induction FEL Optical System Requirements

Optical Systems	Requirements
Input Power	1-10 Joules
Output Power	1-10 Kilojoules
Repetition rate	1-10 Kilohertz
Wiggler length	120 meters
Damage threshold	10 J/cm^2
Divergence length	5 Kilometers

In summarizing the issues associated with such systems the following are seen to be the key issues:

- Optical damage threshold
- Alignment requirements
- Production of sidebands and harmonics
- Use of magnifying aerolenses

1.1.2 Transfer Optics

The purpose of the transfer optics is to condition the optical beam for introduction into the beam director. For both FEL systems this involves establishing the proper beam diameter and phase curvature characteristics, eliminating any unwanted frequency components in the light, correcting any locally introduced phase aberrations and jitter, and compensating for any atmospheric or beam director introduced aberrations which are expected to occur in propagation through the beam director and atmosphere. The conventional approach for correcting these propagation errors is to sample the errors with a beam from a beacon. An aperture sharing element is required to separate the outgoing wave from the incoming beacon beam, a task made more difficult by the requirement that both waves be at approximately the same wavelengths. The analysis of the phasefront errors is performed using a phasefront sensor, and a deformable mirror is used to introduce error compensating phase variations into the beam. To perform this analysis requires a large number of calculation channels of very high speed as well as very complex cooled deformable mirror surfaces. For sufficient phase fidelity, thousands of channels or more will be required. Although some work in this area has been carried out successfully at low powers, the technical effort remaining to make a high quality, high power system is still very large.

1.1.3 Uplink

The uplink system is essentially a very large astronomical telescope operating in reverse. Significant additional requirements are placed on it by the high flux loads, surface figure requirements, and fast slewing required. In the RF case director apertures of a couple of meters are

sufficient to provide resolution of the target and to reduce the thermal flux in the atmosphere to manageable levels. The induction linac's high peak power pulse has an additional constraint imposed by atmospheric Raman conversion which limits the peak flux to less than 1 MW/cm^2. This results in a requirement for the beam director to be on the order of 10 m in output aperture, which may be beyond manufacturing capability for a single unit mirror. If multiple mirror segments are utilized, the alignment and surface tolerance control are issues which require significant technology development for resolution.

1.2 NONLINEAR OPTICS TECHNOLOGY

The nonlinear optics techniques that are candidates for FEL applications are summarized in Table 3. The techniques include stimulated Brillouin scattering (SBS), stimulated Raman scattering (SRS), stimulated Rayleigh-wing scattering (SRWS), four wave mixing (FWM), and, for completeness, pseudo phase conjugation (PPC). Their operational characteristics are also listed for comparison. The SRWS technique is attractive for its short response time and small frequency shift that are the desirable property for a RF linac FEL resonator[15,16]. However, very little of SRWS study has been reported to date. The reflectivity observed was low and the conjugation fidelity was poor. Pseudo phase conjugation using arrays of retroreflective corner cubes[17-19] provides near-unity reflectivity, white-light and instant response, no frequency shift and no minimum power requirement. However, there are two drawbacks for PPC. Due to the finite size of the small corner cubes, it can not correct the phase variations that has a characteristic periodicity smaller than the individual cell dimension. The conjugation fidelity can thus be poor in many cases. Second, the field cannot preserve its initial polarization state upon the reflection[20]. The changes of the polarization could reduce the radiation intensity in the interaction region significantly. In addition, the mirror damage problem is more serious for a PPC mirror because of the sharp surface edges. As a consequence, both SRWS and PPC were not included in our research major efforts.

For SBS, SRS and FWM, the potential applications for RF Linac and induction linac FELs were identified and summarized in Table 4. In general, SBS is a very efficient process if the input pump power is well

Table 3. Summary of Issues and Applications of the Unconventional Adaptive Optics Techniques.

	SBS	SRS	SRWS	FWM	PPC
Issues					
Reflectivity	≤1	≤1	~0.1	>1	1
Bandwidth (cm^{-1})	0.1	10	1	1	0
Response time (sec)	10^{-9}	10^{-12}	10^{-12}	10^{-12}	0
Frequency shift (cm^{-1})	1	>200	1	0	0
Gain (cm/mw)	10^{-2}	10^{-3}	10^{-3}	--	--
Required power	High	High	High	Low	Zero
Fidelity	Good	Fair	Poor	Good	Fair
Polarization	--	--	--	--	X
Thermal Damage	--	--	--	--	X

above the threshold. SBS has the advantage of a small frequency shift that could be buried under the FEL gain spectrum. While its relatively slow response presents initial problems for much shorter RF linac FEL pulses (10-100 ps), the SBS reflectivity can be highly enhanced using the concept of multiple-pulse SBS[21]. In this case, the phonon field decays slowly enough to serve as a starting acoustic field for the next pulse. A theoretical study of multiple-pulse SBS was conducted during this program.

Another major phase conjugation technique studied, FWM[22], is not a stimulated emission process and, thus, has no power threshold. It generates the conjugate reflected wave by parametric mixing of the three input waves where constructive superposition is in the forward and backward directions. High reflectivities up to 100 times have been demonstrated in liquid media. Its fast response and degenerate reflectivity would be suitable for RF linac FEL applications.

For induction linac FEL applications, a new nonlinear optics process was identified and called four-wave stimulated Brillouin scattering (FWSBS). This process is essentially the SBS effect arranged in a four wave mixing configuration[23]. It has the combined advantage of both SBS and

Table 4. Nonlinear Optics Technology For FEL System
(The codes with * are developed in the program)

NLO	FEL	Applications	Issues	Theory/Model	Experiment
SBS	RF	Cavity Alignment Mirror Aberrations	Short Pulse Length Wide Bandwidth System Efficiency	Multiple-Pulse SBS Theory MPSBS Code*	Demonstrated At Garching
	IL	Telescope Aberrations Atmospheric Correction	System Efficiency Bandwidth	Four-Wave SBS Theory FWSBS Code*	EMRLD Data RSELE Experiment PALS Experiment
FWM	RF	Telescope Aberrations Atmospheric Correction Cavity Coupling Energy Outcoupling	Wide Bandwidth System Efficiency Reflectivity ($>10^3$)	Short-Pulse Theory TFWM Code*	FELRD Program/TRW YAG Laser Test
	IL	Telescope Aberrations Atmospheric Correction Beam Conversion	Bandwidth System Efficiency Reflectivity ($>10^3$)	TFWM Code* FWSBS Code*	FELRD Program/TRW YAG Laser Test Coupled Devices Test
SRS	RF	Beam Combination Wavelength Shifting Beam Clean-Up	Wide Bandwidth Short Pulse Length	Multiline RBC Code	RBC Program/TRW
	IL	Beam Combination Wavelength Shifting Beam Clean-Up	Bandwidth	Multiline RBC Code	RBC Program/TRW Excimer and YAG Laser Test

FWM effects as shown in Table 5. This effect was studied in detail in this program. The theory and modeling will be reported in Chapter III and the experimental results will be presented in Chapter IV.

SRS is a optically fast phenomenon with a large vibrational frequency shift. It has been considered for beam combination, wavelength shift and beam clean-up. Research in this area has been carried out in the Raman Beam Combination Program and will not be reported here.

In general, bandwidth and system efficiency are the two major issues of these three techniques for FEL application. The FEL bandwidth is an unsettled issue even from the FEL physics point of view. Some theories indicated that the FEL is an intrinsically wide band laser source. Other theories have argued that the output bandwidth can be extremely narrow if a proper filter or a narrow band injection laser is used. In this program, however, the issue was left open and the bandwidth problem was addressed whenever necessary.

Table 5. Comparison of Characteristics Among the Three Nonlinear Optics Effects: FWM, SBS, and FWSBS

	FWM	SBS	FWSBS
Process	Parametric-mixing	Stimulated emission	Stimulated emission
Reflectivity	High ($\sim 10^2$)	Low (< 1)	High ($\sim 10^6$)
Efficiency	Low (~ 0.1)	High (≤ 1)	High (≤ 1)
Signal power	Low	Low	High
Pump power	Two equal pumps (medium power)	Two unequal pumps (one high and one low)	One high power pump
Fequency shift	No	Yes	Yes
Growing from noise	No	Yes	No
Response time	Fast (10^{-12} sec)	Slow (10^{-9} sec)	Slow (10^{-9} sec)

II. CONCEPTUAL DESIGN

2.1 TASK OBJECTIVE

The objective of the conceptual design task in this FEL resonator development program was to study unconventional adaptive optics concepts in the operational regime of FEL characteristics and provide basic resonator designs, for use in high power FEL systems. To accomplish this objective, the conceptual design effort was divided into three major tasks:

a. Identify the technical issues of conventional resonator designs that are expected to affect critically the performance of a high power free electron laser system.

b. Evaluate the potential of various nonlinear optics techniques for free electron laser system applications.

c. Develop basic resonator designs and identify issues associated with the employed nonlinear optics techniques that will be subject to the following theoretical and experimental studies.

2.2 APPROACH

In order to determine the bases of consideration required for the conceptual designs of a high power FEL resonator, a three-step approach was followed: First, the performance of high power FEL systems using conventional resonator designs were evaluated and the potential problems pertinent to both the RF linac and induction linac FEL systems were identified. Second, the nonlinear optics techniques available for possible applications were reviewed and their characteristics associated with the FEL operational parameters were discussed and included in the Introduction section. Third, a system analysis of the FEL resonator was performed to determine the limit of power losses for a feasible resonator design. These steps led to the conceptual designs described in Section 3.

2.2.1 Conventional FEL Resonator Issues

The resonator configuration used in all demonstrated FEL systems is a linear stable cavity[1-4] (Figure 3). It consists of two spherical mirrors with their centers of curvature overlapped along the optical axis near the wiggler center. At high powers, the resonator requires a very long cavity for the intracavity mode to have a sufficiently large mode size at the

Free-Electron Laser Resonators

Linear Resonator

Ring Resonator

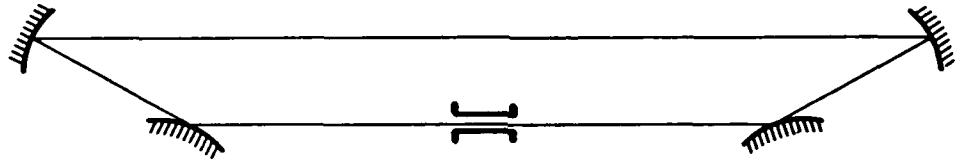

Inverted Ring Resonator

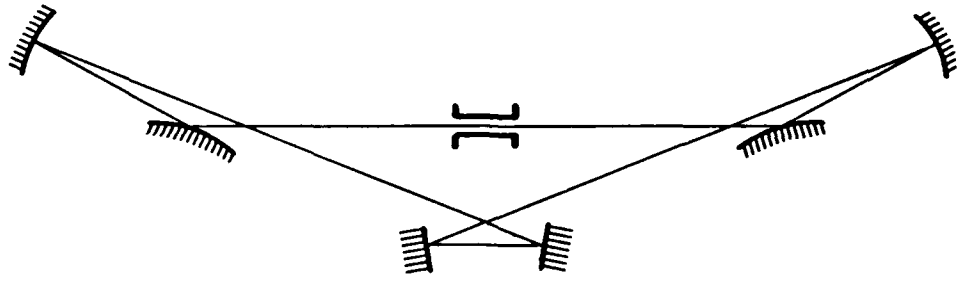

Figure 3. Conventional resonator design for high-power FEL systems

mirror. This long cavity has problems in its engineering aberration control and misalignment sensitivity. A ring resonator configuration with two pairs of hyperboloid-paraboloid mirrors (Figure 3) has been suggested[5-7] to shorten the cavity materially. The grazing-incidence hyperboloid mirror increases the beam divergence and the paraboloid mirror recollimates the beam. The two paraboloid mirrors can be replaced by two spherical mirrors to create an inverted ring configuration (Figure 3). The last configuration avoids the difficulty of fabricating off-axis paraboloid mirrors. However, the aberration effect and the misalignment sensitivity remain the same even though the cavity is much shorter[8-9]. Mirror figure requirements are typically one-hundredth of a wavelength and the alignment sensitivity angle is near 1 μrad or less. These requirements push the mirror and auto alignment technology to their present limits.

The best conventional resonator design for a high power FEL system might be an inverted ring resonator configuration (Figure 3). This configuration has the complexity of the grazing-incidence mirrors, but reduces the engineering difficulty of dealing with an extremely long cavity. However, most of the optical issues associated with linear resonator designs can still be found in this configuration. Those issues that might affect the performance of a high power RF linac FEL or induction linac FEL are summarized in Table 6 and discussed in the following.

The issues can be divided into three groups. The first group is associated with the optical resonator. The second group is related to beam transfer and propagation. The third relates special FEL systems that couple a number of FEL devices.

A. Resonator Optics

Mirror damage is the first major problem that came with the development of a high power FEL system. Although this is a general issue for all high power lasers, the utilization of grazing-incidence mirrors near the high flux region in a high power FEL system presents a serious problems for mirror cooling and optical stabilization technologies. This problem can be less serious using nonlinear optical processes. The medium used to create the process can be liquid, gas or even plasma. Using these

Table 6. Optical Problems and Issues Related to the Conventional High Power Free Electron Laser System

Problems and Issues	RF Linac FEL (Oscillator)	Induction Linac FEL (Amplifier)
Resonator Optics		
Mirror damage	X	X
Higher harmonics	X	X
Beam outcoupling	X	X
Aberration control	X	X
Alignment tolerance	X	-
Up-link Optics		
Telescope correction	X	X
Atmospheric compensation	X	X
Phase Arrays		
Injection locking	X	-
Coupled cavities	X	-
Beam combination	X	-

techniques, it is possible have a much higher thermal damage threshold than a conventional reflector as well as the capability for recovery after damage.

Higher harmonics of the optical beam are generated in the FEL and grow with the fundamental wave. This phenomenon has been observed in previous FEL experiments[2] and found to have serious degradation effect on the mirrors[3]. The suppression of higher harmonics is thus important to ensure the survival of the optical resonator in the visible regime. In a nonlinear optics process, the interaction efficiency is strongly dependent on the

intensity. Since the high harmonics have lower gains than the fundamental, SBS phase conjugation is a naturally selective process that will suppress the growth of shorter wavelength components.

Conventional outcoupling schemes including grating, scraper and transmissive outcoupling (Figure 4) have serious problem. At high power levels, transmissive outcoupling scheme can not be used due to thermal absorption problem and resulting distortions. Grating technology is currently not able to sustain high intracavity fluxes on its corrugated surfaces. Since high power FEL device generally has a very low single-pass gain ($\lesssim$ 10 percent), the scraper outcoupling scheme becomes impractical for either stable or unstable resonator geometries. The output would be a thin annular beam plagued with significant phase fluctuations. An outcoupling scheme using nonlinear optics is an attractive solution for this problem because it can produce a unobscured output beam and is subject to less thermal damage than gratings and scrapers.

With respect to the end mirrors of the resonator, the beam waist inside the wiggler is in the far field region. A small amount of phase nonuniformity generated on the mirrors would produce a significant intensity fluctuation in the interaction region and thus reduce the gain. In general, mirror aberrations must be controlled to within one-hundredth of a wavelength, which is near the limit of current mirror fabrication technology. Phase conjugation using nonlinear optics techniques has been well proven for aberration control in a resonator. The resulting benefit could be two-fold: reduction in the aberration requirements on FEL mirror surfaces and still ensuring good beam quality.

The problem of misalignment sensitivity of a high power FEL resonator has long been recognized[11]. It is due primarily to the long cavity length and narrow interaction region, and is not improved by using of diverging mirrors to shorten the cavity[8]. The tilt sensitivity angle of the end mirrors is approximately one microradian. The resonator thus requires a very sophisticated auto alignment system with an adjustment accuracy in the sub-microradian range. Mirror tilt is a special case of aberrations and

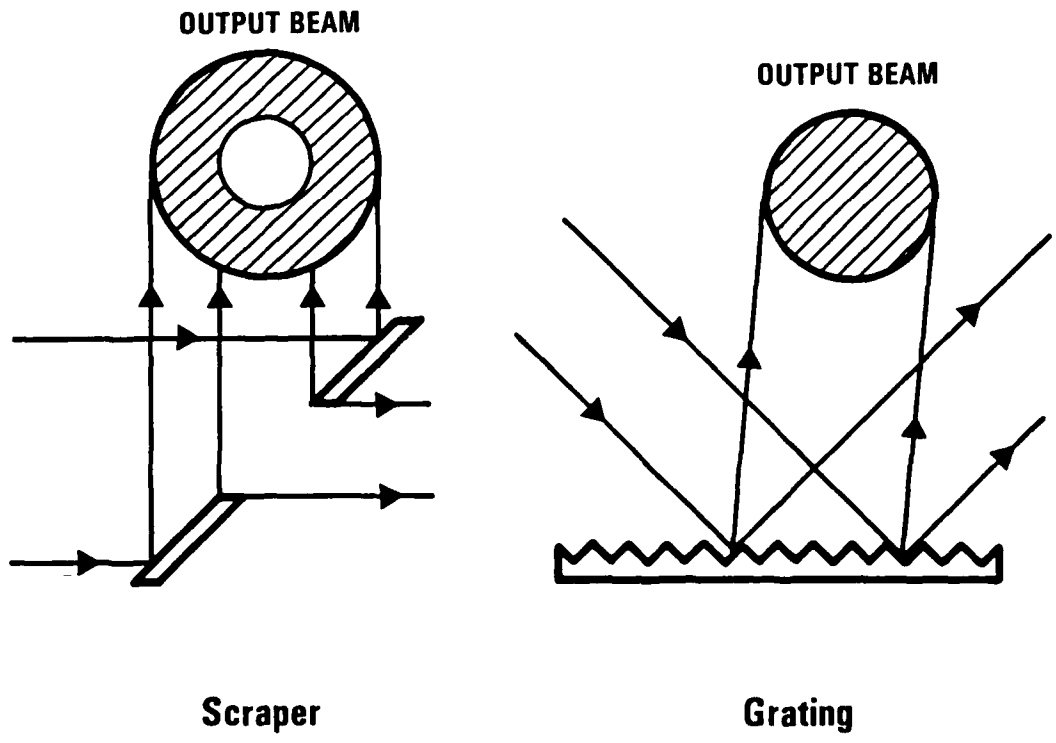

Figure 4. Conventional outcouple schemes for a high power laser resonator

can be corrected by the optical phase conjugation technique. This dynamic correction of the mirror tilt or jitter can reduce the alignment requirement significantly.

B. Up-Link Propagation

For a ground-based high power laser system, the transport of the output laser beam through an optical train and turbulent atmosphere to relay optic in space presents a major challenge[12]. One of the solutions is to place the oscillator in space[13]. A beacon signal coming down from the oscillator would sample atmospheric turbulence. The signal would then be phase conjugated and amplified to high power. The high power beam would be transmitted back into space retracing the optical path thereby compensating the aberrations in the optical train as well as in the atmosphere. This simple scheme will not be effective for a FEL system because the phase information will be completely lost in the high-gain amplification process. A different technique for imprinting the conjugated phase information onto the high power beam is required for an up-link system.

C. Phased Arrays

As a ground-based laser system, a single induction linac FEL is able to produce a very high power beam. However, in the near future, it might be necessary to couple several RF linac FEL devices together to reach the required power level[14]. Therefore, phased FEL arrays are an active research topic which includes different schemes such as injection locking, coupled cavities and beam combination . Since the phased-array concept has been actively pursued in other HEL programs, it is not included in the research scope of this project.

Most of the issues in the resonator and up-link optics are unique to the FEL system. Novel concepts have been explored for developing superior solutions. Recent developments in nonlinear optics technology have demonstrated control of the mirror aberrations and cavity alignment using phase conjugation phenomenon[10]. The feasibility of this approach for FEL applications has been addressed in this program.

In a phase conjugate FEL resonator, the two end mirrors are replaced by two phase conjugate mirrors (Figure 5), which are created by nonlinear

Phase-Conjugated FEL Resonator

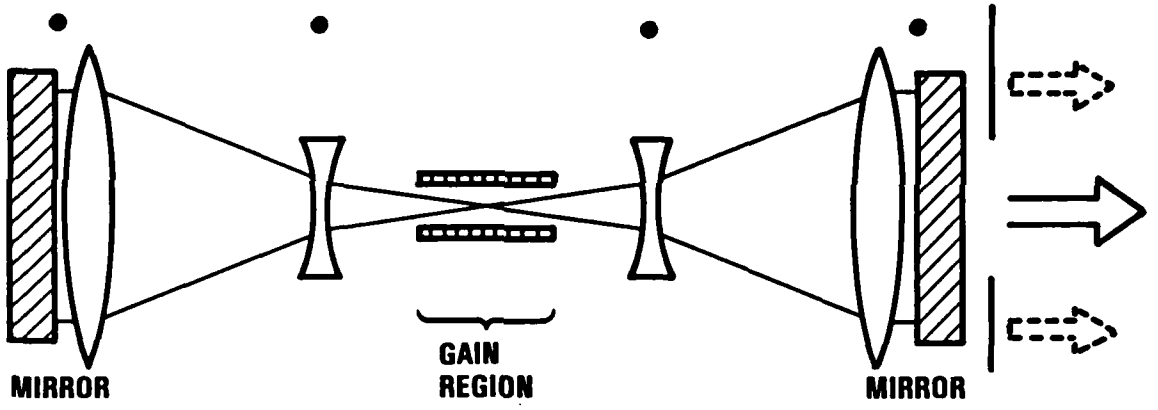

Figure 5. Phase-conjugate REL resonator configuration with conjugators at both ends

optical interactions in a nonlinear medium. The nonlinear effect that is most suitable for this application is stimulated Brillouin scattering (SBS). Because the pulse length in a RF linac FEL is much shorter than the SBS response time (~ nsec), a multiple-pulse SBS approach was investigated in performing the feasibility study.

For a ground-based laser system, the up-link propagation problem through a turbulent atmosphere is another major issues. The concepts of phase conjugate outcoupling for an RF linac FEL and phase conjugate beam conversion for induction linac FEL were developed in this program. The nonlinear optics techniques utilized for the two concepts are short-pulse four wave mixing and four-wave stimulated Brillouin scattering, respectively. These two effects have just begun to receive extensive attention and prove to be promising for the high power beam up-link from ground-based FEL systems.

2.2.2 System Analysis of FEL Resonator

Consider a FEL resonator design utilizing ideal phase conjugate mirrors. In this case a FWM configuration must be ruled out as a candidate because it requires two higher-power pump beams and more power is lost overall than what is reflected. An attractive candidate might be a SBS mirror. However, there are some SBS losses that would impair the resonator characteristics. In order to study this issue with regard to its impact on the device performance, system analyses were conducted for RF linac FEL and induction linac FEL devices.

From the theory of tapered wiggler FEL[24], the variation of the synchronous particle energy can be calculated from the equation

$$\frac{d\gamma}{dz} = \frac{A_w A_s \omega_s}{\gamma c} \sin \Psi \qquad (2.3\text{-}1)$$

where γmc^2 is the synchronous particle energy, ω_s is the optical frequency, Ψ is the synchronous particle phase, A_w and A_s are the dimensionless amplitudes of the magnetic field and the optical field. Assume the change of γ is

small. A_w and Ψ are kept constant. The change rate of γ is found to be proportional to the square root of the optical power, P,

$$\frac{d\gamma}{dz} \sim - P^{1/2} \qquad (2.3\text{-}2)$$

Since the FEL interaction gain and efficiency are defined as

$$G = \frac{\Delta P}{P} \qquad (2.3\text{-}3)$$

$$\eta = \frac{\Delta P}{P_{eb}} = \frac{\Delta \gamma}{\gamma} \quad , \qquad (2.3\text{-}4)$$

the Equation (2.3-2) can be integrated to obtain

$$(G + 1)^{1/2} - 1 = \frac{k}{P^{1/2}} \quad , \qquad (2.3\text{-}5)$$

where k is a proportional constant. Equation (2.3-5) was derived without any restriction on the magnitude of the gain. For an induction linac FEL amplifier, the gain is much larger than 1. Equation (2.3.5) gives the gain dependence on power,

$$G = \frac{k^2}{P} \qquad (2.3\text{-}6)$$

and η is a constant. For a RF linac FEL amplifier with a gain much lower than 1, the gain-efficiency relation is

$$G\eta = \frac{4k^2}{P_{eb}} \qquad (2.3\text{-}7)$$

Similarly, for a RF linac FEL oscillator where the power is not at the resonance, the relation can also be found to be

$$G\eta^3 = k'^4 P_{eb} \qquad (2.3\text{-}8)$$

where k' is another constant

The analysis for FEL amplifiers is straightforward and is not of interest here. However, the situation is more involved for a FEL oscillator because of the dynamical response of the intracavity power to changes in the FEL gain. To complete the equations required for the system

analysis, the gain and the system efficiency, η_S, are expressed in terms of the outcoupling fraction, C, and other losses, L,

$$G = \frac{C + L}{1 - C - L} \tag{2.3-9}$$

$$\eta = \frac{PC}{P_{eb}} \tag{2.3-10}$$

Now, with the help of gain-efficiency relations, the system efficiency can be found to be

$$\eta_S = k\, P^{1/4} \frac{C}{C + L} (1 - C - L)^{1/4} \tag{2.3-11}$$

The result is shown in Figure 6. The curve for L = 0 is an ideal condition. The value of η_S is normalized to have the maximum of 1 at C = 0 on this curve. For $L > 0$, η_S is zero when C = 0 or C + L = 1. The curves show that there is an optimum outcoupling fraction for any given losses. However, no significant variation was found between C = 0.2 and 0.6. For the loss of 5 and 10 percent, it was found the efficiency is reduced by 20 and 30 percent, respectively.

2.3 SYSTEM CONCEPTS

Based on the problems identified for conventional FEL resonators and our understanding of the unconventional adaptive optics techniques, three novel resonator concepts have been developed using the nonlinear optics technology. The first one is the phase-conjugate resonator concept that would correct the aberration effects and misalignment while also alleviating the mirror damage problem. The high reflectivity resonator mirrors are created by the multiple-pulse SBS process. The second concept is the phase-conjugate outcoupling of a RF linac FEL resonator using the four wave mixing process. It simplifies the problem of outcoupling optics and produces a conjugate beam. The third concept is the phase-conjugate beam conversion of the induction linac FEL device using the FWSBS technique. It

Free-Electron Laser System Efficiency for Fixed Intrinsic Efficiency

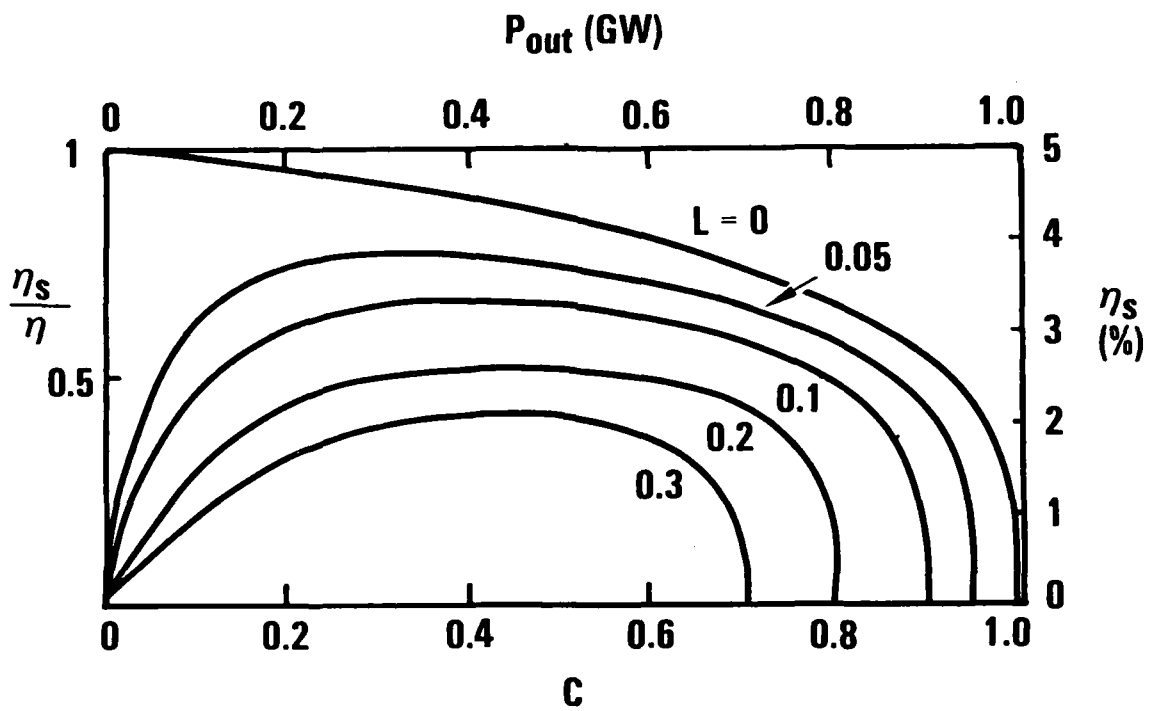

P_0 = 1 GW; K = 0.05 $(GW)^{1/4}$; P_{eb}/G = 20 GW

Figure 6. FEL resonator sytsem study. System efficiency verse outcoupling fraction for different losses. The numerical example is shown on the top and righthand coordinates

converts the high power output beam into the conjugate of a probe beam with high reflectivity and high efficiency.

2.3.1 Conjugate FEL Resonator

The simplest conjugate FEL resonator design replaces both mirrors of the linear resonator configuration with two gas medium SBS cells. Since gases can sustain much higher fluxes than mirrors, the SBS cells can be placed near the wiggler and thus reduce the overall cavity length substantially. The reflectivity from the SBS cells may be sufficiently high to permit oscillation. However, the phase conjugation property that is important for aberration control and misalignment corrections, might be absent completely in this configuration. In order to a phase conjugate wave, the pump beam has to be focused so that the phase information on the beam transformed into an intensity distribution in the focal volume-interaction region. The reflected field following this intensity variation would have the highest SBS gain, thereby generating the conjugate of the input beam.

A concern associated with the use of gaseous medium SBS cells is optical breakdown. The optical breakdown in gases consists of two steps, initial ionization and avalanche ionization. At an intensity of 100 Gw/cm^2, multiphoton ionization process can readily take place in gas molecules. For low pressure gases and short laser pulses, the secondary effect of ionization by electron collisions with atoms that causes the avalanche, might be negligible. However, a complete breakdown may occur for intensities of 1 TW/cm^2. For intermediate power RF linac FEL devices anticipated to be developed in the near future, SBS cells using inertial gas media, such as Xenon, may be sufficient for the application. For higher power devices, plasma media should be used. However, little is understood of the SBS effect in plasma as a phase conjugation process. More studies, particularly experimental work should be conducted before a conclusion can be drawn.

Since the phase conjugation process in SBS requires a focused beam, concave grazing-incidence mirror can be used to focus the beam into the SBS cell (Figure 7). The mirrors are configured as a ellipsoid with foci at the wiggler and at the phase conjugate cell. A spherical mirror can be

Grazing Incidence Ellipsoidal Mirror for Focusing the Radiation into the SBS Cell

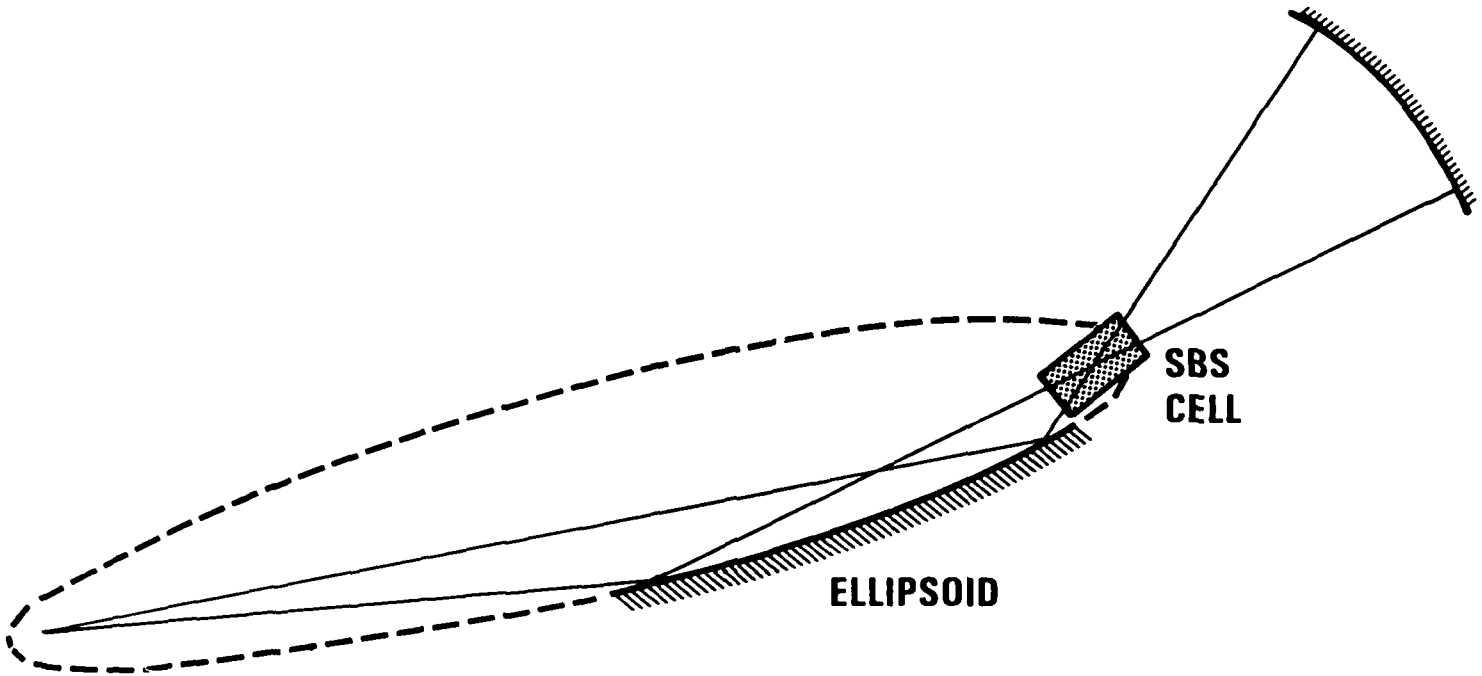

Figure 7. The conjugate mirror assembly on one side of the wiggler. The spherical mirror reflects the radiation that escapes the SBS interaction.

placed at some distance behind the cell . This spherical mirror functions as a conventional resonation mirror at oscillator start-up and at low powers when there is no SBS action. As the intracavity power increases above the SBS threshold, the optical wave is increasingly reflected at the SBS cell. The spherical mirror then intercepts escaping radiation and reflects the wave into the SBS cell as a back-injection signal to enhance the reflectivity.

A complete phase-conjugate FEL resonator can be formed by placing the set of elliposoidal-SBS-spherical mirrors on the both sides of the wiggler (Figure 8). A grating outcoupler is included just to show a complete configuration. In general, use of gratings is less favorable inside high-power resonators.

The pulse length in RF linac FEL devices ranges from 3 to 100 psec, depending on the accelerator type. However, the characteristic response time of the SBS effect is in the nanosecond regime. The laser field does not stay in the SBS medium long enough to permit the Stokes wave to build up from noise. However, if the pulse-to-pulse interval is comparable to or shorter than the phonon relaxation time, the acoustic wave will persist in the medium until the next pulse arrives. A significant SBS reflectivity is thus possible even with extremely short pump pulses[21]. This multiple-pulse SBS phenomenon is essential for a successful conjugate FEL resonator and is a subject of theoretical studies in this program.

2.3.2 Phase Conjugate Outcoupling

The identification of a satisfactory FEL outcoupling scheme has been a major problem in designing a high power RF linac FEL resonator. A grating can produce an unobscurred beam. However, there are two output directions and, gratings exhibit much lower damage thresholds. Scraper outcoupling is practical only if the outcoupling fraction is significant. For most RF linac FEL systems, the gain is approximately 10 percent. The result is an undesirably thin annular beam. To solve this problem, a phase conjugate outcoupling scheme using nonlinear four wave mixing process has been identified.

Phase-Conjugate Free-Electron Laser Resonator

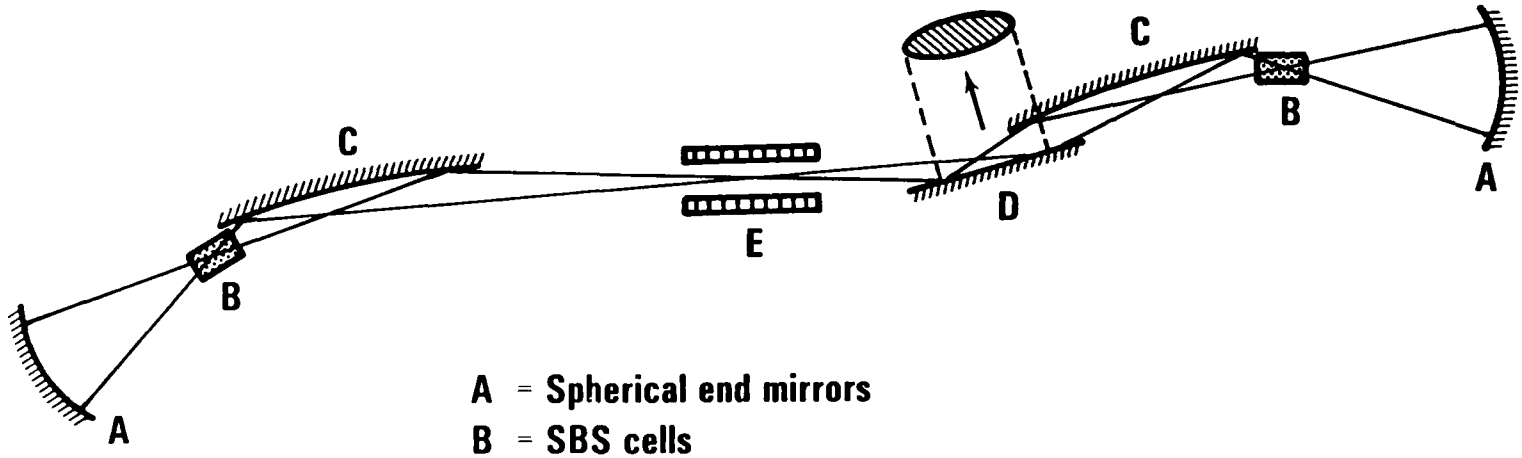

A = Spherical end mirrors
B = SBS cells
C = Concave grazing incidence mirrors
D = Planar grazing incidence grating
E = Wiggler

Figure 8. Phase-conjugate free electron laser resonator design

The FWM cell, containing nonlinear gas media, is placed inside the resonator (Figure 9). Its position is adjusted such that the counter-propagating short pulses overlap inside the cell. There is no stringent alignment problem of the pump pulses because only the on-axis pulses can survive the oscillation. A low power probe signal with aberrated phases is incident into the interaction region. The nonlinear mixing process generates a conjugated field propagating in the direction opposite to the incoming signal. This outcoupling scheme has the following advantages:

a. The output is a well-filled beam suitable for propagation

b. The reflectivity can be much larger than 1, such that a weak signal can induce a high power return[26]

c. Typical maximum energy transfer efficiency of FWM is 5 to 10 percent which is roughly equal to the FEL single-pass gain

d. The reflected wave is a conjugate of the signal and can correct the phase aberration on its return path

e. Typical response time of FWM are several picoseconds, which are much shorter than the pulse length

f. The outcoupling is negligible at low powers which can shorten the time for the intracavity field to reach saturation

g. The damage threshold of gas media is much higher than conventional mirror surfaces.

However, there is an equal amount of energy scattered in the forward direction accompanied with the conjugate reflection. This reduces the outcoupling efficiency by 50 percent. Several designs have been considered to alleviate the problem. One possible solution is to inject the forward wave back into the resonator for further oscillation. The second concept is to reflect the forward wave by another phase conjugate mirror, such as an SBS cell. Therefore, there are two conjugate return pulses for each interaction. The third method takes advantages of the short pulse length and finite relaxation time of the index grating formed in the medium (Figure 10). By adjusting the arrival time of pump pulses with respect to the signal, it is possible to create different gratings to reflect the pump beams selectively into the forward or backward direction respectively. It is called

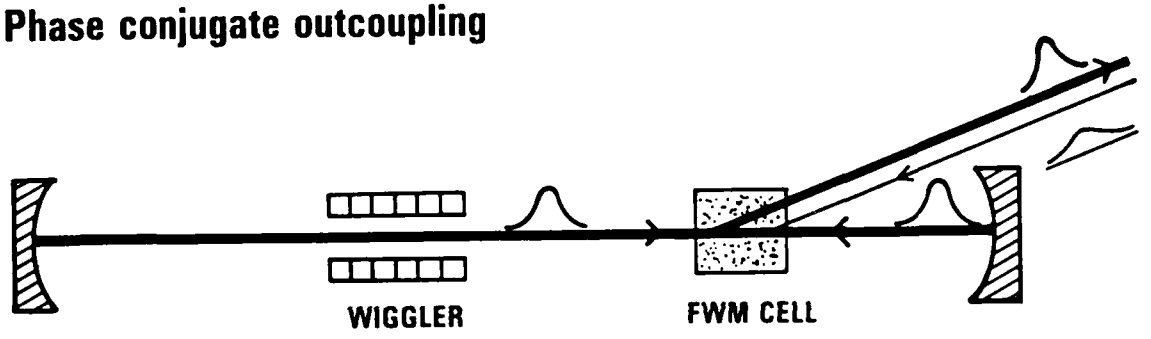

Figure 9. Phase-conjugate outcoupling from a FEL resonator, using the four wave mixing effect

Reduction of Transmitted Wave in Transient FWM

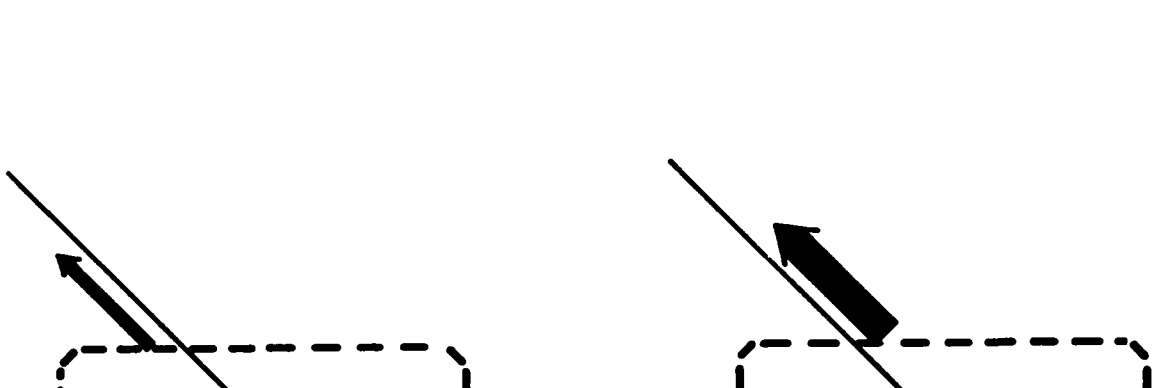

Figure 10. Selective scattering of the FWM process by adjusting the arrival time of pump pulses

"Discriminative scrattering" of FWM. In this way, the back scattering efficiency can be enhance.

2.3.3 Phase Conjugate Beam Conversion

For the output beam from an induction linac FEL amplifier or from a RF linac FEL oscillator without phase conjugate outcoupling, the transmission through the turbulent atmosphere would degrade the beam substantially. The FWM scheme described in the previous subsection can not be applied here because it requires two counterpropagating pump beam and the energy conversion efficiency is very low. For this purpose, a completely new nonlinear optics concept has been evaluated. It is a SBS process arranged in a FWM configuration (Figure 11) and, therefore, is called four wave stimulated Brillouin scattering (FWSBS).

The system consists of a SBS cell placed in the path of the high power beam. A much lower power laser beam at the same frequency is incident from the opposite direction. The signal to be conjugated interacts at a very small angle with the two pump beams. The signal frequency is slightly higher than the pump frequency and the difference is equal to the acoustic wave frequency of the SBS medium. The result is a substantial energy flow from the high power beam into the direction opposite to the signal beam. The reflected wave is the phase conjugate of the signal field. This process has a high reflectivity (10^6 demonstrated) and high efficiency effect. Since the response time of the SBS process is in nanoseconds, it is appropriate for the induction linac FEL.

This new effect was studied in detail, both theoretically and experimentally, in this program. The results are discussed in Chapter III and IV respectively.

Phase conjugate beam conversion

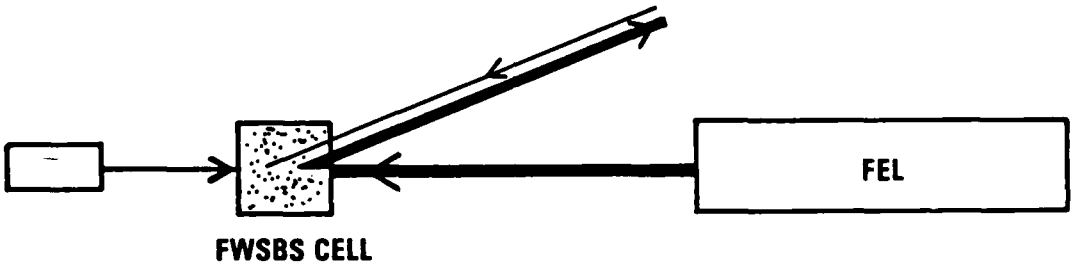

Figure 11. Phase-conjugate beam conversion from a high power laser output, using the four-wave SBS effect

III. THEORY AND MODELING

3.1 TASK OBJECTIVE

The objective of the theory and modeling task in the FEL resonator development program is to develop analytical tools for the study of the nonlinear optics phenomena that have been identified for FEL applications and included in the conceptual resonator designs. To accomplish this objective, the approaches of formulating analytical theory and developing numerical modeling were followed for each phenomenon. The tasks performed are summarized

	Theory	Modeling	Analysis
Conjugate FEL Resonator	-	2-D Code	Yes
MPSBS	Yes	1-D Code	Yes
SPFWM	Yes	2-D Code	Yes
FWSBS	Yes	1-D Code	Yes

3.2 CONJUGATE FEL RESONATOR

Conjugate resonators for general laser system have been an active research area for nearly a decade. Many analytical and numerical studies have been reported and were included in the reference list of two recent review articles[27,28]. However, most of the studies considered high Fresnel number cavities and assumed a large aperture conjugator with collimated input beams. In the conjugate FEL resonator design, the Fresnel number is low because of the highly focused beams. The fields at the conjugators and at the wiggler are in the far-field region of the field at the converging lens. The effects of aperturing on the conjugation process may not be the same for both resonator configurations. To facilitate the analysis of the

effectiveness of conjugate FEL resonators, a two-dimensional steady-state simulation code was developed in this program. The code was used to analyze both conventional and conjugate FEL resonators. The results show the difference in mode structure and the improvement in aberration and alignment control, when the conjugate reflector is used.

3.2.1 FEL Resonator Modeling

The phase conjugate FEL resonator code, FELPCR, was developed using wave optics and a simplified FEL gain model. The configurations include the conventional resonator with diverging lenses and the conjugator resonator with converging lenses. Schematics of both resonators investigated during the numerical studies are shown in Figure 12.

The code uses cylindrical coordinates with radial grid point spaced for employing gaussian quadrature. The fields are propagated with propagators derived from the Fresnel-Kirchhoff integral. For convenience, the fields are decomposed into angular Fourier components. These components are coupled to each other at the tilted or aberrated mirrors. The aberrations are modeled by fifteenth-order Zernike polynomials. At the conjugator, the fields are complex conjugated assuming perfect conjugators.

Since an RF linac FEL is essentially a low-gain device, the intracavity mode structures are dominated by the resonator configuration. The FEL interaction provides simply the energy increase for the radiation, with an aperturing effect due to the small electron beam cross-section. Based on these considerations, a simplified gain model has been developed for the FEL mode-medium interaction. It requires no particle simulation and generates a two-dimensional gain distribution on a single individual gain sheet. Considering the effect of betatron oscillation, the gain as function of radius is expressed as[29]

$$G(R) = \frac{\int_R^\infty g\ (\tilde{I}(r))\ f_e(r)dr}{\int_0^\infty f_e(r)dr}, \qquad (2.1\text{-}1)$$

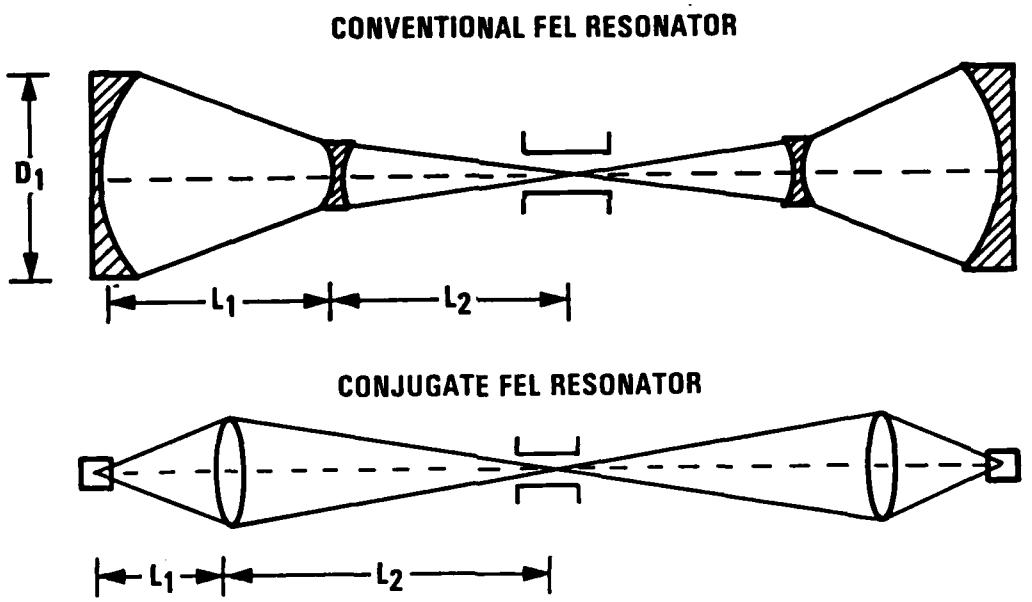

Figure 12. Resonator configuration for resonator analysis

where $f_e(r)$ is the electron density distribution, $\tilde{I}(r)$ is the average optical intensity within the radius r, g(I) is the saturated FEL gain depending on the interaction intensity, I,

$$g(I) = \frac{g_{ss}}{I + \left(\frac{I}{I_s}\right)^{3/4}}, \qquad (2.1\text{-}2)$$

In the above gain expression, g_{ss} is the small signal gain and I_s is the saturation intensity which is found to be near the resonance intensity for a tapered wiggler. This gain model is quite different from that for conventional lasers. There the gain is saturated by the local intensity and is thus, for example, lower in the high intensity region of the center of a gaussian optical beam. In the FEL gain model, however, the gain at a given radius is determined non-locally from the properties of all of the medium external to the given radius, properties which in turn depend on the average inner intensity. The result is higher gain near the center of the beam. This peaking gain provides a natural aperturing effect for the FEL mode-medium interactions.

3.2.2 FEL Resonator Analysis

A comparison of the behaviors of both conventional and conjugate resonators was made using the code, FELPCR. The dimensions of the conventional resonator were chosen to be L_1 = 85 m, L_2 = 24 m and L_{eff} = 370 m. The effective cavity length, L_{eff}, is the distance between the end mirrors of the cavity which has the same mode size at the mirrors without using any diverging lenses. The choices of these values may not represent the actual design, but are largely limited by the Fresnel number that can be handled by the code. For the conjugate resonator, the converging lens is placed 30 m from the wiggler and focuses the beam into the conjugator located 1.5 m from the lens. The beam size in the conjugator is approximately 50 μm. The mode structures are shown in Figure 13. The mode profile in a conjugate resonator is close to a dome, instead of gaussian shape. This is consistent with the observations in other reports.

The relative brightness has been obtained for different tilt angles and aberrations in both resonators. For the conventional resonator, the

Mode Intensity Profile

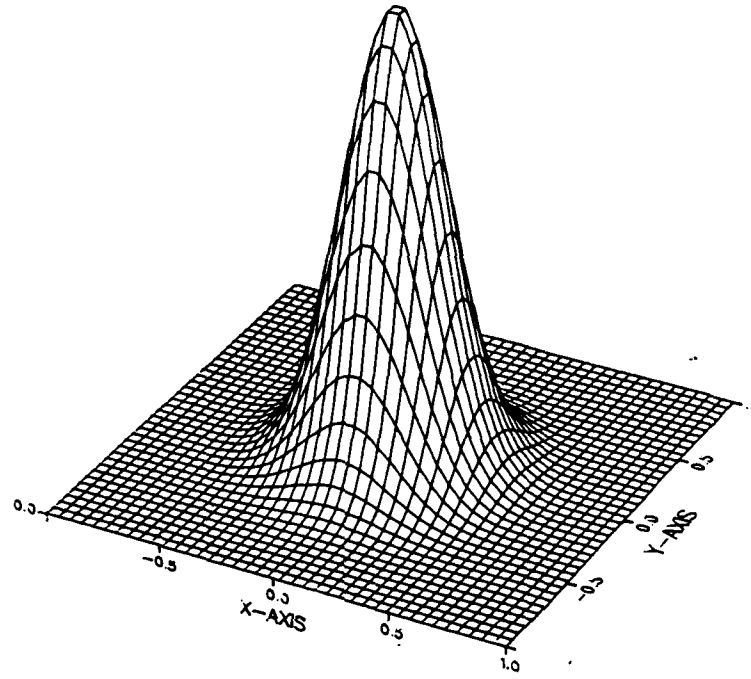

Conventional FEL Resonator

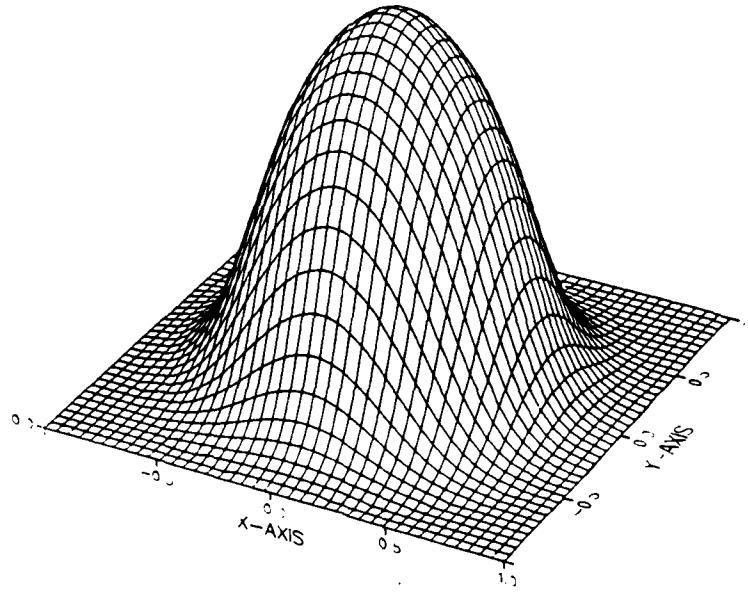

Conjugate FEL Resonator

Figure 13. Mode structuries in conventional and conjugate FEL resonators

misalignment sensitivity was found to be within 10 μrad (Figure 14). In particular, the end mirror tilt is a factor of 5 more sensitive than the diverging mirror tilt. For the conjugate resonator, no obvious decrease in the brightness was observed up to 10 μrad. Beyond this angle, the code showed oscillation in the output and can not converge properly, probably due to the small aperture size set at the conjugator. The clipper begins to interfere with the side-lobe field at the focus and causes the instability.

For the study of the aberrations, we used the phase screen previously measured for NACL optics (Figure 15). The phase screen is scaled to obtain different rms values of the optical path difference (OPD). The effect of beam aberration was observed by applying the phase screen on the end mirror or the diverging lens of the conventional resonator, and on the converging lens of the conjugate resonator. It was found that the effect of aberration is more profound for the end mirror compared to the diverging lens (Figure 16). The aberrations have less effect on the performance of the resonator with phase conjugate mirrors.

In general, we have found that the mode size in a conjugate resonator is larger than the mode size in a conventional resonator. The peak mirror loading is thus much lower. For alignment control tolerances, we observed that the sensitive tilt angle is well beyond 10 μrad and might be near the mrad regime which is beyond the analytical capability of the code. The aberration control requirements were found to be relaxed by a factor of ten. The mirror surface requirement can be largely relaxed in a conjugator resonator.

3.3 MULTIPLE-PULSE STIMULATED BRILLOUIN SCATTERING

For backward SBS using a single short pump pulse, the reflected wave may not be observable because field does not have enough time to grow. For example, the pulse length from a RF linac FEL is typically 3 to 30 psec which is much shorter than the typical relaxation time of phonons (~ nsec) in most SBS media. However, if the next pump pulse arrives at the interaction region before the phonon field disappears, it permits the phonon field to grow (Figure 17). The result is the build-up of the phonon field from pulse to pulse. At steady state, the reflectivity near 100 percent even

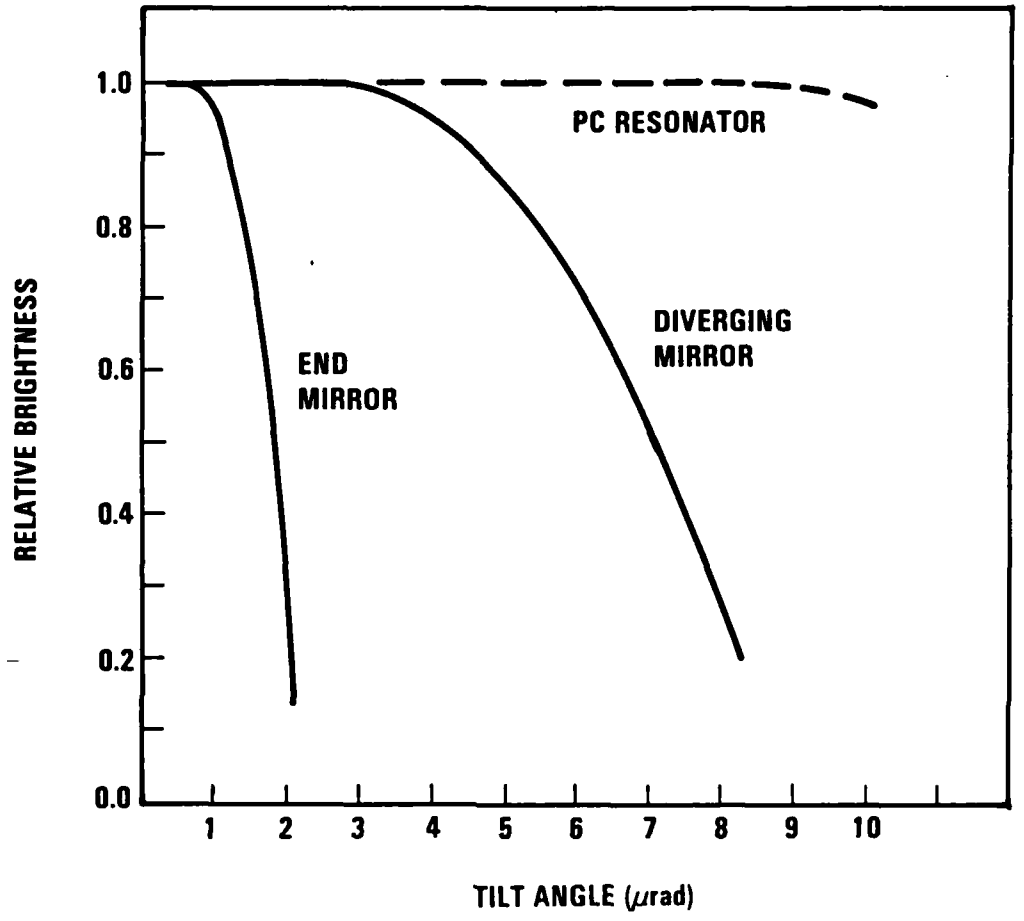

Figure 14. Cavity alignment sensitivity shown in brightness versus tilt angle for convertional (solid curves) and conjugate (dotted curve) FEL resonators.

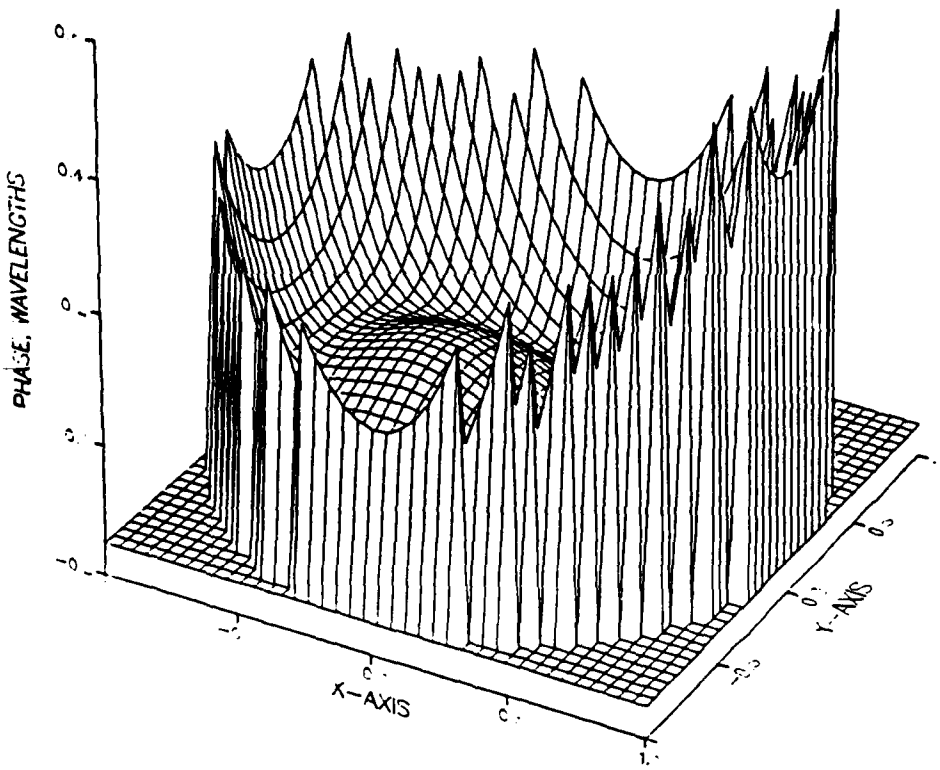

Figure 15. Phase screen used in the resonator analysis

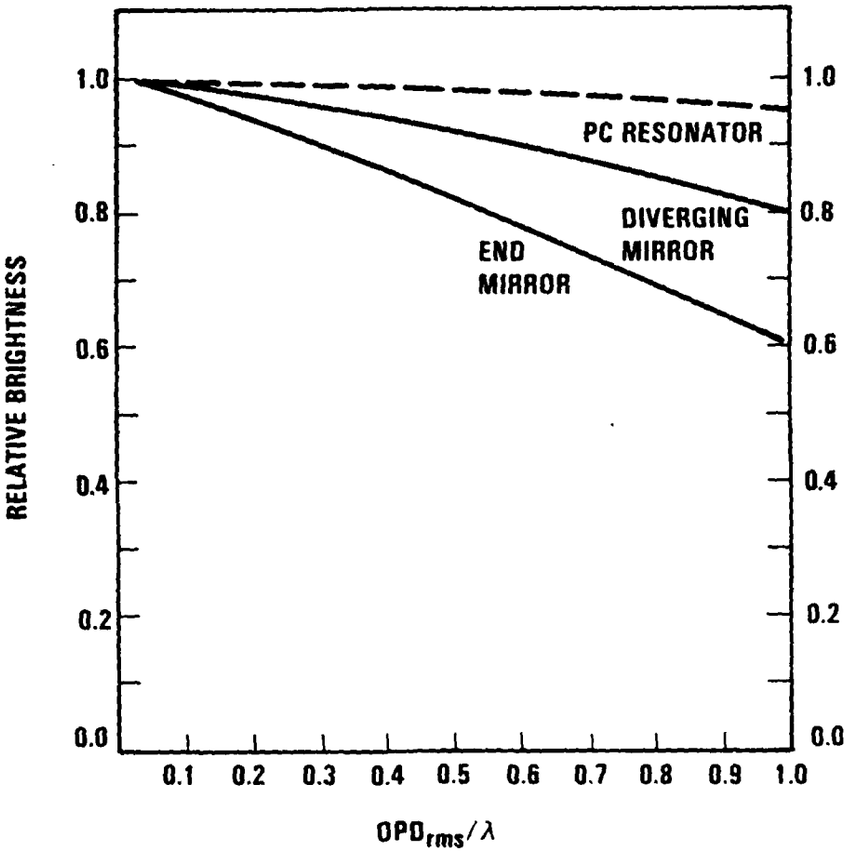

Figure 16. The dependence of brightness on mirror aberrations

Multiple-Pulse Stimulated Brillouin Scattering

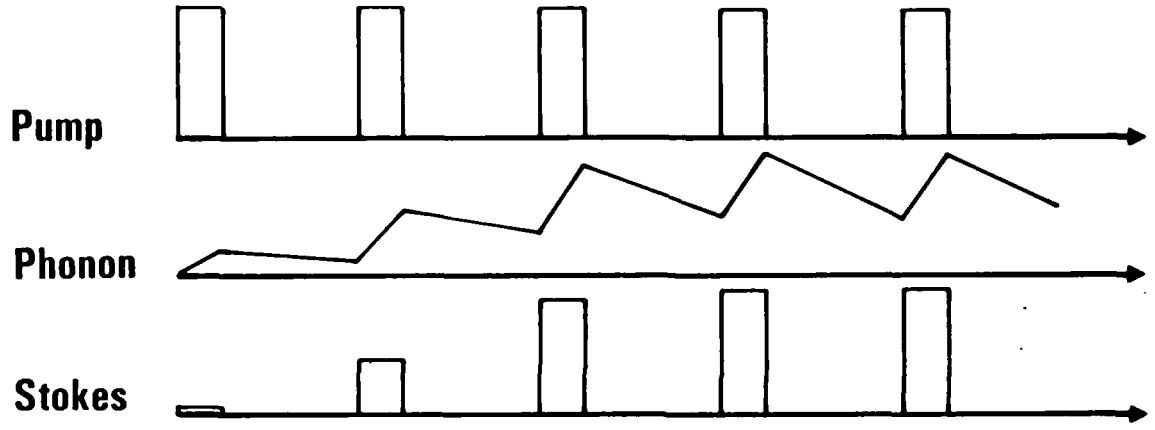

Experiment in SF_6 (CLEO Conference 1985, FG 4)

	Pulse 1	Pulse 2	Pulse 3
Pump	51 mJ	17 mJ	10 mJ
Stokes	<1 mJ	4 mJ	9.6 mJ
Reflectivity	< 0.2%	24%	96%

Figure 17. Multiple-pulse SBS phenomenon. The first observation was reported to have a reflectivity of 96 percent.

the individual pulses are very short. This multiple-pulse SBS (MPSBS) phenomenon was first demonstrated at Garching using three consecutive pulses[21]. The reported reflectivity was 96 percent. This effect can be applied to the phase conjugate FEL resonator and is studied in this program.

3.3.1 MPSBS Theory

The interaction of the pump, Stokes and phonons in a SBS medium can be described by the following one-dimensional equation,[30]

$$\left(\frac{\partial}{v\partial t} + \frac{\partial}{\partial z} \right) E_p = -ig_1 Q^* E_s \qquad (3.1\text{-}1)$$

$$\left(\frac{\partial}{v\partial t} + \frac{\partial}{\partial z} \right) E_s = -ig_1 Q E_p \qquad (3.1\text{-}2)$$

$$\left(\frac{\partial}{\partial t} + \Gamma \right) Q = -ig_2 E_p^* E_s, \qquad (3.1\text{-}3)$$

where E_p, E_s and Q are the slowly varying envelopes of the pump, Stokes and phonons, g_1 and g_2 are the coupling coefficients, v is the light velocity in the medium, Γ is the phonon relaxation rate. For most SBS media, the field Q grows slowly compared to the response time of the photon fields. In most cases, the optical fields are able to reach equilibrium within a few round trips of the medium length, which is of the order of 0.1 nsec. Therefore, the time derivatives in field equations can be neglected. In other words, for time scales longer than 0.1 nsec, it can be assumed that the fields response instantly to the change of phonon field, Q.

An analytical solution of the Equation (3.1-1, 2, 3) has not been found with time dependence. However, if Γ is small enough it can be seen that the phonon field actually neglects the existence of the gap between the pulses. The SBS effect will be the same as if the pulses are packed together back-to-back. For the pulse length of 30 psec, it means that steady-stated can be reached in a couple of ten pulses.

3.3.2 MPSBS Analysis

In order to understand quantitatively the transient response of the SBS medium to short pump pulses, a one-dimensional code was developed based

on the equations (3.1-1, 2, 3). The code was designed to process every ten pulses as a group. At the beginning of each pulse, the Stokes intensity was assigned at noise level. Between pulses, the phonon field decays with the relaxation rate, Γ, (or relaxation time, $\tau = 1/\Gamma$). The reflectivity and the Stokes wave profiles are the output.

Equations (3.1-1, 2, 3) can be converted into simpler forms in terms of a dimensionless quantity, $G = gIL/\tau$, where $g = g_1 g_2$, I is the pump intensity and L is the interaction length. A parametric study was performed to study the effect of relaxation time on MPSBS. The medium and the pump intensities were chosen such that G = 750/nsec. The pulse length was selected to be 0.1 nsec with a repetition rate of 2 GHz. For a gaseous medium, the relaxation time can be adjusted by changing the pressure. The interaction gain, g, is proportional to the relaxation time. The calculated variation of the reflectivity from pulse to pulse for different values of τ are shown in Figure 18. The reflectivity was found to reach near the steady-state value within three pulses, which is consistent with the experimental observation reported earlier[21]. The steady-state value of reflectivity, however, increases with the relaxation time primarily due to the increasing SBS gain.

The reflected pulse profiles for the case of τ = 1 nsec were examined and are shown in Figure 19. The pump intensity and length are normalized to one. In general, the pulse profiles have a sharp-rising front and fast-decreasing tail. The difference in steady-state reflectivity is mostly due to the difference in time for the pulse to reach the maximum intensity.

For practical reasons, the case of a RF linac FEL using a xenon SBS cell was studied. For xenon gas at 39 atm, the SBS gain is 0.044 cm/MW and the relaxation time was 2 nsec[31]. Assuming that the medium length is 1 cm, the pulse length is 30 psec with a repetition rate of 0.5 GHz. The case here shows that the relaxation time is equal to the pulse-separation time but several hundred times longer than the pulse length. The pump intensity varies from 10 to 100 GW/cm^2 and the noise level is chosen to be 0.1 MW/cm^2. The actual noise intensity may be much lower than this value. The change of intensity below the chosen level can be estimated by taking the spatial average of Eq. (3.1-2) assuming E_p constant. For an intensity of

Multiple Pulse SBS

Pulse length = 0.1 ns

Pulse separation = 0.5 ns

$$\frac{gIL}{T} = 750/ns$$

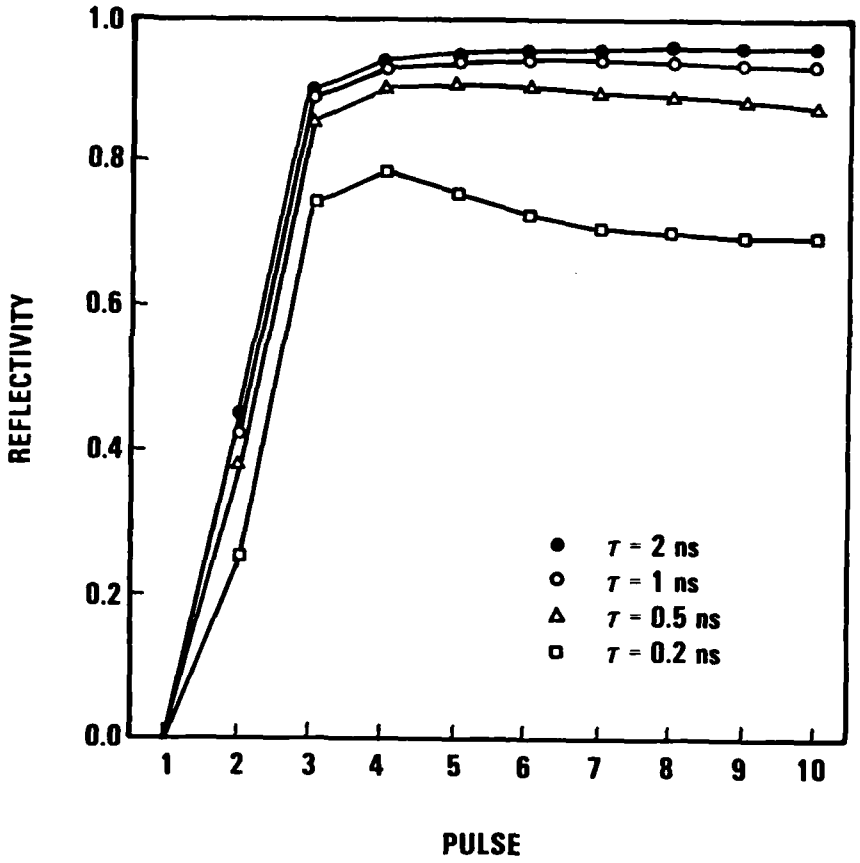

Figure 18. Reflectivity build-up for different values of relaxation time

Multiple Pulse SBS

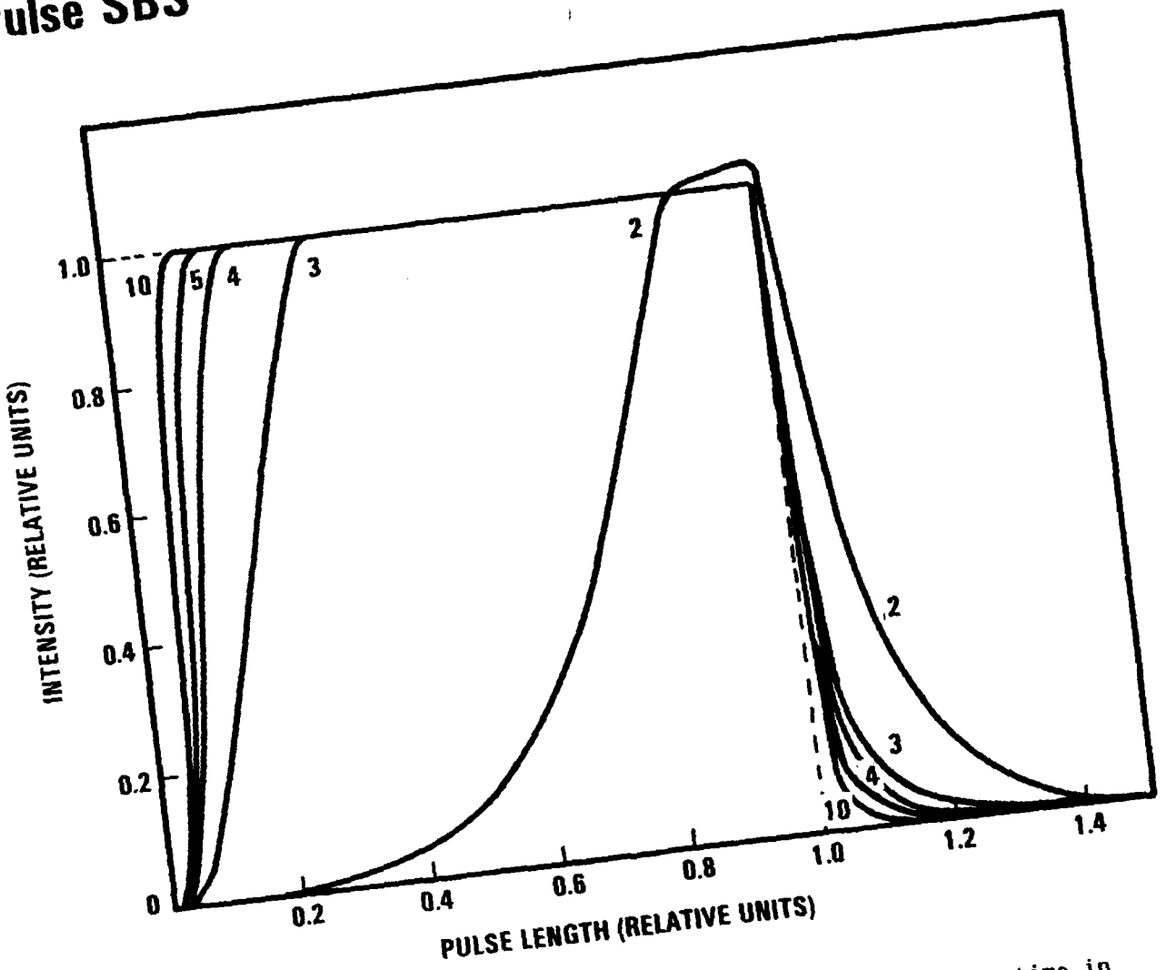

Figure 19. Reflected pulse profiles for 1 nsec relaxation time in Figure 18

10 GW/cm^2, the Stokes intensity doubles after every pulse. For high intensities, the rate should be proportionally increased. Thus, for every three orders of magnitude reduction in the noise level, the required number of pulses grows by ten.

From Figure 20, it can be seen that the SBS reflectivity can reach its steady-state value within 10 or 20 pulses. For the cases of 50 GW/cm^2, the reflected pulse profiles are shown in Figure 21. The first three reflected pulses are too weak to be seen in the linear scale. As the pulse number increases. The pulse profiles becomes closer to the shape of the input square pump. The steady-state reflectivity is 93 percent.

In summary, the MPSBS effect has been studied numerically in real time domain. Choosing the RF linac FEL pulse structure and a practical SBS medium, it was shown that high reflectivity can be obtained after a small number of pulses. The reflectivity is close to unity that is high enough for FEL resonator applications. The reflected pulse shape is also close to the input profile. The FEL interaction is thus less perturbed.

3.4 SHORT-PULSE FOUR WAVE MIXING

The four wave mixing effect was considered as a phase conjugate outcoupling scheme for RF linac FEL resonators (Figure 22). For the analysis of this phenomenon in the FEL characteristics regime, it was found no analytical theory and numerical modeling are available in the literature. Most of the theories presented the solutions either in steady-state or in long-pulse regime where the time varying pump fields are assumed to be uniform across the medium[32]. However, the pulse length of a RF linac FEL device is around 0.1 - 1 cm, which is probably shorter than the interaction region. The phenomenon is definitely in the transient regime and requires a full space-time representation in the coupled equations. In the area of numerical modeling, only the one-dimensional steady-state solutions have been reported. For the purpose of demonstrating the conjugation, field of view, beam misalignment and self-focusing effects, a two-dimensional simulation code is necessary to accomplish the task. The analytical theory and the numerical code developed in this program are described in the next two subsections followed by some detailed analysis.

Multiple Pulse SBS

Medium: Xe at 39 atm
$L = 1$ cm
$g_B = 0.044$ cm/MW
$\tau = 2$ ns

Laser: RF linac FEL
Pulse length = 30 ps
Pulse separation = 2 ns

Power:
- ◉ 100 GW/cm^2
- ○ 50 GW/cm^2
- △ 20 GW/cm^2
- □ 10 GW/cm^2

Noise 0.1 MW/cm^2

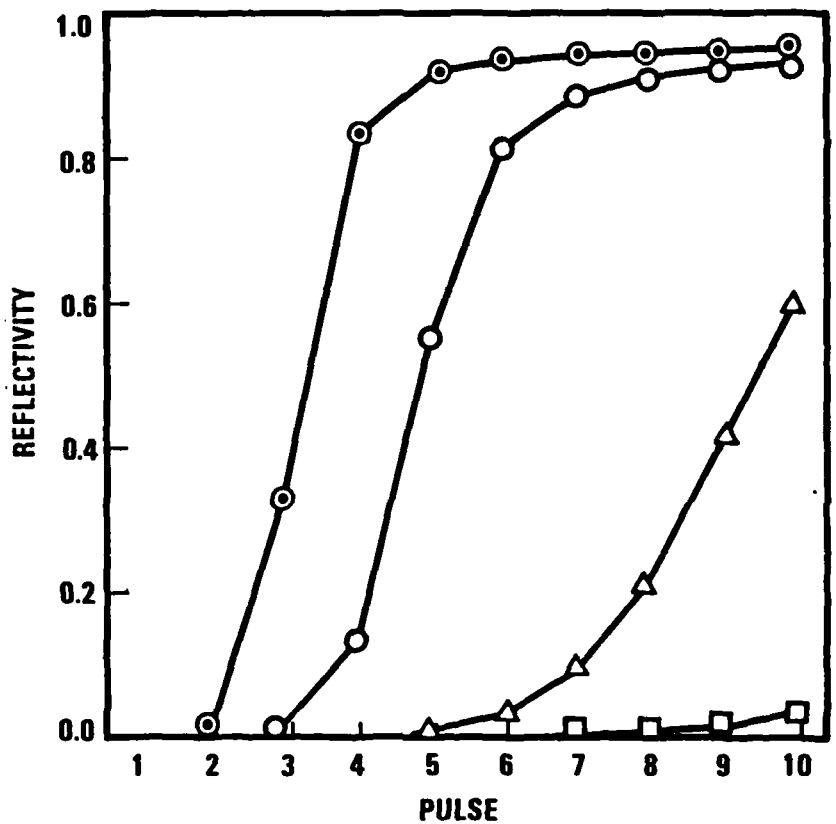

Figure 20. Reflectivity build-up for the case of xenon SBS medium and typical short-pulse RF linac FEL at different intensities

Multiple Pulse SBS

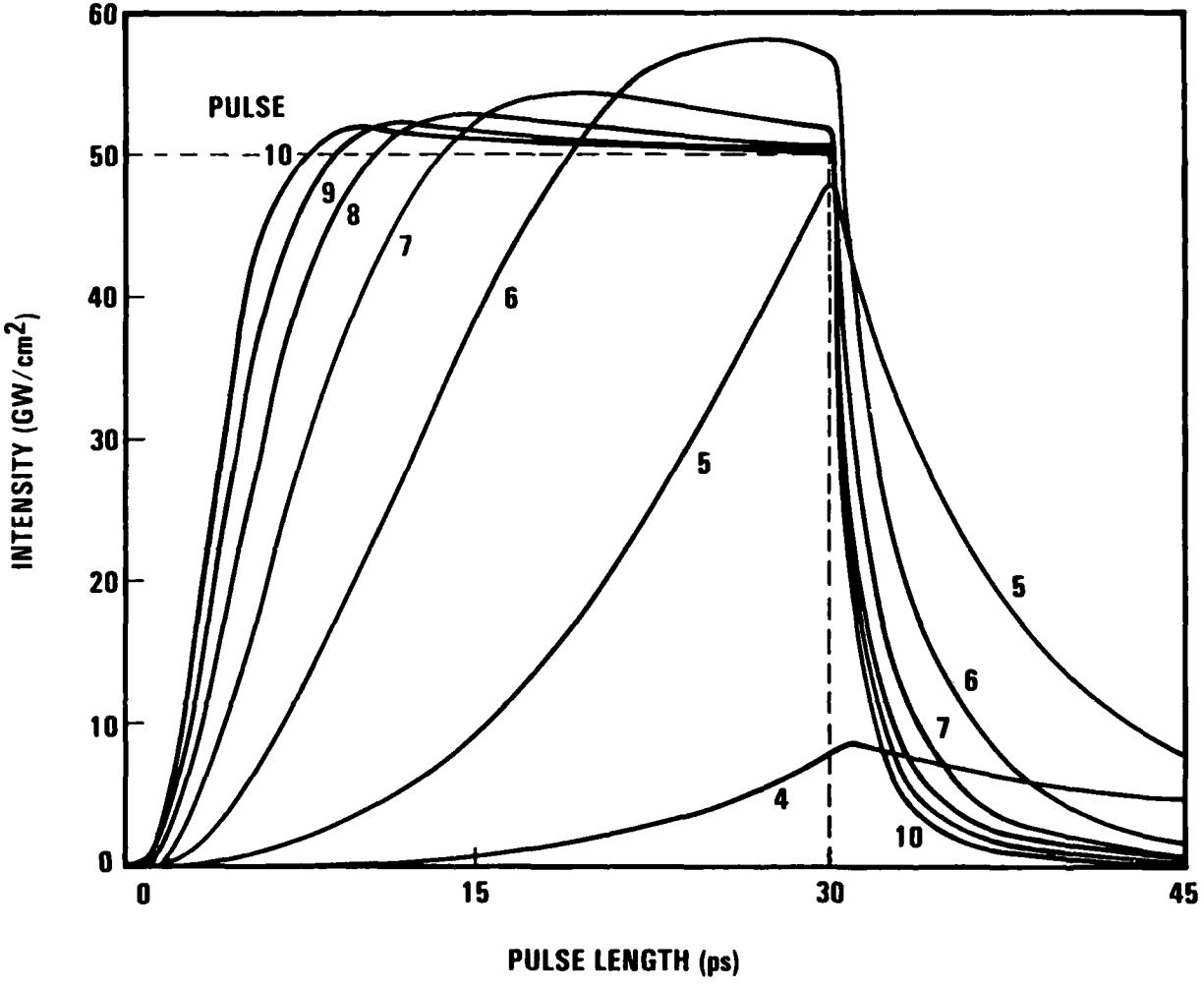

Figure 21. Reflected pulse profiles for the intensity of 50 GW/cm^2 in Figure 20

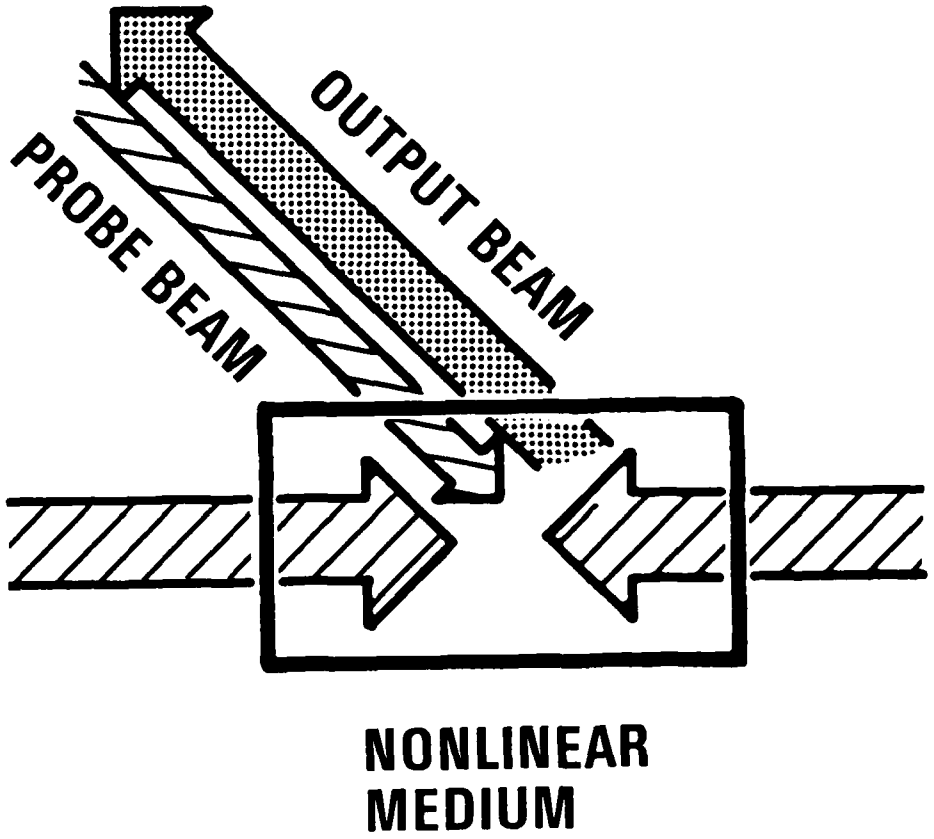

Figure 22. FWM as an outcoupling scheme for FEL resonators

3.4.1 SPFWM Theory

The details of the analytical theory for SPFWM are shown in Appendix A, which is a preprint of the paper submitted for publication. The theory starts with the coupled-mode equations describing the four wave interactions. The equations can be solved exactly in the no-pump depletion regime. For arbitrary pulse profiles, the result is given in Equation (A-13). For a special case where the three input beams have the same pulse profiles, a closed-form reflectivity expression was obtained as shown in Equation (A-17). The result is quite different from the steady-state or long-pulse solution in earlier theories[22,32]. The reflectivity is independent of the pulse shape and monotonically increases with the pump fluences (Figure A-2 and A-3).

Since bandwidth is one of the major issues for the FEL device, the theory is generalized to the cases where the coherence length is much shorter than the pulse length. The main results is in Equation (20), where γ is also the ratio of bandwidth to the transform-limited bandwidth. The dependence of reflectivity on this ratio is shown in Figure A-4.

Consider a practical example for RF linac FEL pulses at 0.5 μm wavelength. The pulse is 1 cm (i.e. 30 psec) and the pulse energy density is 10 J/cm^2. If the bandwidth is one percent, the coherence length is 0.05 mm. For a nonlinear optical medium similar to CS_2, the reflectivity is found to be

$$R = 200 \left[I_0^2 (3) + I_1^2 (3) - 1 \right] \sim 9000 \; ! \qquad (4.1\text{-}1)$$

which is readily adequate for our requirement ($> 10^3$).

The reflectivity expression was derived assuming collinear polarization of the three beams. In this case, the equation for the conjugated field can be written as

$$E_4' \sim \chi_{1111} E_1 E_2 E_3, \qquad (4.1\text{-}2)$$

where prime means spatial derivative and χ_{1111} is the nonlinear optical susceptibility. For circularly polarized input beams, as in our experiments, the x and y components of E_4 have contributions from different

combinations of the three input field components. Based on the nonzero third-order susceptibilities, the component E_{4x} has the following contributions,

$$E'_{4x} \sim \chi_{1111} E_{1x} E_{2x} E_{3x} + \chi_{1122} E_{1x} E_{2y} E_{3y} + \chi_{1212} E_{1y} E_{2x} E_{3y} + \chi_{1221} E_{1y} E_{2y} E_{3x}. \quad (4.1\text{-}3)$$

For CS_2, the off-diagonal suscepalibilities are related to χ_{1111} as

$$\chi_{1122} \sim \chi_{1212} \sim \chi_{1221} \sim \chi_{1111} / \sqrt{2}. \quad (4.1\text{-}4)$$

Since $E_{ix} = E_{iy} = E_i$ for i = 1, 2, 3, we have

$$E^1_{4x} \sim \frac{3 + \sqrt{2}}{4} \chi_{1111} E_1 E_2 E_3 \sim 1.1 \chi_{1111} E_1 E_2 E_3 \quad (4.1\text{-}5)$$

Similar result should be obtained also for E_{4y}. In the low reflectivity limit, the return intensity is thus about 2.4 times larger than the value in the collinear polarization case if the input intensities are the same in both cases.

3.4.2 SPFWM Modeling

For the purpose of studying numerically the SPFWM effect, a two-dimensional simulation code, called TFWM, has been developed in this program.

In the four wave mixing configuration, beam 1 and 2 are the colinear pump beams propagating in opposite directions. Beam 3 is the probe beam incident at a small angle with respect to beam 1. The plane defined by these three beams is the two-dimensional interaction plane for the system and no variation of physical parameters is assumed in the direction normal to this plane. The z axis is defined as the line bisecting the angle between beam 1 and 3 (Figure 23), although the incident angle of each beam can be input independently. The return signal (beam 4) is expected to propagate on the same plane and in nearly opposite direction of beam 3.

The region of the nonlinear medium extends from 0 to L in the z direction and has an area large enough to cover the four beams. At the beginning (t = 0), the pulse fronts of beams 1, 2 and 3 are placed against

Two Dimensional Model of Four Wave Mixing

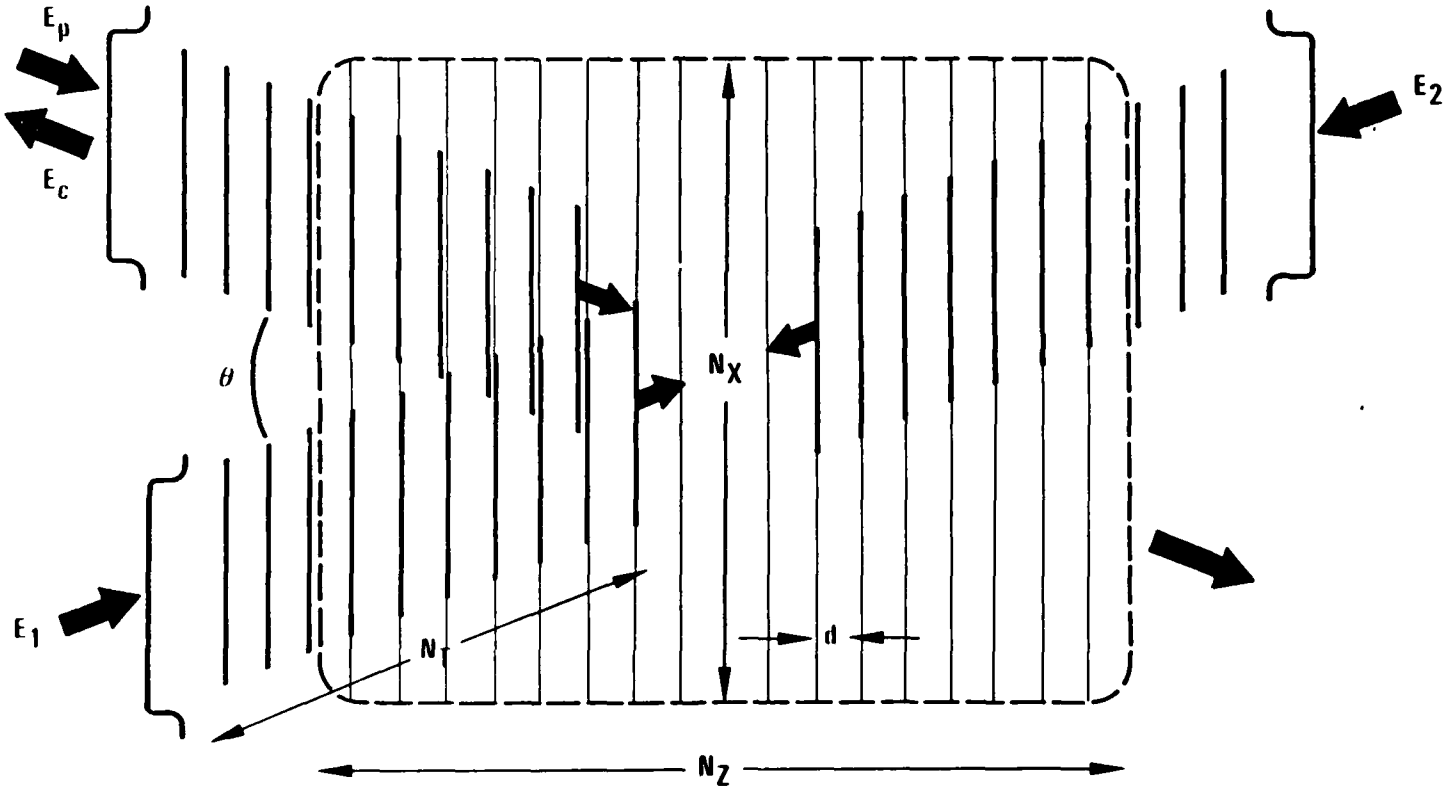

Figure 23. Schematic of the two-dimensional FWM modeling

the front and rear edges of the medium. The advance of the pulses into the medium can be adjusted if a pulse delay is assumed in any one of the beams. For longitudinal sampling, the pulses are sliced into equally spaced sheets perpendicular to the z-axis. The slice distance should be twice that of the propagation distance in each time step, such that the field on each sheet will interact with every field sheet in the opposite-direction pulse.

Transversely, the fields are sampled in equally spaced grid points across the whole aperture. The beam area is defined by either a gaussian profile or a smoothed square window function. The smooth window edges reduce the diffraction effect. Because the field sheets are not perpendicular to the actual direction of beam propagation for non-zero incidence angle, a linear phase variation is applied to the field across the beam. For short pulse applications, several different longitudinal pulse profiles have been used in the study (Figure 24).

Before the pulses enter the interaction region, a phase screen representing the phase aberration can be applied to the complex field. The phase screen consists of five sinusoidally varying functions. With different variation amplitudes and periods, various phase screens can be created independently for each beam. The phase screen of beam 3 should be applied to the exiting beam 4 to check how well the aberration is corrected. In each case, the beam quality is calculated in terms of the Strehl ratio.

The pulses advance in the medium using the near-field propagation scheme. In each propagation step, the one-dimensional field array is Fourier-transformed. For CW cases, the propagation continues until a steady state is reached. For pulse interaction, the propagation stops when the trailing edge of every pulse completely leaves the medium. At the end of the run, the reflectivity and Strehl ratio are calculated. The field arrays are stored for three-dimensional plots of pulse intensity and phase profiles.

In the nonlinear medium, every field interacts with itself and with each other through the nonlinear optical susceptibility. The code models such interactions in Kerr-like media as well as in saturable absorbing (or

Four-Wave Mixing Code
Pulse Profiles

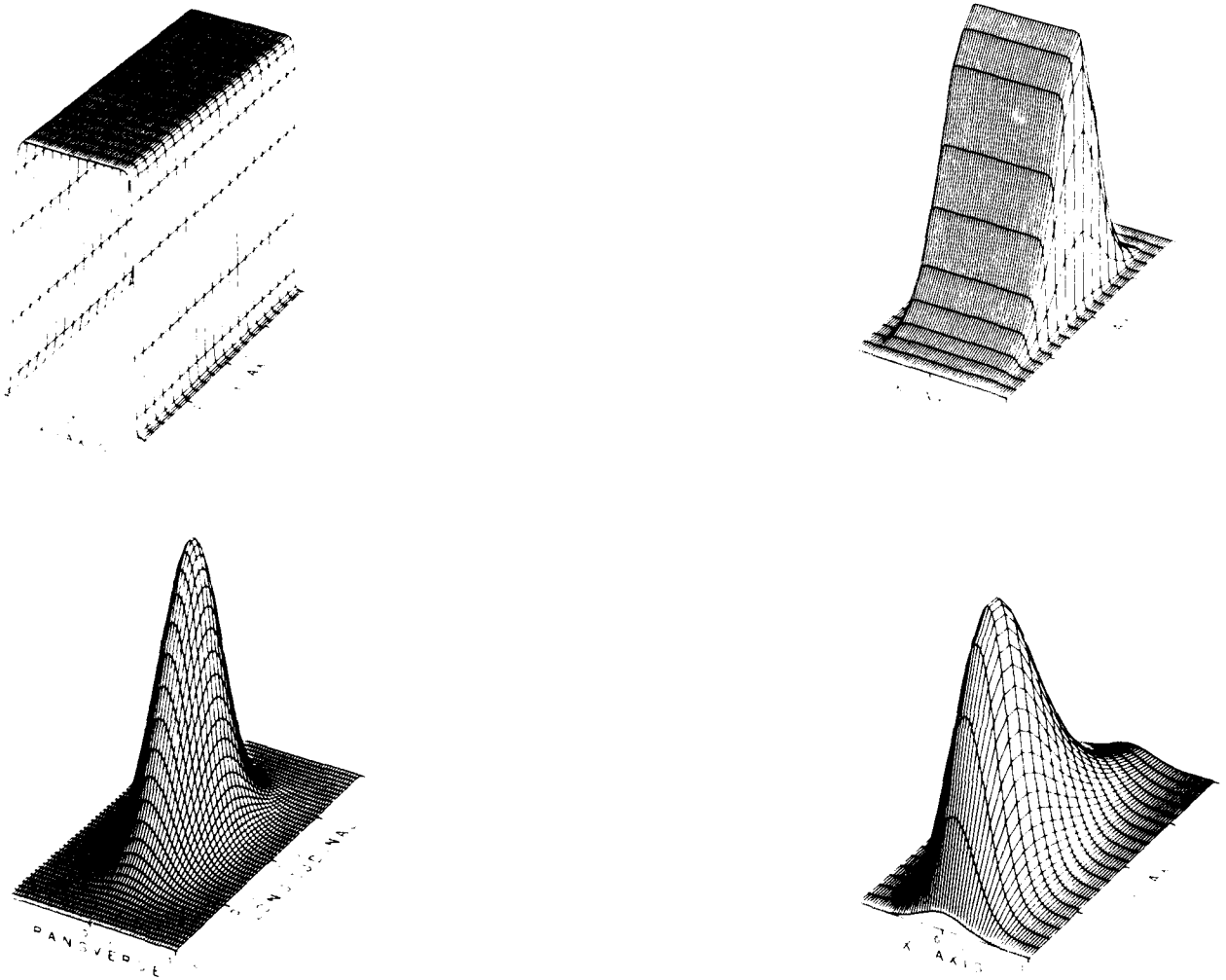

Figure 24. Different pulse shapes used in the FWM modeling

gain) materials. In a Kerr-like medium nonlinearities can be described by an effective index of refraction n:

$$n = n_0 + n_2 \langle E^2 \rangle, \tag{4.2-1}$$

where $\langle E^2 \rangle$ is the time average of the square of the total field. Before each propagation, the complex field array, A_j (n_x, n_z), are updated according to the formula

$$\Delta A_j = -i \left[(2I_0 - I_j)A_j + 2A_k^* A_m A_n \right] \frac{2n_2 k_0 \Delta z}{\cos\theta_j}, \tag{4.2-2}$$

where the indices are

j	k	m	n
1	2	3	4
2	1	3	4
3	4	1	2
4	3	1	2,

(4.2-3)

and

$$I_j = |A_j|^2, \tag{4.2-4}$$

$$I_0 = I_1 + I_2 + I_3 + I_4$$

$$i = \sqrt{-1}$$

k_0 is the vacuum wave number, θ_j is the incident angle of beam j and Δz is the propagation distance.

Equation (2) can also be transformed into coupled intensity and phase equations. Both methods are available in the code. Although using coupled intensity equations guarantees energy conservation, it is necessary to be very careful in the region where the intensity is zero because the intensity variable appears in the denominator of the accompanied phase equations. In general, the first term in Equation (2) represents the self phase modulation which would result in nonlinear self-focusing for a non-uniform beam. The second term represents the four wave interaction which generates the conjugated return signal.

3.4.3 SPFWM Analysis

The two-dimensional code, TFWM, was developed for the observation of phenomena that have the nature of transverse field variations. The phenomena of interest related to SPFWM include self-focusing, effective field of view, conjugation fidelity and the saturation effect.

In a nonlinear medium, self-focusing and FWM should have comparable effects because both are the results of electric field interactions through the third-order optical susceptibility[35]. In order to make sure that the self-focusing effect is properly included in the code, the process is isolated from FWM by inputing only one beam. The beam profile in the medium is carefully followed. At intensities above several GW/cm^2, the self-focusing effects occur. A typical beam profile is shown in Figure 25 for peak intensity of 2.5 GW/cm^2. It is important to point out that the self-focusing observed is in only one transverse direction. It might be quantitatively different from the two-dimension self-focusing effect. For our purpose, one-dimensional self-focusing is sufficient and was well simulated by the code.

Most analytical theories and one-dimensional codes of FWM considered only collinear interacting beams. However, the probe beam was incident at small angle with respect to the pump beam in most experiments and also in our applications. It is important to determine the dependence of the reflectivity on the incidence angle. The angular dependence was studied for the low reflectivity case so that it could be compared with the theoretical prediction. The medium used was CS_2 in a 1 cm long cell. The length and the spatial width of the pulses were 1 cm and 0.25 mm, respectively. The pump and the probe intensities were 124 MW/cm^2 and 12.4 MW/cm^2 respectively. As the incidence angle was increased, the reflectivity decreased nearly linearly (Figure 26). The results were agreement with the dotted curve which was calculated considering that the reflectivity is proportional to the beam overlap. It was found that the beam-overlap argument was valid in most cases.

FWM has been demonstrated experimentally as having a high conjugation fidelity. However, the FWM phase conjugation process has not previously been studied by a simulation code because no two-dimensional code was

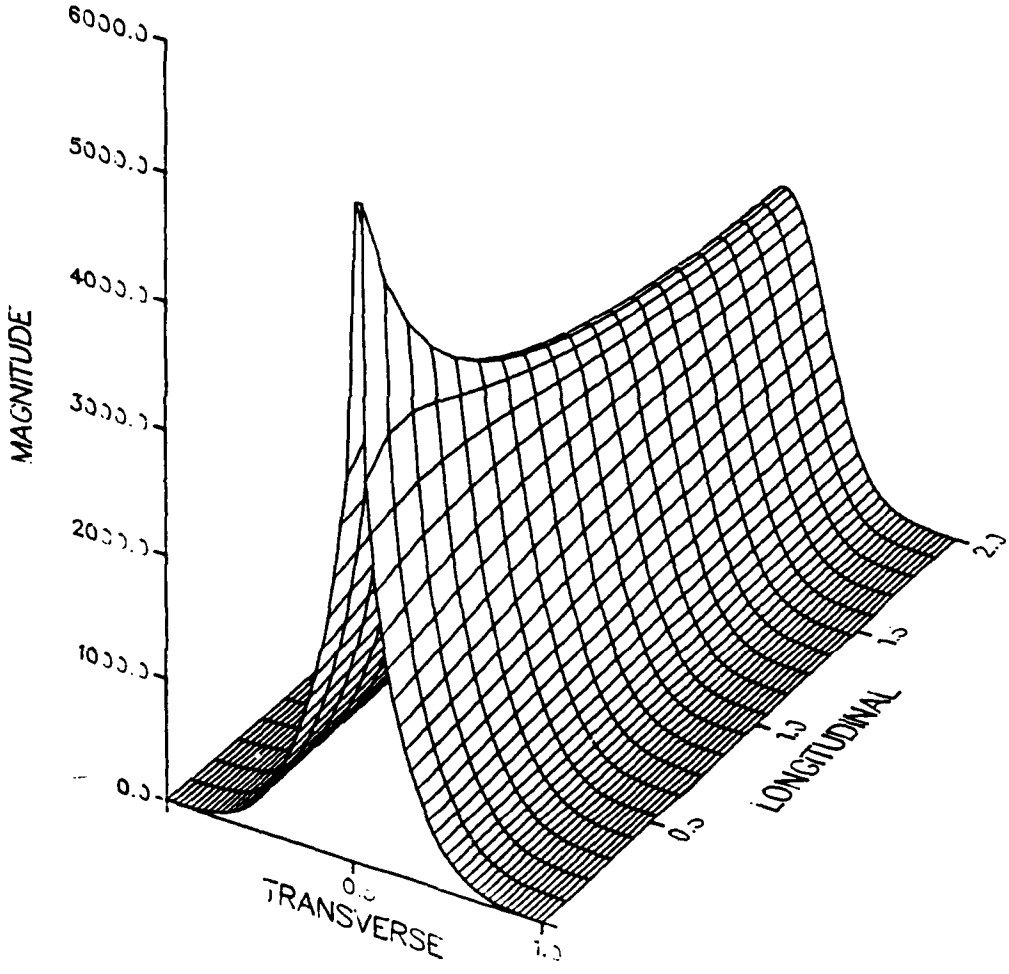

Figure 25. Narrowing of pulse intensity profile (self-focusing) in a kerr medium (CS_2). The peak input intensity is 2.5 GW/cm^2

Noncolinear Four-Wave Mixing
Angular Dependence

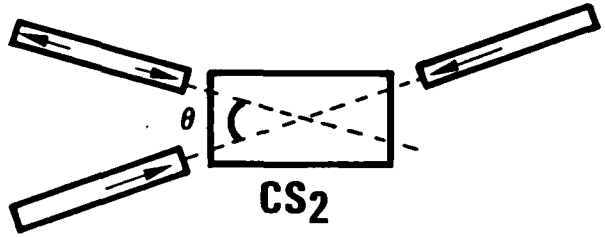

Medium: length 1 cm
width 1 mm

Pulse: length 1 cm
width 0.25 mm

Intensity: pump 124 MW/cm^2
probe 12.4 MW/cm^2

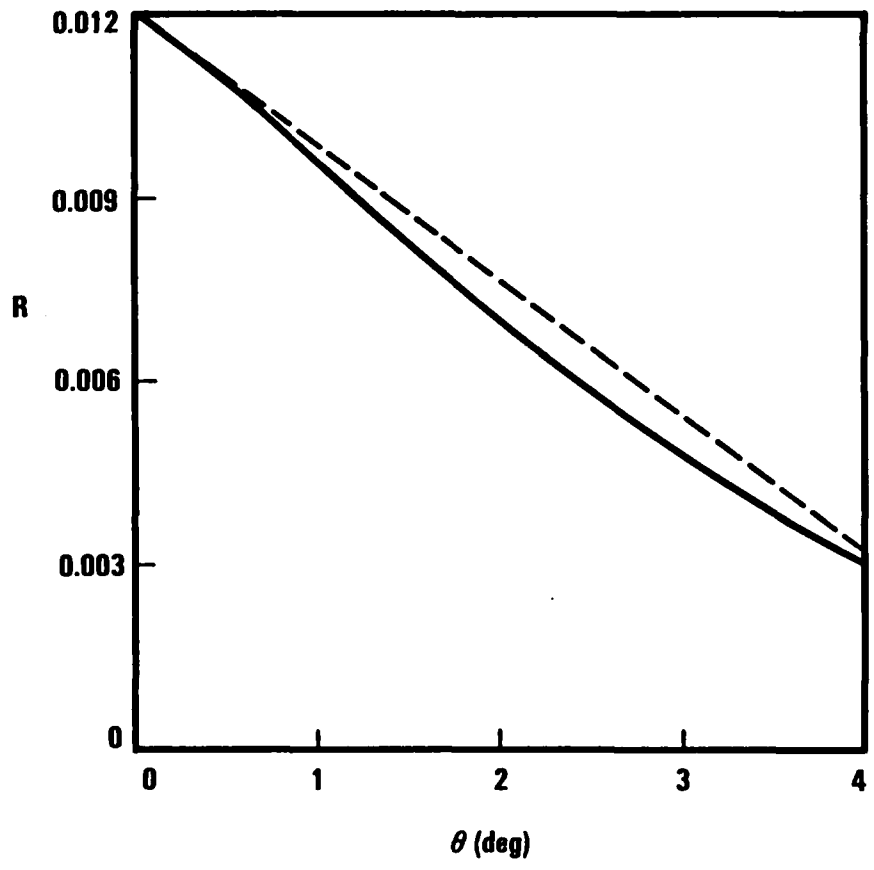

Figure 26. Angular dependence of reflectivity in FWM shown in simulation (solid curve) and calculation from beam overlapping (dotted curve)

available. For demonstration, the intensity and the phase of an aberrated probe beam are shown in Figure 27. The aberration represents a Strehl ratio of 0.77. The beam interacts with two good quality pump beams in the CS_2 medium. The intensity and the phase of the reflected beam after passing through the aberrator again are shown in Figure 28. The intensity profile is found to rise toward the trailing edge. This effect can be understood since the FWM energy transfer efficiency is proportional to the square root of the intensity product $(I_1I_2I_3I_4)^{1/2}$. Since $(I_1 + I_3)$ and $(I_2 + I_4)$ are constants of the interaction, the intensity product will become higher as I_3 and I_4 increase. Therefore, the energy transfer is more efficient near the end of the pulse. The phase of the output field is uniform in most of the area. The correction of the aberration is nearly complete and the final Strehl ratio is calculated to be 0.997.

The code is also used to demonstrate high reflectivities and the saturation effect. Figure 29 shows the theoretical prediction (solid curve) based on the constant pump approximation, and the simulation results (dots). It is demonstrated that high reflectivity can be obtained in the SPFWM effect. However, the output beam quality begin to degrade when saturation occurs. For η = 5, where the saturation is first observed, the output fields with square and gaussian input pulses are shown in Figure 30 and 31, respectively. The intensity profiles are rich in structure and peak near the end of the pulse. The Strehl ratio of the reflected beam is found to be 0.84 and the energy transfer efficiency is 9.4 percent at a reflectivity of 800.

3.5 FOUR-WAVE STIMULATED BRILLOUIN SCATTERING

The concept of using four wave mixing in a RF linac FEL resonator was found to be useful in outcoupling the high power beam that is the phase conjugate of a suitable weak probe signal. However, it was found impractical for FWM to be used for the induction linac FEL device due to the following reasons: First, although the FWM process requires two counterpropagating pump beams, there is only one high power output beam available. Second, the energy transfer efficiency in FWM is low, which is acceptable in a resonator because the remaining energy will continue to circulate. For the induction linac FEL, the non-transferred part of the

Four-Wave Mixing
Input Probe Pulse

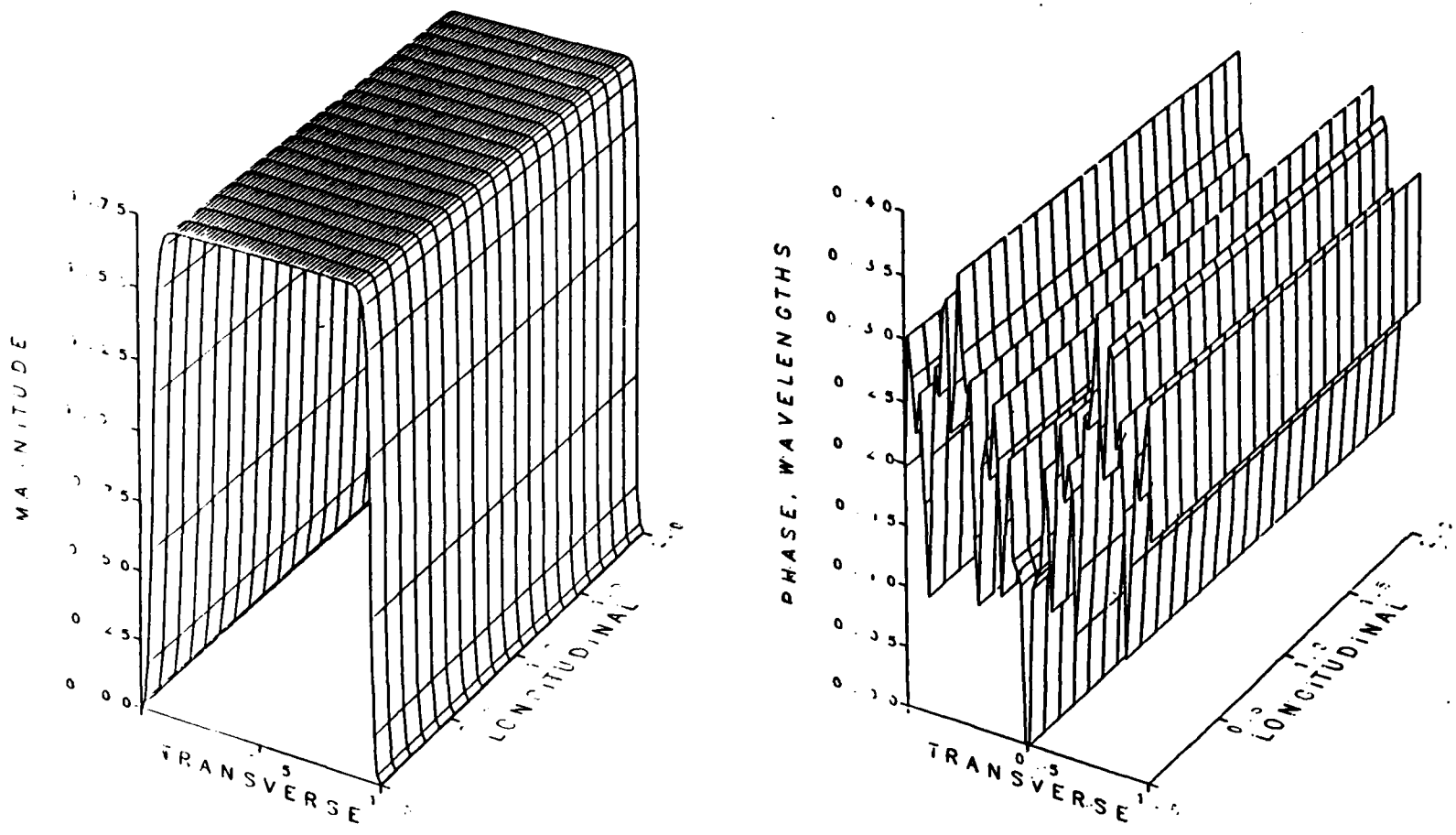

Figure 27. The intensity and phase of an aberrated probe beam

Four-Wave Mixing
Output Conjugated Pulse After Aberrator

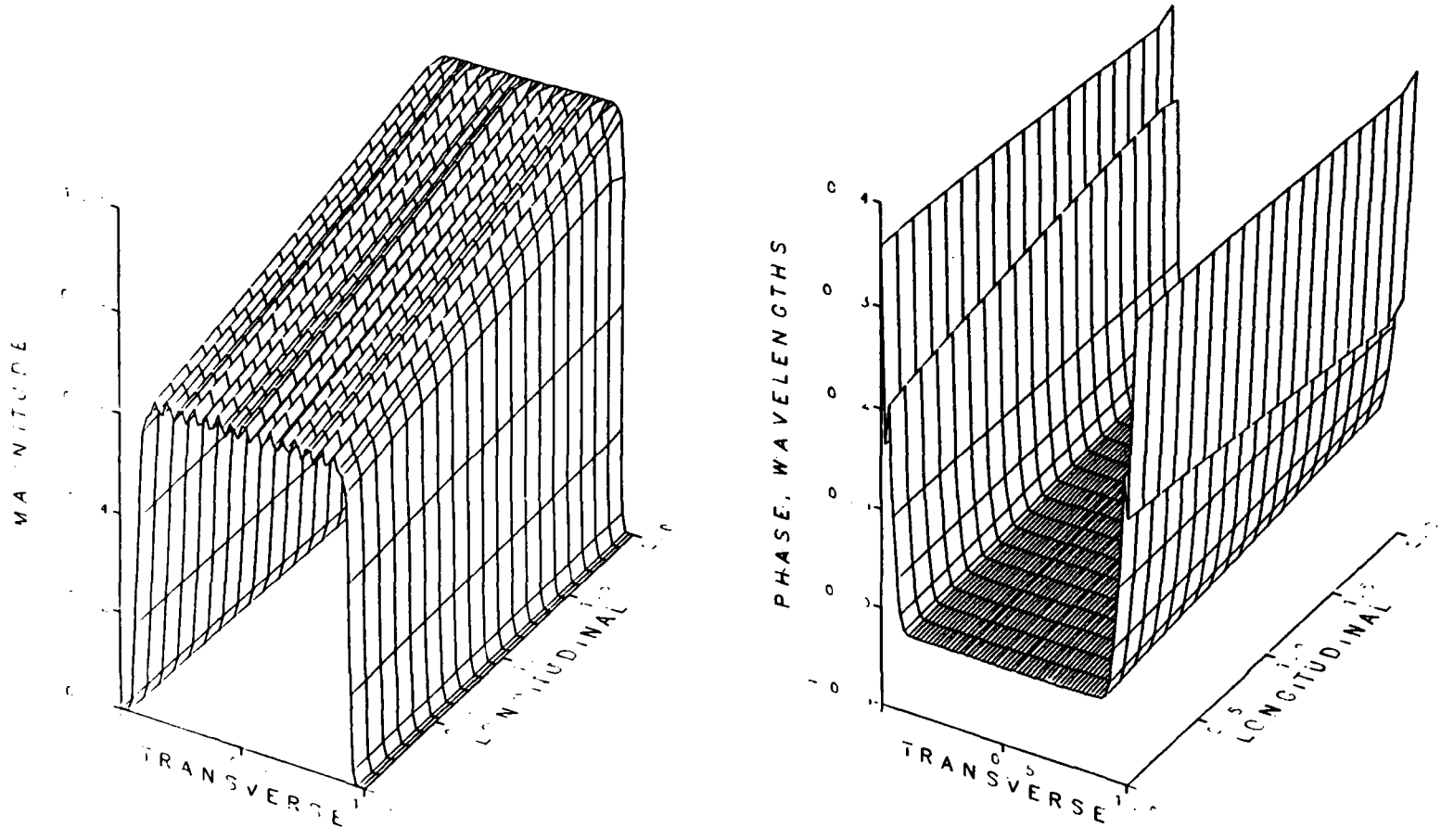

Figure 28. The intensity and phase of the conjugated and corrected beam using the aberrated probe beam shown in Figure 27

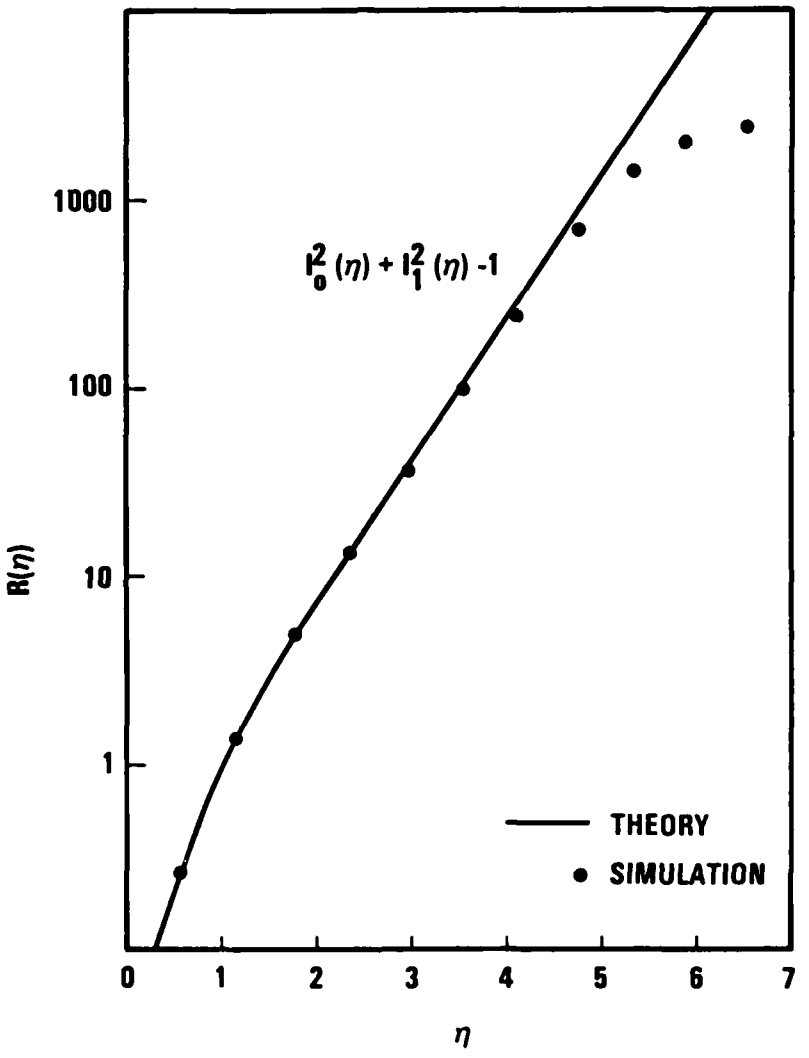

Figure 29. The saturation effect observed in simulation (dots) compared to the result from the non-depletion theory (solid curve)

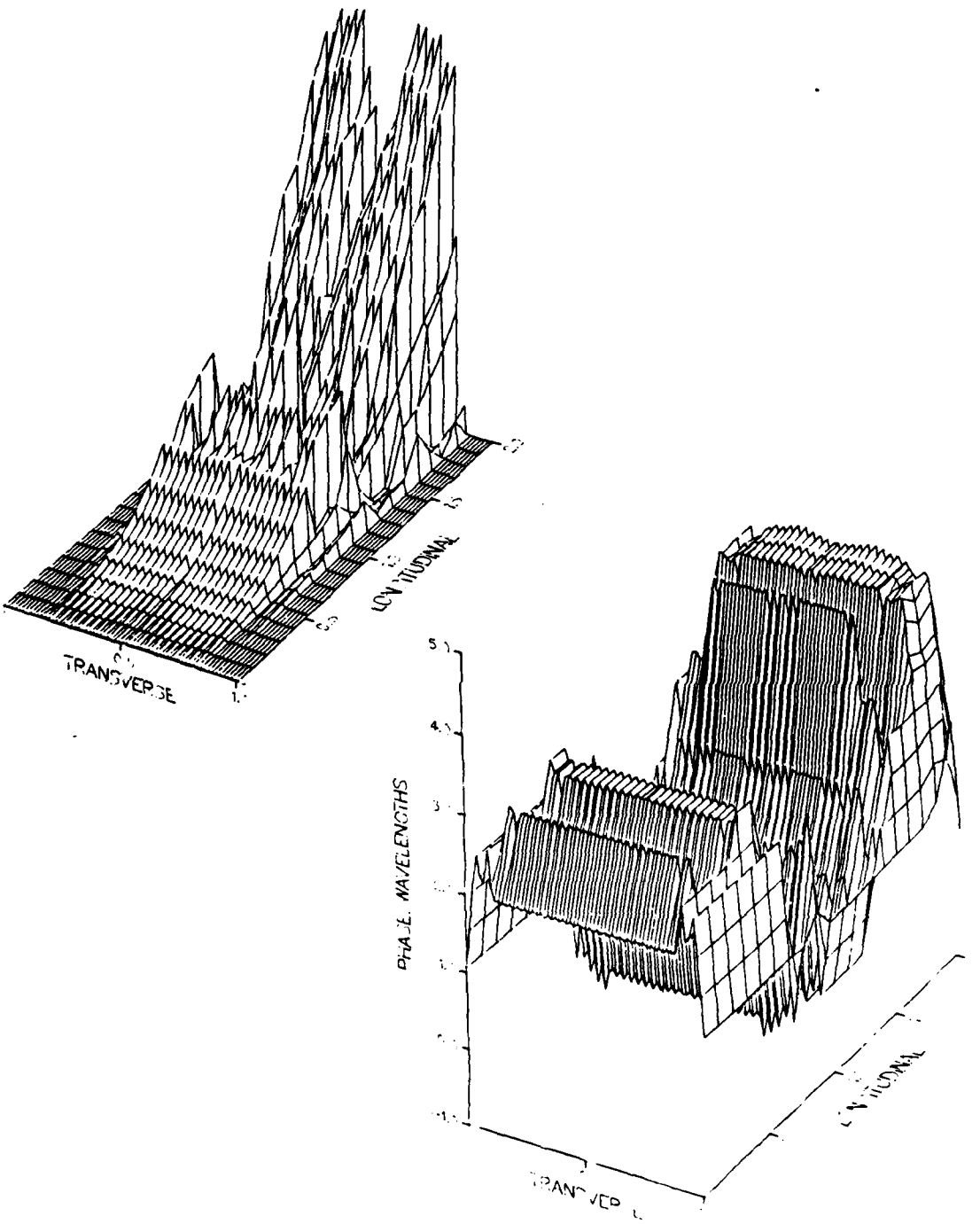

Figure 30. The intensity and phase of the reflected purlse at η = 5 for a square input pulse

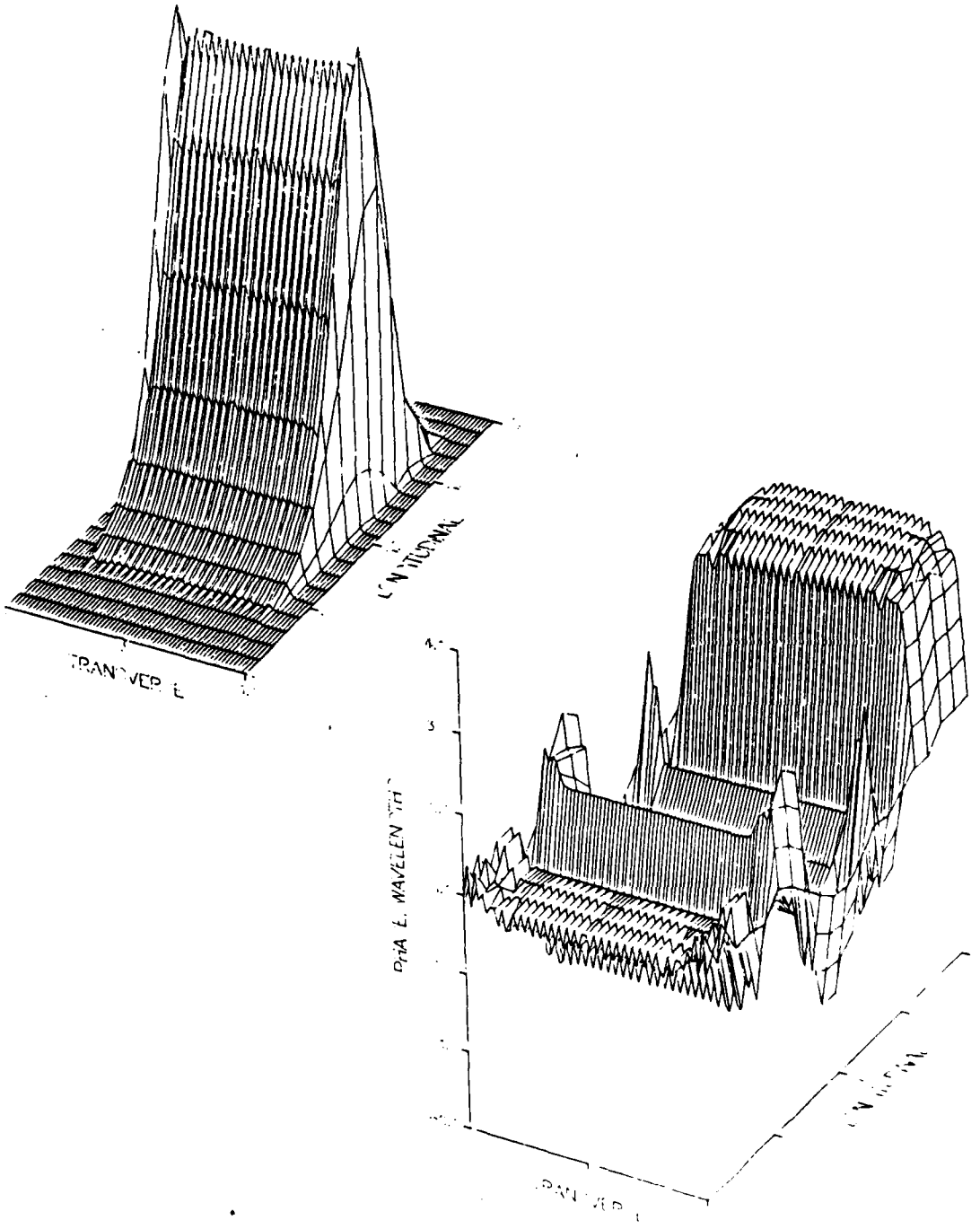

Figure 31. The intensity and phase of the reflected pulse at $\eta = 5$ for a gaussian input pulse

beam energy would be lost. For successful induction linac FEL applications, a nonlinear process must have the properties of high reflectivity, high efficiency and require only a single high power beam. We have found a new nonlinear optics concept that meets these requirements. The new process, called FWSBS, was shown to be extremely efficient in converting the high power beam into the phase conjugate of a selected weak probe beam[23,36]. Both theoretical and experimental studies have been carried out on this program.

3.5.1 FWSBS Theory

In the FWSBS process, two pump beams, one at high power and one at low power, and having the same frequency, ω, counterpropagate and meet in a SBS cell (Figure 32). The probe beam of frequency, $\omega + \Omega$, where Ω is the phonon frequency, is incident at a small angle with respect to the high power pump beam. The arrangement is similar to the ordinary nondegenerate FWM configuration. An acoustic grating is created initially by the SBS interaction between the probe beam and the weak pump beam. This grating is further enhanced by the stimulated scattering of the high power pump beam in the opposite direction of the probe beam. The scattered field is a conjugate of the probe signal.

No detailed theoretical study, especially concerning the saturation effect, can be found in the literature[37]. Since high reflectivity and high efficiency of FWSBS is of primary interest for the induction linac FEL applications, we have developed an analytical theory of FWSBS in this program. The detail of the theory is shown in Appendix B, which is a preprint of the paper submitted for publication.

In the theory, the steady-state coupled equations of the four waves were formulated and solved analytically. The coupled equations (7) show that there are two kinds of interactions responsible for the FWSBS effect. The four wave mixing through the phonon interaction generates the initial return field. The mixing process ensures that the return field is the conjugate of the probe signal. As the return field becomes sufficiently strong the SBS amplifying process will take over and saturate the return field. The reflectivity and the efficiency in the nonsturation and

Four-Wave Stimulated Brillouin Scattering

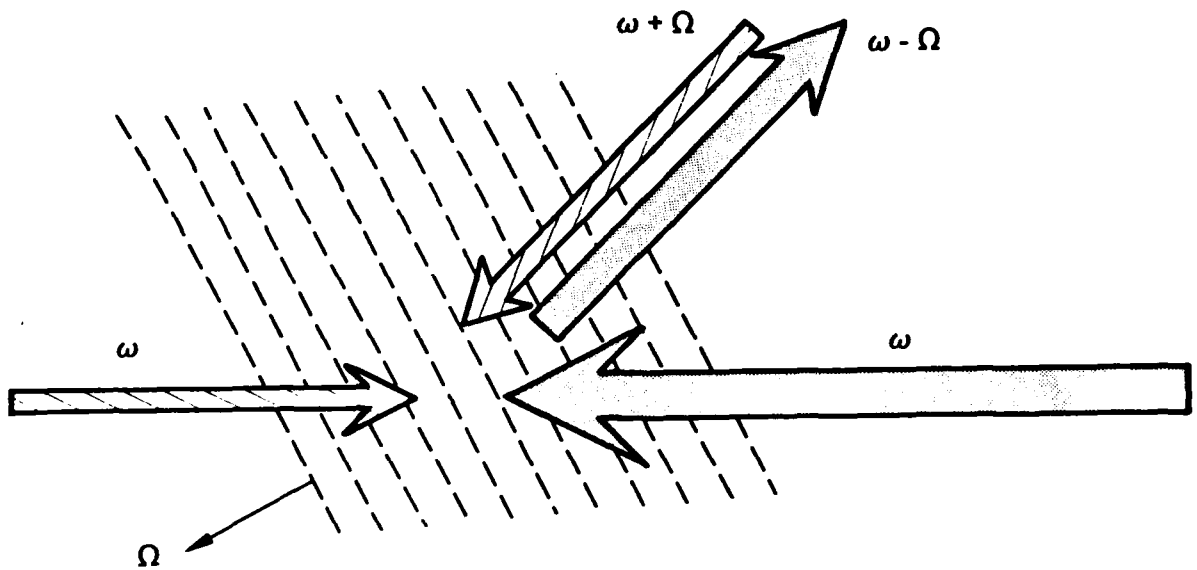

Figure 32. Schematic of four wave stimulated Brillouin scattering

saturation regimes were found to be given by the approximate expressions, which describe the dependence quite well, particularly when I_3 is less than I_2,

$$R = \frac{I_1}{I_2 + I_3} \tag{5.1-1}$$

$$\eta = \frac{I_3}{I_2 + I_3}, \tag{5.1-2}$$

where I_1, I_2, I_3 are the intensities of strong pump, weak pump and probe beam, respectively. With properly chosen input intensities, both the reflectivity and the efficiency can be very high. These relations are compared to the experimental observations. No simulation code has been developed for FWSBS in this program.

3.6 SYSTEM REQUIREMENTS

Based on the analytical results obtained in previous sections. System analysis were performed for an up-link FEL system. The system is either an RF linac FEL resonator with FWM outcoupling or an induction linac FEL device with FWSBS beam conversion. the power requirements of the pump beam and the beacon can be readily determined from the required reflectivity and efficiency. In general, the results show that both nonlinear optics approaches are capable of accomplishing the atmospheric compensation for the high power FEL system.

3.6.1 RF Linac FEL

A four wave mixer in an RF linac FEL resonator can be used to outcouple the energy and convert it into the phase conjugate of a beacon signal which interacts with the intracavity pump beams. The fraction of the pump energy that goes into the conjugated wave is defined as the efficiency of the FWM process. From the resonator optics, it also represents the outcoupling fraction. The interaction is assumed to take place in CS_2 or other media with comparable nonlinear optical coefficient.

In the sort-pulse FWM phenomenon, the reflectivity was found to depend on the pump pulse fluence. It has a quadratic dependence in the low fluence region and increases exponentially at high fluences (See Figure 2

and 3 in Appendix A). Although it is highly underrepresenting at high reflectivities, the quadratic dependence is used in our analysis for simplicity. Figure 33 shows the relations of beam energies for different outcoupling fractions. For example, assuming 10 percent outcoupling fraction and 2 J/cm^2 pump fluence, the required probe fluence should be 20 $\mu J/cm^2$ and the reflectivity is 10^4.

Figure 34 shows the system requirement for different linewidths, assuming 10 percent efficiency. The lowest curve is for the case of transform limited pulses that are 3 psec long. The corresponding linewidth is 0.1 percent at 1 μm wavelength. The curves move to higher pump fluences with increasing linewidths. Therefore, the effect of wider linewidth can be compensated by higher pump fluence in order to have the same efficiency. However, the reflectivity in this case is increased by the same factor.

3.6.2 Induction Linac FEL

The FWSBS interaction in an SBS cell can be used to convert the output beam from an induction linac FEL into a high power conjugate beam of a beacon signal. This is a high reflectivity and high efficiency process. If the power ratio of the two pump beams is sufficiently large, both reflectivity and efficiency are medium-independent quantities and are determined from the beam intensities only. Thus it is convenient to express the requirements in terms of intensity ratios (Figure 35). The relations were based on the approximate formulas in Equations (5.1-1) and (5.1-2). In general, the reflectivity can be very high depending on the pump intensity ratio. Efficiency near 50 percent should be easy to obtain if the probe intensity is close to the backward pump intensity. However, efficiency higher than 90 percent may be difficult because of the fast increase in the requirements of the probe intensity.

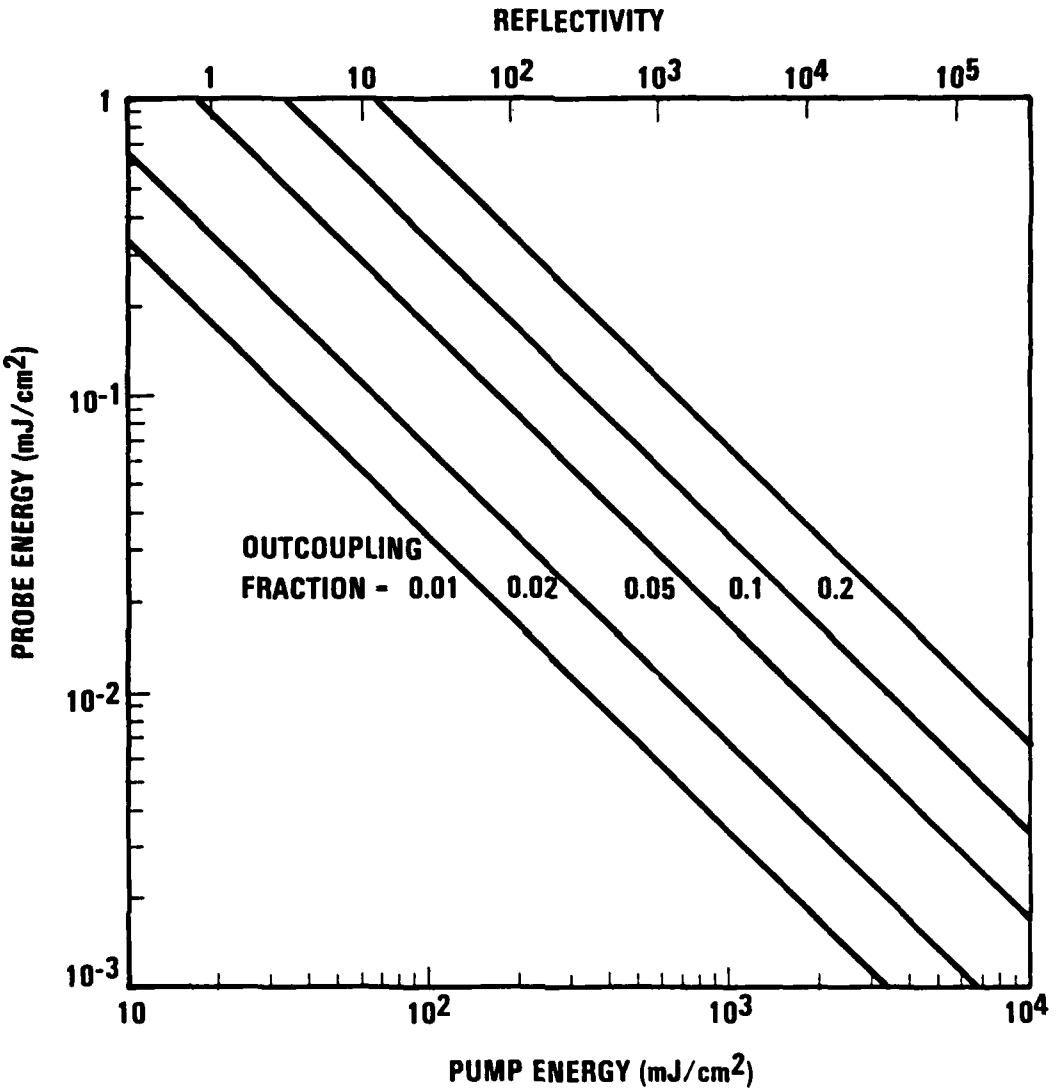

Figure 33. System requirements at different efficiencies for an RF linac FEL using the FWM outcoupling

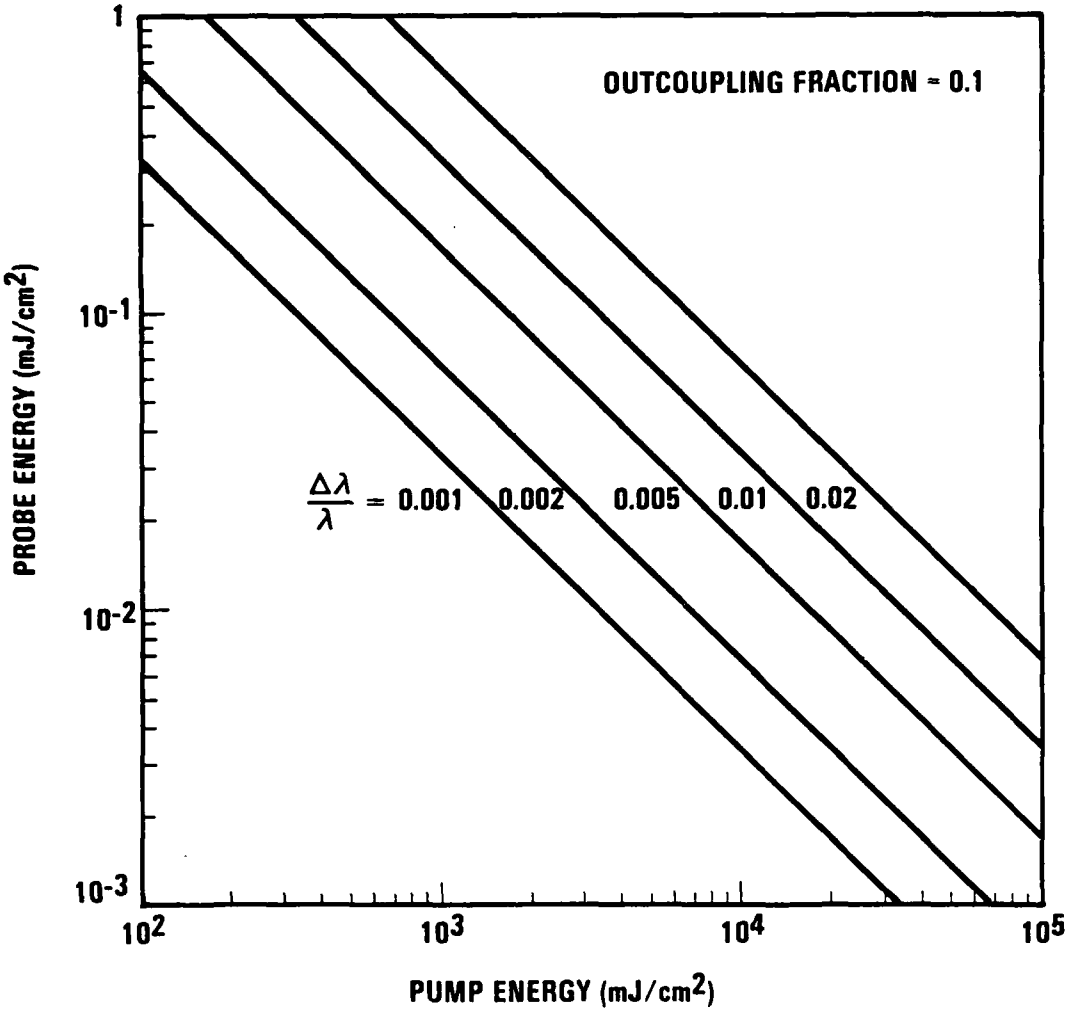

Figure 34. System requiremetns at different linewidths for an RF linac FEL using the FWM outcoupling scheme

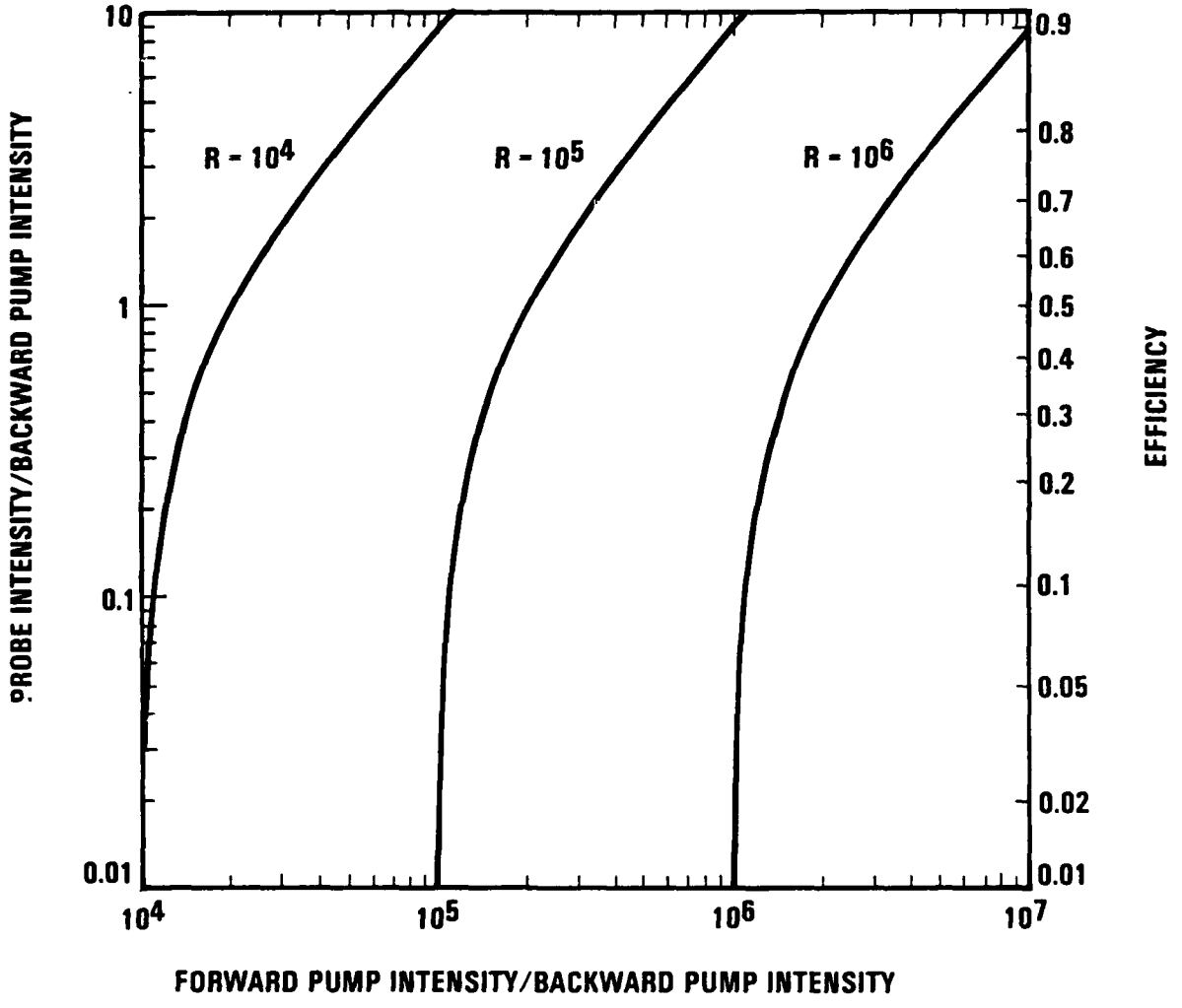

Figure 35. System requiremetns for an induction linac FEL using the FWSBS beam conversion scheme

IV. EXPERIMENTS

In the experimental portion of the program, experiments were performed to establish the viability of phase conjugators in FEL system configurations. Two four wave mixing phase conjugators were investigated. Liquid carbon disulfide was used to phase conjugate RF linac FEL-like short pulses to establish the scaling of reflectivity with pump intensity. Linear scaling of reflectivity up to 60% was observed for pump pulse fluence up to 15 mJ/cm^2. In the second series of experiments, SBS enhanced four wave mixing in acetone was used to phase conjugate induction linac FEL-like pulses to obtain reflectivities as high as 100 000% and 16% conversion efficiency. Both of these techniques show promise for the production of atmospheric aberration compensated high power beams in response to weak satellite beacons as described in Chapter II.

This chapter consists of four sections. The first two describe how the two system concepts were studied experimentally, and how closely aspects of the experiments bear on those concepts. The two remaining sections describe the four wave mixing (FWM) experiments in detail. The first section describes the short pulse four wave mixing experiments which used a doubled mode-locked Q-switched Nd:YAG laser source. Time averaged and time resolved reflectivity measurements are presented and analyzed. The second section describes the SBS enhanced four wave mixing (FWSBS) experiments, a type of non-degenerate four wave mixing, using Brillouin shifted pump beams. Measurements of reflectivity variation with probe, forward and backward pump beam intensities are presented.

4.1 EXPERIMENTAL OBJECTIVES

The objectives of the experiments were to evaluate the performance of high reflectivity/high efficiency phase conjugating mirrors used in FEL system concepts. Two types of four wave mixing phase conjugators were proposed in system concepts. In one concept, an extracavity phase conjugator is used to convert a high power pump beam supplied by an induction linac FEL into the phase conjugate of a weak beacon beam. High conversion efficiency is needed to avoid spoiling the overall system efficiency. In the second concept, an intracavity four wave phase conjugator is used to

outcouple an RF linac FEL, as well as provide compensation of atmospheric aberrations. Here, the conversion efficiency can be relaxed to the desired outcoupling, usually around 10% for high power RF linac FELs. Hence, an experimental objective was to measure efficiency.

Our primary objective was to measure reflectivity scaling to anchor calculations of phase conjugate mirror reflectivities for high power FELs. In both system concepts, a weak beacon propagates through the atmosphere to the phase conjugating mirror, where the beam is time reversed with enormous gain.

4.2 EXPERIMENTAL APPROACH

The applicability of the experimental results derives from essential similarities between the FELs and our FEL simulators. For example, our experiments were performed in similar time regimes at similar wavelengths. However, the laser powers were much lower, and the linewidths much narrower than the FEL's. We sought to establish scaling relationships in power to predict performance at high powers. Also, our experiments did not facilitate investigation of the effect of large FEL bandwidth on the four wave mixers. Although attempts were made to expand the bandwidth of the mode-locked laser using self phase modulation, no significant broadening was achieved. Also, in attempts to emulate the induction linac FEL a second, relatively broad bandwidth laser source would not yield four wave mixing. (At the available power levels, narrow bandwidth pulses were necessary to achieve four wave mixing. Theoretically, increases in power can compensate for increase in bandwidth). Hence, the scope of the four wave mixing experiments was limited to the determination of reflectivity and efficiency scaling with pump and probe beam intensity variation.

4.2.1 RF Linac FEL Phase Conjugator Experiments

To investigate the RF linac FEL intra-cavity phase conjugator, short pulse degenerate four wave mixing (DFWM) experiments were performed in a carbon disulfide; a fast Kerr-like medium. A mode-locked laser was used to produce a train of 25 ps pulses at 532 nm to simulate the optical pulse trains circulating inside the RF-linac FEL cavity. We chose to use CS_2 for the experiments because it is a Kerr-like medium a class which includes

other scalable, transparent, damage resistant candidates for high power devices, including liquids and plasmas.

The short pulse DFWM experiments essentially replicate the geometry of the RF linac FEL intracavity four wave mixer. In the experiments, the three applied pulses are produced by a mode-locked laser. Note that in the system concept, the probe beam need not be a short pulse. A longer probe pulse would relax the difficult timing requirements set by the low duty cycle of the pump beams ($\sim 10^{-3}$).

The FEL simulator for the short pulse (degenerate) four wave mixing experiments was a Q-switched, mode-locked doubled Nd:YAG laser. Table 7 compares the intracavity FEL pulses to the FEL simulator output. Figure 36 shows a schematic of the simulator output defining several time constants listed in the table. The laser emits a burst of pulses every 100 ms. Each burst consists of approximately 12 pulses with energies distributed under a Gaussian envelope. The pulses have an average duration, of 25 ps. (The uniformity of the pulse duration over the burst is discussed in section 4.3.3).

Table 7 shows that the performance of the mode-locked laser is similar to an RF linac FEL in many respects, including the pulse peak power, energy per pulse, pulse width, pulse spacing and wavelength. The pulse energy of 5 mJ compares favorably with the minimum FEL pulse energy of 10 mJ; however, it must be borne in mind that the FEL pulse energy inside the cavity is about ten times as great, and that the pump pulse supplied to the four wave mixer is reduced by a factor of four by losses in the optical train and division of the pulse into two pump pulse. Also, note that because a fast medium is used in the experiment, with a picosecond response time, the temporal profile of the pulse train is not important. The medium responds to each pulsed interaction as a separate event.

4.2.2 Induction Linac FEL Phase Conjugator Experiments

To indicate the potential for the application of a four wave stimulated Brillouin scattering (FWSBS) phase conjugator to an induction linac FEL, Table 8 compares the nominal characteristics of the (induction linac) FEL simulator with the FEL. The "demonstration requirements" use

Table 7. FEL System Performance and Current Simulator Capabilities

Parameter	FEL	Quantel 501
power	1-10 MW	620 kW [1,3]
peak power	1 GW	210 MW [1]
energy/pulse	10-100 mJ	5.2 mJ [1]
pulse width	10-100 ps	25 ps [2]
pulse spacing	2-10 ns	7.1 ns [1]
wavelength	Visible	532 nm [1]
bandwidth	0.5 - 1.0%	<0.04% [1]

Notes

1. Measured
2. Manufacturer's specification
3. Averaged over the 6 most energetic pulses

Table 8. Nominal Laser Characteristics for FWSBS

Demonstration Requirement	Does the Induction linac FEL Capability meet the demonstration requirement?
Pulse Duration, $>$ 15 ns	Yes
Peak Power $>$ 2 MW	Yes
Beam Quality $<$ 1.04	Yes
Wavelength $\simeq$ 1.06 μm	Yes
Relative Bandwidth, $\Delta\nu/\nu < 2 \times 10^{-7}$	No

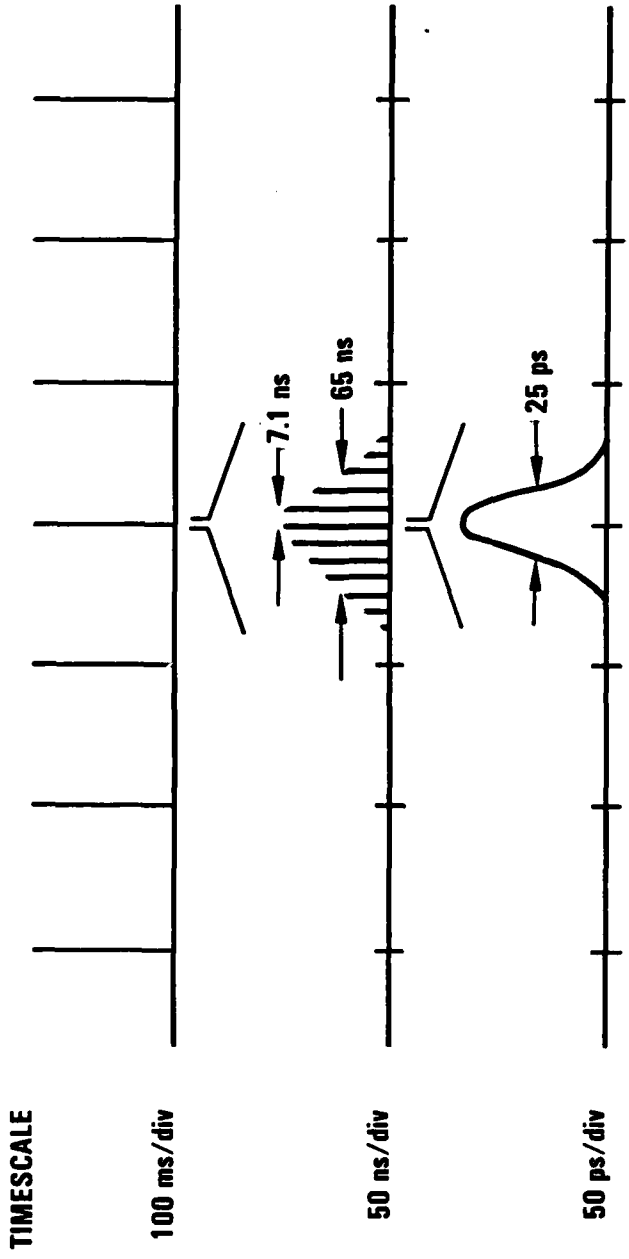

Figure 36. Temporal structure of mode-locked, Q-switched Nd:YAG laser.

the FEL simulator characteristics as the minimum requirements for FWSBS. For this type of four wave mixing, the FEL characteristics equal or exceed those of the simulator, with the exception of linewidth. As was the case for the DFWM experiments, reflectivity scaling with power may compensate for the much larger linewidth.

As mentioned previously, FWSBS is a nondegenerate type of four wave mixing that requires a small frequency difference between the pump and probe pulses. In our experiment, we obtained this shift by using a Brillouin scattered pulse for the pump. However, an actual FEL implementation of a FWSBS phase conjugator would not pre-shift the pump beam wavelength as we did in our experiment. Instead, the small wavelength difference between the pump beams and the probe beam necessary for SBS enhancement can be obtained by design of the FEL and the beacon. This avoids the losses of an additional SBS cell in the FEL pump beam.

The FWSBS investigation consisted of several reflectivity measurements and an experiment which optimized the pump beam conversion efficiency. The variations are shown in the test matrix presented in Table 9. For each matrix entry, reflectivity was measured as the probe beam intensity was varied over four orders of magnitude. This data was used to study the dependence of the reflectivity on I_3, I_1 and I_2/I_1 where I_1, I_2 and I_3 are the forward pump, backward pump and probe beam intensities. In addition to these experiments, an experiment in which the pumped volume was enclosed by the probe beam was performed to maximize the pump energy extraction.

Table 9. FWSBS Test Matrix

I_2/I_1 I_1	4%	1%	0.048%
46 MW/cm^2	X		
80 MW/cm^2	X	X	X

4.3 SHORT PULSE DFWM EXPERIMENTS

This section describes the degenerate four wave mixing experiments using green picosecond pulses in carbon disulfide that were performed to study phase conjugation reflectivity scaling with pump pulse fluence. The experiments showed a power law dependence of reflectivity on pump pulse fluence, with reflectivities ranging up to 60% for pump pulse fluences up to 15 mJ/cm^2. Fluence was predicted to be the correct scaling parameter, rather than intensity or energy, for short pulse four wave mixing in Appendix A.

A power law dependence was observed in both pulse train average and single pulse experiments. An active-passive mode-locked Nd:YAG laser oscillator and amplifier were used to produce a pulse train of about 12 pulses under a Gaussian envelope. Each pulse was split into pump and signal pulses and used in the four wave mixing geometry to obtain a phase conjugate reflection. In pulse average reflectivity experiments, the integrated pulse train reflectivity was measured with respect to the pulse train fluence. In the single pulse measurements, reflectivities were obtained from fast photodiode traces of the probe and phase conjugate reflection, with scaling by pulse train energy measurements.

4.3.1 Experimental Set-Up

The experimental set-up is shown in Figure 37. Bursts of short pulses are emitted at 10 Hz by the double mode-locked, Q-switched Nd:YAG laser (to be described in detail below). The pulses first pass through a polarizer and quarter wave plate which provide isolation to the laser. A 4% beamsplitter samples the pulses to form the probe beam while the pump pulse passes on to a spatial filter. This round-about path was chosen to allow the introduction of a self-phase modulator, (SPM), to increase the pump pulse bandwidth. Then, at BS, the pulse is split into two pulses which are made to cross paths at the four wave mixing cell (FWM). After the 4% beamsplitter, the probe beam is demagnified by a long focal length telescope, passed through a variable delay line, through a 50% beam sampler and on to an insertion mirror which steers the probe towards a "collision" with the pump pulses.

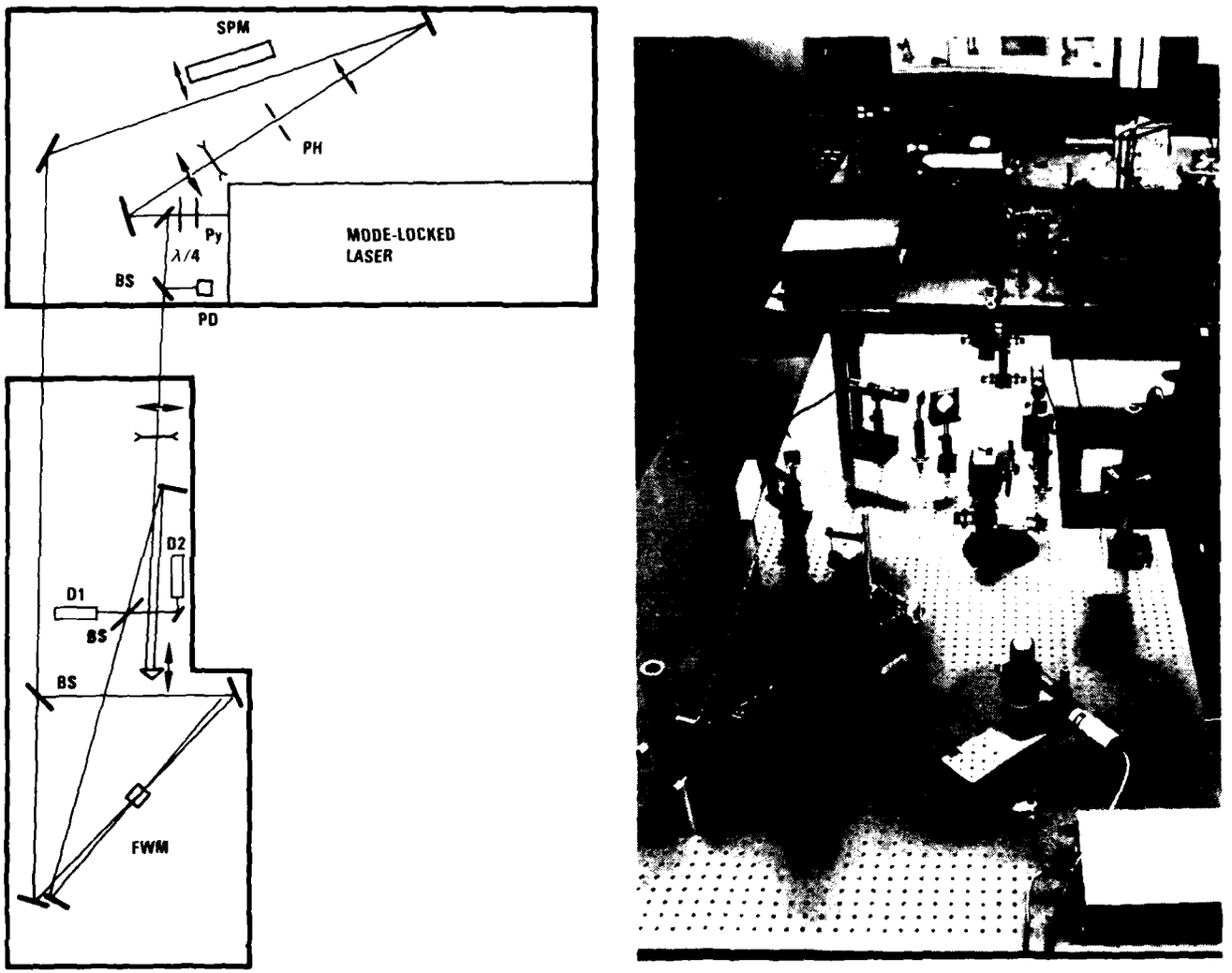

Figure 37. Short pulse DFWM set-up. P_y: vertical polarizer; BS: beam splitter; PH: pin hole; SPM: self-phase modulator; D1, D2: pyroelectric energy detectors; PD: photodiode; FWM: four wave mixing cell.

A mode-locked laser system, with peak powers as high as 1 GW, was used for these experiments. The system consists of a mode-locked Q-switched Nd:YAG oscillator and amplifier, followed by a second harmonic generator. As shown in Figure 36, the system emits trains of 10-12 short pulses (25 ps duration) at 10 Hz. The unit was modified by the removal of the standard pulse selector, so that the entire pulse train is output. The performance specification of our modified Quantel YG-501-10 are given in Table 10.

Table 10. Quantel YG 501-10 performance specifications

Parameter	Performance	Notes
repetition rate	10 Hz	
wavelength	532 nm	
beam diameter	7 mm	
polarization	vertical	
pulse train energy, E	2 mJ< E <25 mJ	Variable with amplifier flashlamp voltage
peak single pulse energy, E_p	12%	Photodiode trace analysis
pulses per mode locked train	10-12	
period between pulses	7.1 ns	
pulse duration	25 ps	Manufactures specification TPA measurement
pulse train stability	5%	
bandwidth	<2.5 A	Resolution limit of monochrometer
	>0.17 A	Transform limited linewidth

The pulse train energy is the total of the individual pulse energies in a train. The distribution of energy among the pulses was monitored by a photodiode. A typical photodiode signal is shown in Figure 40. The apparent fractional nanosecond width of the signal peaks is due to instrument broadening by the detector in combination with oscilloscope. In this

trace, the pulse energies may be inferred from the relative heights of the peaks. Typically, the peak pulse contains approximately 12% of the pulse train energy.

No rigorous measurements of the pulse duration or bandwidth were made. The manufacturer claims a pulse duration of 25 ps, which we corroborated qualitatively with a two photon fluorescence measurement of the fundamental 1.06 μm pulse width [40]. Limits on the bandwidth were established by the transform limit of 0.17Å, determined from the pulse duration, and instrument limited linewidth measurements of 2.5 Å. Also, a Michelson interferometer gave good fringe contrast over about 1 cm of path length difference, from which we estimate a bandwidth of about 0.27 Å.

An optical schematic of the laser system is shown in Figure 38 The oscillator is an active/passive mode-locked Nd:YAG laser [38,39]. Simultaneous mode-locking and Q-switching is caused by a cell containing a saturable absorber in the cavity. For this purpose, a flowing dye cell in contact with the rear mirror is used to circulate a solution of Kodak 9740 Q-switching dye in 1, 2 dichloroethane. In the presence of sufficient dye concentration, the laser mode-locks and Q-switches, resulting in a burst of pulses spaced by the cavity round trip time of 7.1 ns. With increasing dye concentration, the energy of the burst increases, fewer pulses occur in the burst and the pulse width is shortened, with the net effect of increasing the second harmonic generation. The mode-locking properties of the dye tend to decay over a few days, necessitating regular dye changes for energetic pulses.

The introduction of the acousto-optic mode-locker into the cavity has the effect of stabilizing the mode-locking. The pulse train energy stability was found to be approximately 5%.

The pulses were mixed in an 8 mm thick spectrophotometer cell containing spectroscopic grade carbon disulfide. The pump beams were made to focus at the cell by slightly defocussing the spatial filter, giving an elliptical spot of 1.05 mm x 1.31 mm. The probe beam was demagnified by about 3 and brought to focus at the cell using a 1 m lens (not shown), giving a spot size of 0.46 mm at the cell. The probe beam was introduced into the pump beam path at an angle of about 10 mr.

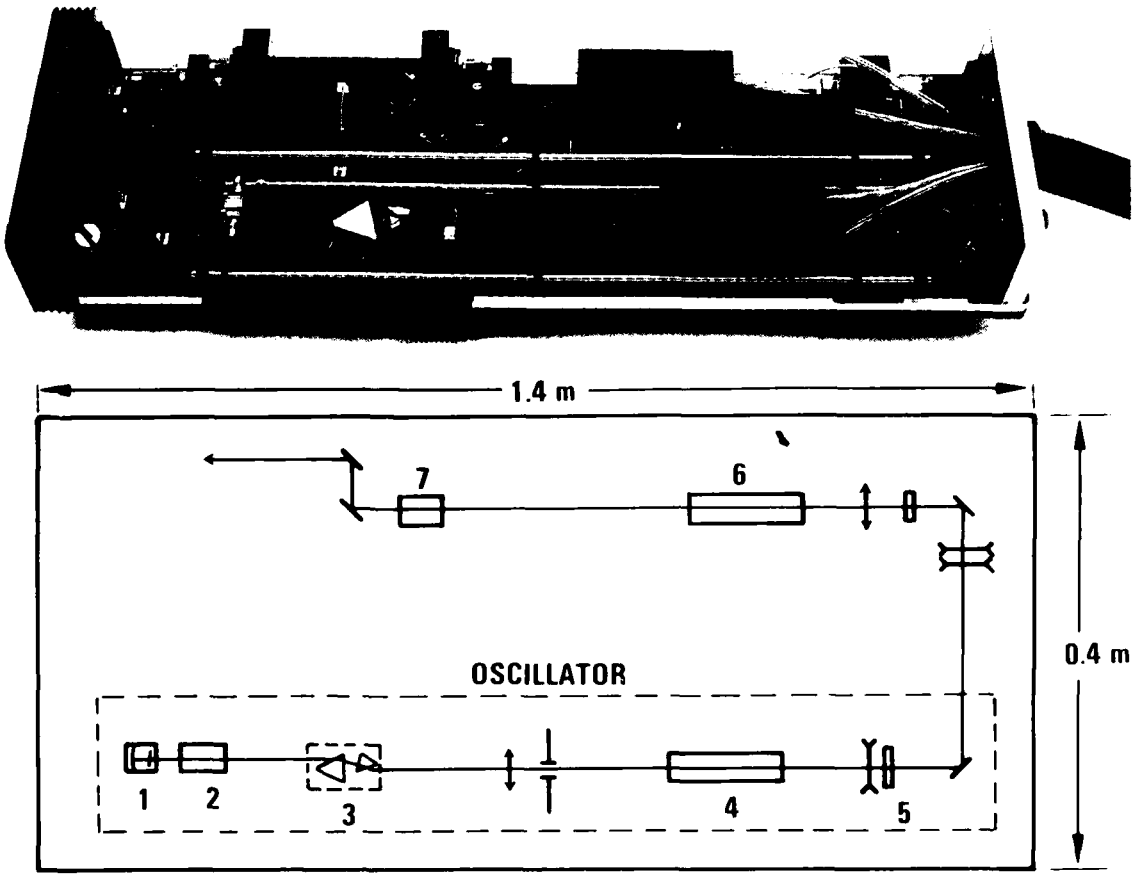

Figure 38. Quantel Mode-Locked Nd:YAG Laser System. 1: flowing dye cell; 2: acousto-optic mode-locker, 3: variable delay line; 4: Nd:YAG amplifier; 5: oscillator output coupler; 6: YAG amplifier; 7: second harmonic generator.

The coincidence of the three incident pulses was obtained interferometrically. First, to determine the location at which the pump pulses crossed, a front surface mirror was inserted at the approximate location of the crossing such that the two pulses were retroreflected. Then, using a beam sampler placed upbeam of the pump pulse splitting, the retro-reflected pump beams were projected onto a screen. When the front surface of the mirror located the pump crossing, interference fringes could be observed on the screen. Similarly, when properly timed, the inside edges of the forward pump and probe pulse could be made to interfere when the two beams were made nearly parallel. The timing of the probe pulse was adjusted using the right angle prism optical delay line.

Data was collected at the three positions occupied by PD, D1 and D2. The output from PD, a fast photodiode, was used to display the mode-locked pulse train on a 500 MHz bandwidth oscilloscrope (Tektronix 7844), as in Figure 40. Because oscilloscope traces at 10 ns/division are faint, visible film records of pulse trains required as many as 200 multiple sweep exposures. Detectors D1 and D2 were pyroelectric detectors (accessories to the Laser Precision Rj 7200 energy meter) used to measure probe and signal pulse train energies. To perform time resolved reflectivity measurements, D1 and D2 were replaced by fast photodiodes.

In order to measure the pulse energies, transmission factors with respect to the energy detector (the instrumentation is described below) D1 were measured. Since the probe and pump beams were both proportion to the laser output, a measurement at D1 gave all of the incident beam energies. In addition, because the probe beam energy was proportional to the pump beam energy, the efficiency of the four wave mixing process was proportional to the reflectivity.

In an effort to study the dependence of reflectivity on bandwidth, we attempted to modify the pump pulse bandwidth using self phase modulation [41]. As shown in the figure, the layout was designed to accommodate the insertion of a 20 cm cell of CS_2. Self phase modulation was evidenced by several experimental results, but was difficult to quantify as discussed below.

4.3.2 Time Averaged Reflectivity

Figure 39 shows a plot of probe pulse train reflectivity measurements versus pump pulse train energy. In the data, the pump pulse train energy refers to the sum of the pulse energies in one of the pump beams, $E_1 = \Sigma E_{1i}$, where the E_{1i} are individual pump pulse energies. The summation is performed by the pyroelectric detectors which cannot resolve the individual pulses in the pulse train. Similarly, the average reflectivity is given by $R = (\Sigma E_{4i})/(\Sigma E_{3i})$ where the E_{4i} and E_{3i} are individual signal and probe pulse energies, respectively. In the plot, the data is seen to have a powerlaw dependence on the pulse train energy, given by the slope of the line fit to the data, $R \alpha E^{1.3}$. Another notable feature of the data is the sharp drop in reflectivity at fluences in excess of about 200 mJ/cm^2. The drop may be caused by the onset of self-focusing in the CS_2, or the onset of self phase modulation in the Nd:YAG amplifier rod with high pulse intensities, broadening the pulse bandwidth.

For comparison, a plot of the theoretical reflectivity for negligible pump depletion is shown. The calculated pulse train reflectivity is calculated from $R_i = 1.8\ \eta_i^2$, where $\eta_i = 63 \cdot F_i$ (J/cm^2) (specific to CS_2) and F_i is the individual pump pulse fluence in units of J/cm^2. (See the following section for discussion of this expression.) The disagreement between the slope of the curves is probably due to the significant pump depletion at these probe intensities. Although the probe pulse energy was less than 5% of the pump pulse energy, the relatively small probe spot size gave the probe 27% of the pump pulse fluence. Certainly the peak pump pulses, with reflectivities in excess 65%, experienced significant ($> 17\%$) pump depletion.

4.3.3 Time Resolved Reflectivity

Time resolved reflectivity measurements were used to obtain single pulse reflectivity dependence on pump intensity. Typical time resolved reflectivity data is shown in Figure 40. Traces of the probe and phase conjugate signals were recorded simultaneously using photodiodes and a dual beam oscilloscope. The upper and lower traces correspond to the phase conjugate and probe signals, respectively. Notice that the envelope of the phase conjugate reflection rises and falls more sharply than the probe beam

AD-A168 950 APPLICATION OF NONLINEAR OPTICS TO FREE ELECTRON LASER SYSTEMS(U) TRW ELECTRONICS AND DEFENSE SECTOR REDONDO BEACH CA C SHIH ET AL. 06 JUN 86 N00014-84-C-0668 2/2

UNCLASSIFIED F/G 20/5 NL

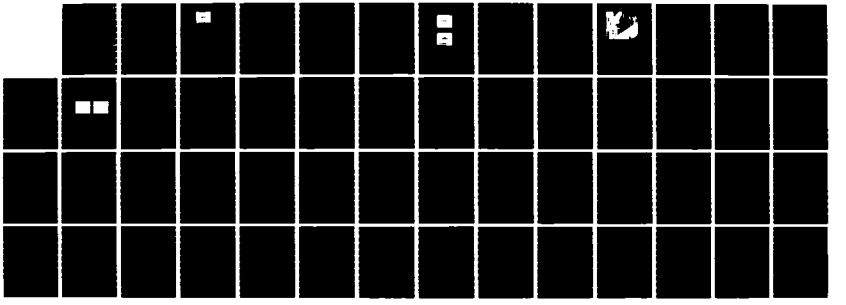

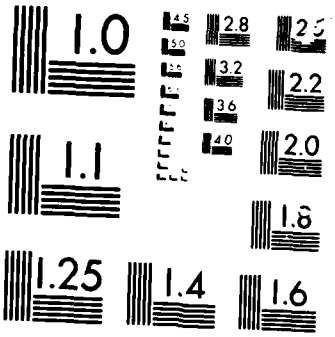
1.0
1.1
1.25
1.4
1.6
1.8
2.0
2.2
2.8
3.2
3.6
4.0
4.5
5.0

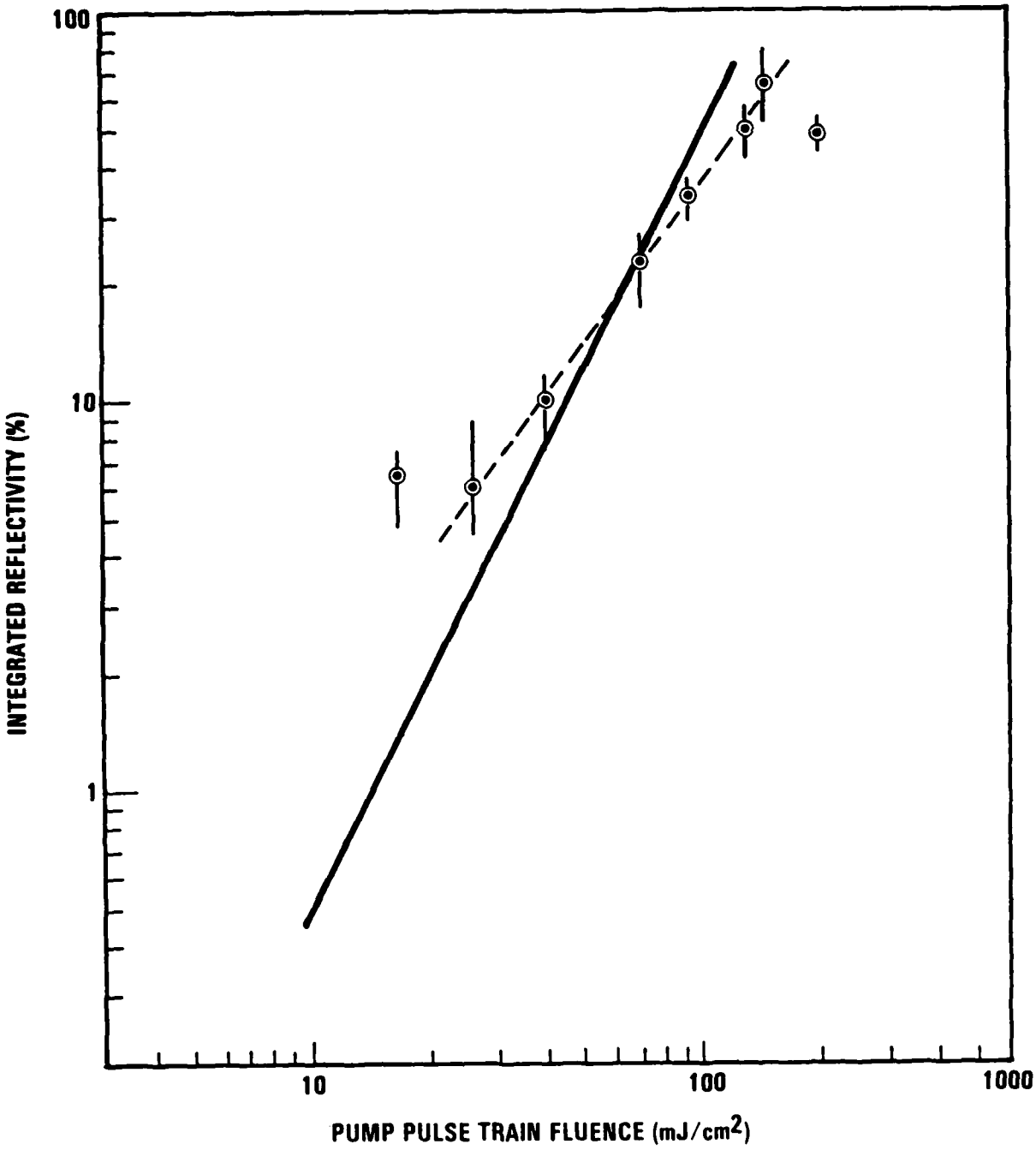

Figure 39. Time averaged reflectivity measurements.

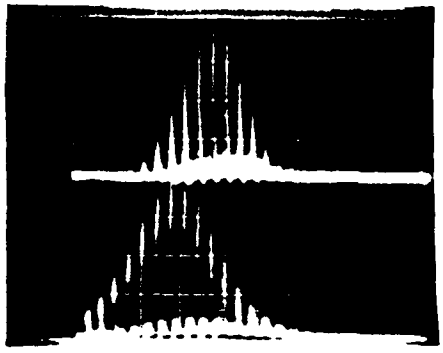

Figure 40. Typical time resolved reflectivity measurement. The upper trace corresponds to the phase conjugate reflection, the lower to the probe pulse train. (20 ns/division).

envelope, indicating a nonlinear reflectivity for pulses at the leading and trailing edges of the pulse train.

Figure 41 is a plot of individual pulse reflectivities as a function of pump pulse fluence. The numbers next to the data points refer to the pulse position in the pulse train, showing a rise to a peak reflectivity of 65% for the sixth pulse. The points are well fit by a straight line in the log-log plot, which has the nearly linear form $R \alpha F^{0.96}$. The four wave mixing efficiency for each reflection as given by the right hand vertical axis of the figure. Since the probe was proportional to the pump beam is these experiments, the efficiency, or fraction of pump energy transferred to the phase conjugate beam, was proportionate to the reflectivity. To take the small size of the probe beam into account, only the portion of the pump beam overlapping the probe beam was considered.

For comparison, the predicted reflectivity of a transform limited pulse in the non-depleted pump regime is shown. The theoretical curve is derived from the expression for the reflectivity given by eq. 17 of Appendix A. That expression considered the interaction of linearly polarized beams; the reflectivity must be increase by a factor of ~2 to discribe circularly polarized beams (as was the case in our experiment), as explained in Seciton 3.4.1. Hence, the dependence can be expressed as, R =

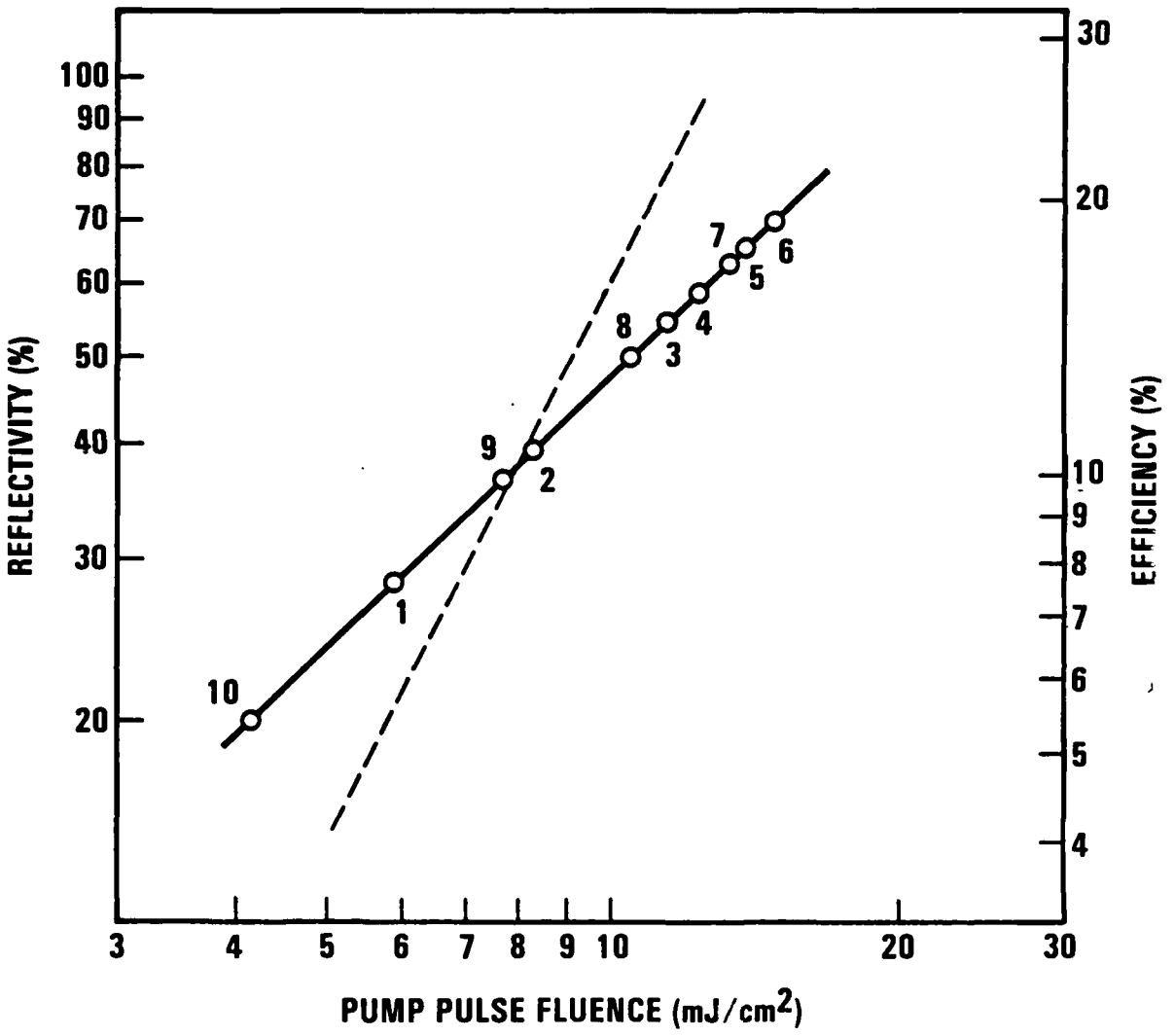

Figure 41. Time resolved reflectivity. The numbered points refer to pulse position in the pulse train. The dashed line represents the predicted reflectivity in the nondepletion regime. The efficiency gives the percentage of the pump beam overlapped by the probe that is transferred to the signal beam.

$1.8\ \eta^2$, where η is a parameter proportional to the nonlinear optical susceptibility and the pump fluence. Using the $\chi^{(3)}$ value of 2.025×10^{-31} in SI units for CS_2, η is about 63 times the pump fluence in units of (J/cm^2), as given in Equation (19) of Appendix A.

Although the experimentally measured reflectivity agrees with the theory for a pulse fluence of about 12 mJ/cm^2, the data does not show the predicted quadratic dependence of reflectivity on pump fluence. Two plausible explanations for the discrepancy are: (1) Pump beam depletion reduces the reflectivity or (2) the pulse bandwidth was proportional to pulse intensity, reducing the reflectivity to a linear dependence on fluence. With a peak conversion efficiency of 27%, pump depletion certainly affected the results. With respect to the second explanation, bandwidth modulation over pulse train produced by mode-locked Nd lasers has long been observed in passively mode-locked neodynium lasers [42,43] and recently measured in doubled active/passive mode-locked Nd:YAG laser system quite similar to ours by Nathel [44]. Nathel's simultaneous time resolved measurements of pulsewidth and bandwidth showed that both quantities vary significantly over the duration of the pulsetrain. Up to the peak pulse, the seventh in a train of 13 pulses, the pulse train exhibited a nearly constant pulse duration (about 30 ps), but has bandwidths that increased in proportion t the pulse energy. By the peak pulse, a four-fold increase in bandwidth over the first pulse has occured. After the peak pulse, the bandwidth stabilized with the accompaniment of a rapid decrease in the pulsewidth to just a few picoseconds.

Such evolving pulse characteristics may explain our results. According to predictions of the theory (see Appendix A), the reflectivity should be inversely proportional to the bandwidth. With bandwidth proportional to the pulse energy and therefore fluence, the pulsetrain reflectivities are expected to be linear in pulse fluence. Pulse reflectivities after the peak may be degraded as the error in the pulse timing becomes increasingly significant with respect to the pulsewidth.

4.3.4 Bandwidth Effects on Reflectivity

Experiments investigating the bandwidth dependence of short pulse DFWM were performed, but difficult to quantify with our limited bandwidth

resolution capabilities. However, two indications of our success in achieving nominal bandwidth expansion were observable effects on the time resolved reflectivity measurements and a narrowing of the four wave mixing reflectivity versus probe delay characteristic.

We attempted to use self phase modulation (SPM) to control pulse bandwidth. Self phase modulation, (SPM), the process responsible for the dynamic bandwidth modulation in mode-locked neodymium lasers, occurs when an intense transient pulse propagates through a medium with non-linear refractive index n_2, such as Nd:YAG ($n_2 \simeq 4 \times 10^{-13}$ esu) or CS_2 ($n_2 \simeq 1 \times 10^{-11}$ esu) [45]. The dependence of the index of refraction on the pulse intensity causes portions of the pulse to propagate with differing phase velocities. For $n_2 > 0$ (as in CS_2), this has the effect of red-shifting the leading edge of the pulse and blue-shifting the trailing edge, giving the pulse a frequency sweep or "chirp." We performed experiments with a 20 cm cell of CS_2 introduced into the path of the pump beam to investigate the properties of DFWM with an SPM-broadened pump pulse and relatively narrowband probe pulse. However, because we could not broaden the pump pulses beyond the resolution limits of our monochrometer (2.5Å), we were not able to quantify bandwidth dependence.

The effects of the SPM are demonstrated by the time resolved reflectivity oscillograms shown in Figure 42. The figure compares the phase conjugate signal (upper trace) for pump pulses in and out of the regime of significant self phase modulation. In (a) and (b) the intensity of the peak pulse at the SPM was about 310 MW/cm^2 and 470 MW/cm^2, respectively. In (b), SPM broadening of the peak pump pulses causes the suppression of the phase conjugate signal.

The broadening of the pump pulse bandwidth by the SPM is also evident is measurements of the reflectivity with probe delay. Leading and trailing edges of the pump beam which have been frequency shifted by the SPM destroy the degeneracy of the four wave mixing and spoil the reflectivity. Figure 43 shows measurements of the reflectivity with probe pulse delay, with and without the self phase modulated pump pulses. The characteristics have widths of 25 and 19 ps, for measurements with and without the self phase modulator, respectively.

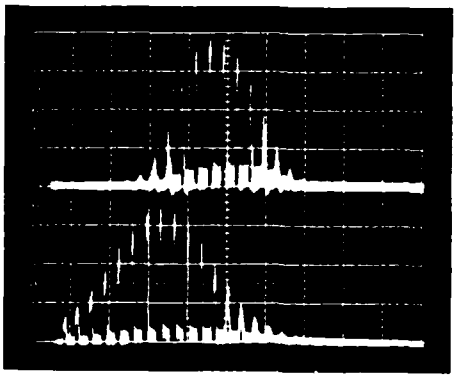

(a)

Conjugate return beam

probe beam

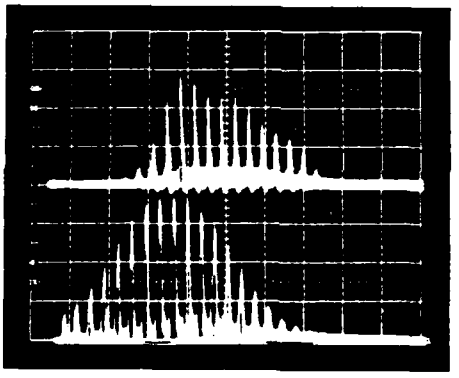

(b)

Conjugate return beam

probe beam

Figure 42. Effect of self phase modulation on time resolved reflectivity measurements. The two oscillograms show time resolved reflectivity measurement with the self phase modulator in the pump beam path. In (a), the peak pulse intensity at the SPM reaches about 310 MW/cm^2 and in (b) 470 MW/cm^2. At the higher pump pulse intensities (b), the broadening becomes significant, and the reflectivity is reduced.

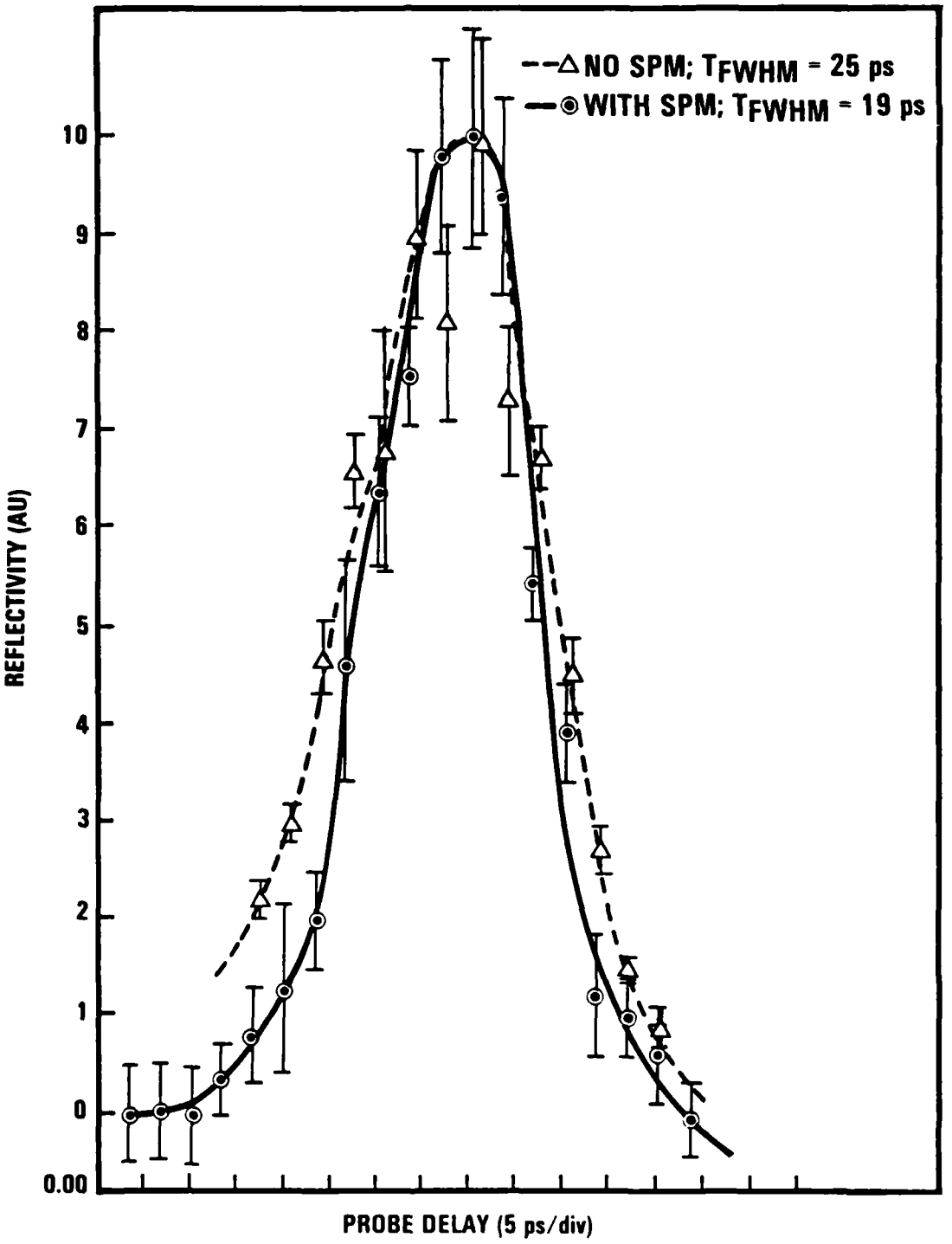

Figure 43. Reflectivity versus probe pulse delay with and without the self phase modulator.

4.3.5 Conclusion

In the short pulse DFWM experiments, we were able to observe phase conjugate reflectivities as high as 65%, the highest value ever observed for short pulse DFWM as far as we know (compare Reference 48), and an efficiency as high as 27%. The observed scaling of reflectivity with pump pulse fluence did not obey the quadratic scaling law predicted by the theory, but this discrepancy is most likely due to variations in the pulse bandwidth in the course of our experiments.

The difficulty imposed by the bandwidth variation over the pulse train can be remedied by the use of a single pulse selector. By selecting the same pulse from each pulsetrain, fixed bandwidth experiments could be performed.

Bandwidth control might be achievable using schemes other than self-phase modulation. One possibility would be to broaden single pulses by propagation through long single mode fibers followed by a relatively broad-band Nd:glass amplifier. The use of optical fibers to introduce chirp into short pulses is part of a widely used technique for pulse compression. Another approach might be to use the doubled output of the mode-locked laser system to synchronously pump a dye laser with intra-cavity bandwidth tuning elements.

4.4 FOUR WAVE STIMULATED BRILLOUIN SCATTERING

This section describes and analyzes the Four Wave Stimulated Brillouin Scattering (FWSBS) experiments which produced reflectivities as high as 100,000% and efficiencies as high as 16%. First, the experimental set-up and its characteristics are described, followed by presentations of reflectivity and efficiency measurements. Reflectivity measurements with varying forward pump, backward pump and probe intensities are presented and compared to simple theoretical predictions. The results of an extraction efficiency experiment are presented and compared to a simple theoretical prediction.

4.4.1 Experimental Set-Up

The experiment was arranged as shown in Figure 44. A Q-switched Nd:YAG laser system (described in detail below) produced a 12 ns pulse

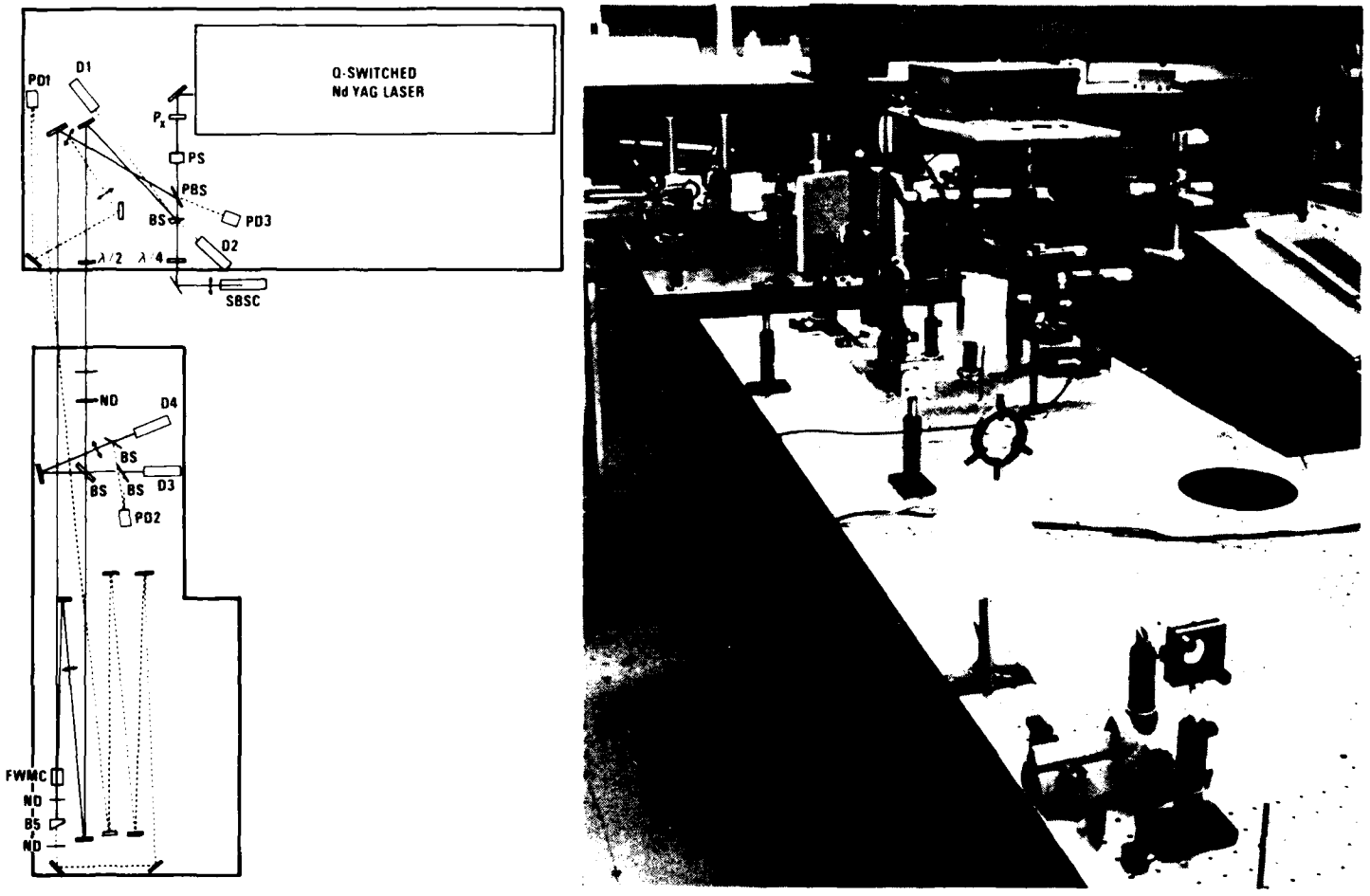

Figure 44. Four-wave SBS set-up. The solid lenes represent the optical paths of the pump, probe and signal beams. The dashed lines reprecent beam samples. P_X: x polarizer; PS: pulse selector; PBS polarizing beam splitter; D1, D2, D3, D4: pyroelectric energy detectors; PD1, PD2, PD3: photodiode detectors; SBSC: stimulated Brillouin scattering cell; BS: beam sampler; ND: neutral density filter; FWMC: four wave mixing cell.

which was first sampled at BS to produce the probe beam and then back-scattered by the acetone SBS cell (SBSC) to form the strong forward pump beam. The pump beam polarization was turned 90° by two passes through a quarter wave plate and reflected out of the retrobeam path by the polarizing beamsplitter (PBS). The strong pump is then focused by a 3 m focal length meniscus lens to an elliptical spot of 1.5 mm x 2.3 mm at the acetone four wave mixing cell, FWMC. After passage through the cell, the beam encountered the normally oriented surface of an uncoated wedged beam splitter which provided the weak backward pump. After being split off the main beam, the probe beam was sampled by a 50% beamsplitter, focused by a 1 m focal length lens and clipped in to the strong pump beam path at an angle of about 10 mr.

We used a Q-switched Nd:YAG laser system operating at 10 Hz to produce pulses in a horizontally polarized beam, which we clipped to a roughly circular cross-section 7 mm in diameter. The laser system, which consisted of an oscillator and amplifier, was capable of producing pulses of up to 250 mJ, although we were limited to energies of 150 mJ by the onset of damage to our Brillouin shifter. A typical temporal profile of the pulse as shown in Figure 46. The pulses were smooth with widths of approximately 12 ns as long as single axial mode operation was maintained by the oscillator. Well tuned single axial mode operation could be maintained for minutes at a time, before modulation in the pulse envelope had increased noticeably. Hence, the laser was frequently fine tuned to minimize modulations in the pulse envelope due to the presence of additional mode components. This instability contributed to scatter in the experimental data.

The laser pulse was Brillouin shifted upon backscattering by the SBS cell (SBSC) to obtain the pump pulse at the desired wavelength. The SBS cell consisted of a 8" x 1" ϕ tube with optical windows expoxied to its ends. The cell was half filled with spectrophotometric grade acetone, and topped with argon gas to avoid combustion of the acetone vapor in air. The cell is shown in the plane of the optical bench for purposes of the schematic; in fact, the cell was oriented with its axis slightly off the vertical. This allowed the f/20 beam to enter the cell at a relatively low intensity, avoiding damage to the cell window, while reaching focus at

about 2 cm below the surface of the acetone, which optimized the SBS reflectivity. Typically the SBS reflectivity was about 70%.

The four wave mixing cell, labelled FWMC in Figure 44, consisted of a 4 cm x 1" ϕ cell, capped by optical windows and filled witl spectrophotometric grade acetone. The cell axis was always misaligned with respect to the pump and probe beams to avoid multiple weak backward pump beams and to avoid retroreflecting the probe beam.

Energy and pulse profile measurements were made by pyroelectric probes (accessories to the Laser Precision R_j 7200 energy meter) D1, D2, D3, D4 and photodiodes PD1 and PD2 (PD3 was used to trigger oscilloscopes). D1 and D2 were used to monitor the SBS and FWSBS reflectivities, respectively. The photodiodes were used in conjunction with Tektronix 7104 oscilloscopes, which were capable of producing bright enough traces to record nanosecond signals on film. PD2 was used to monitor the shape of the probe and phase conjugate signals. PD1 was used to monitor the shape of the forward pump beam before and after transmission through the four wave mixing cell. Since the backward pump was produced by sampling the forward pump pulse after transmission by FWMC, the second pulse signal monitored by PD1 may be viewed as either the backward pump pulse or the post four wave mixing forward pulse.

Because thermal lensing of the forward pump pulse into the phase conjugate signal path occurred for operation at 10 Hz, a pulse selector was used, shown as PS in Figure 44. At 10 Hz operation, a false "phase conjugate" signal would grow over the course of a few seconds with the probe beam blocked. This occurred as the pump beam heated the the acetone, and thermally induced refraction steered scattered rays into the signal beam path. To avoid this, we used an electro-mechanical shutter, synchronized with the laser flashlamp timing to pass a single pulse upon command. By waiting about 10 seconds between shots, the false signal with the probe beam blocked was eliminated.

4.4.2 FWSBS Reflectivity Experiments

FWSBS reflectivity measurements were made while varying pump and probe intensities. Figure 45 summarizes data collected from four reflectivity

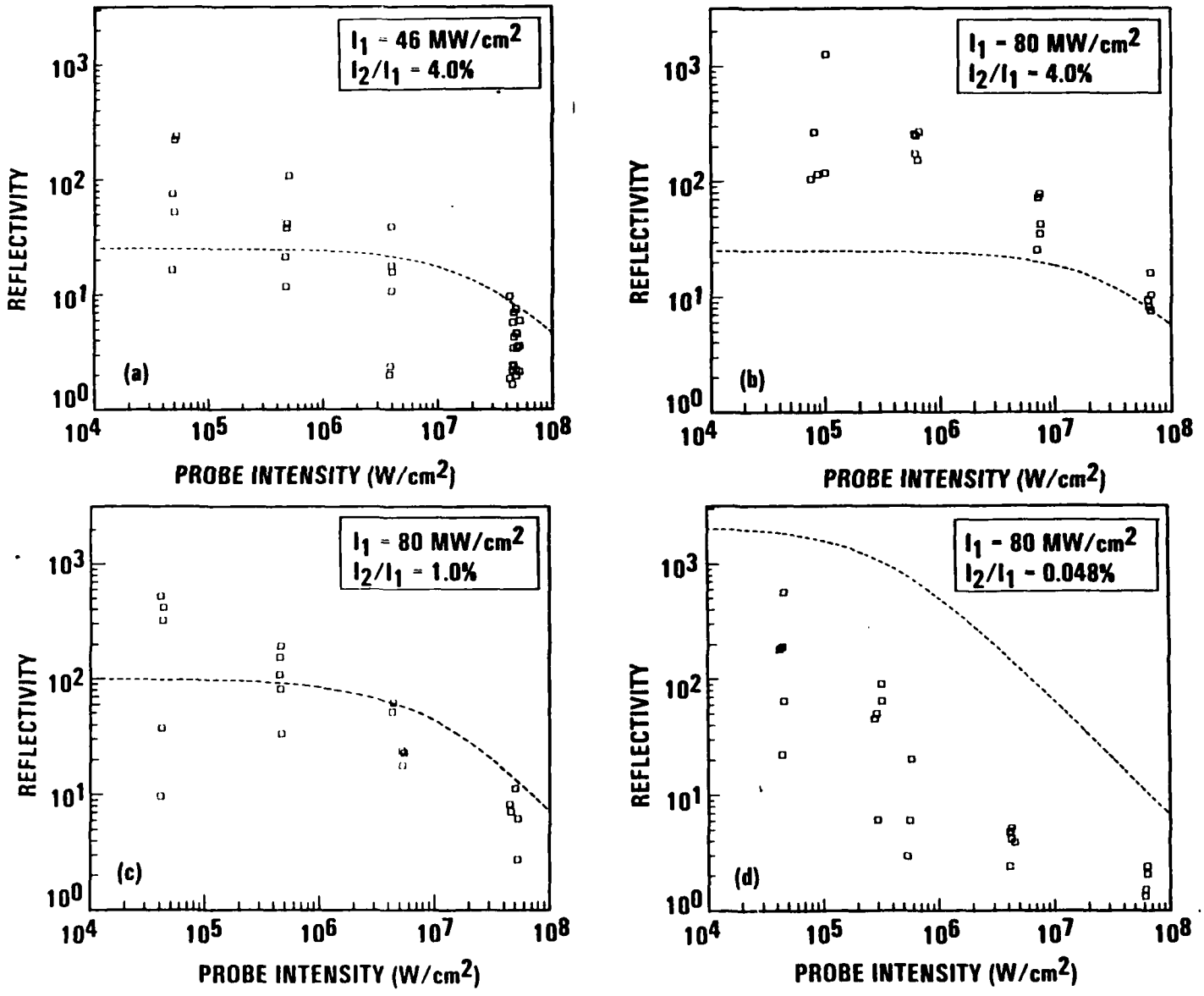

Figure 45. Summary of FWSBS reflectivity data. I_1 and I_2 refer to the forward and backward pump intensities respectively. The dashed lines give the theoretically predicted reflectivity.

experiment. Each point represents a single four wave mixing event. In each of the plots, the reflectivity variation with probe intensity is shown. Note that is comparing (a) and (b), only the pump power was changed. Plots (b), (c) and (d) differ only in the magnitude of the backward pump beam relative to the forward pump beam.

Each of plots includes a theoretical reflectivity given by:

$$R = \frac{I_1}{I_2 + I_3} \qquad \text{(B-27)}$$

where I_1, I_2 and I_3 are the intensities of the forward pump, backward pump and probe beam, respectivity. (See Appendix B for the derivation of Equation B-27). This characteristic asymptotically approaches the value of I_1/I_2 for small values of probe intensity, and falls as $1/I_3$ for $I_3 > I_2$. The theory appears to characterize the data well in the regime where $I_3 \lesssim I_2$; however, much larger reflectivities than were predicted by the theory were obtained for small I_3.

This discrepancy between the theory and the data can not be explained in terms of signal noise. Background noise was measured for the data in plots (a), (b) and (d), by blocking the probe and measuring the signal in the return beam path. The noise level during the I_2/I_1 = 4% experiments was stable and small, and has been subtracted out of the phase conjugate signal energies. In plot (d), where the backward pump intensity was reduced by two orders of magnitude, the background noise was significant for probe intensities under 1 MW/cm^2. However, because the scatter in the background noise measurements was large, no systematic error could be discerned. In plot (d), the four smallest reflectivities for I_3 = 0.5 MW/cm^2 and 0.05 MW/cm^2 may be entirely due to noise.

Typical FWSBS pulse profiles are shown in Figure 46. It is seen that the return pulse is about 50% narrower than the probe pulse. Because the FWSBS medium is short compared to the pulse lengths (in space), the shape of the return pulse envelope is related to the product of the envelopes of the three incident pulses. Note that the backward pump pulse, which is also a sample of the forward pump pulse after transmission through the acetone cell, has been considerably shortened. This shortening may

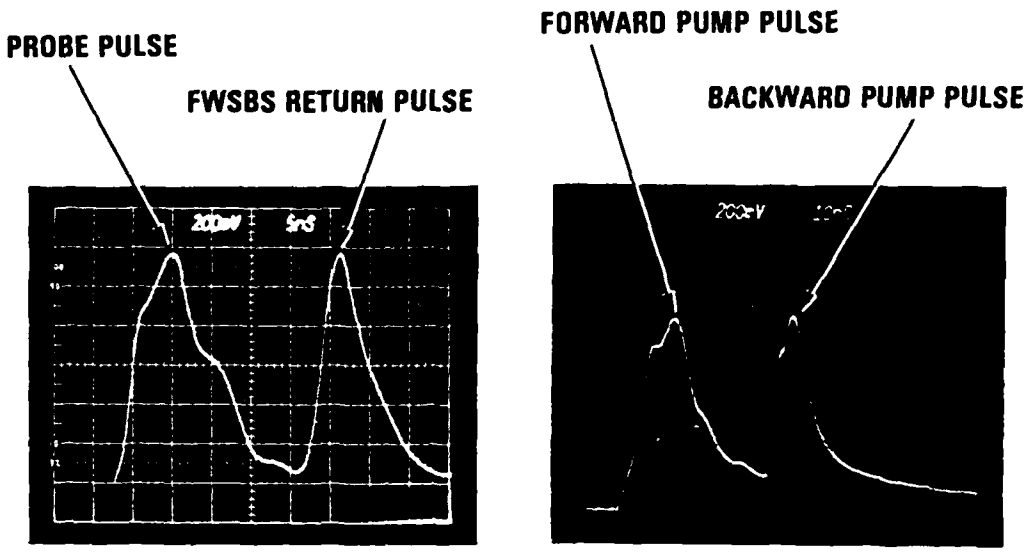

Figure 46. Typical FWSBS pulse profiles.

correspond to significant depletion of the trailing edge of the pulse after the onset of SBS enhancement of the four wave mixing. The risetime of the SBS enhancement is approximately the phonon lifetime in acetone of 2 ns.

A summary of the experimental investigation into the dependence of reflectivity on pump power is shown in Figure 47. In the figure, the data presented in Figure 48(a) and (b) is replaced by averages and error bars, and fit using linear regression. The error bars are constructed such that they enclose all of the data points at a fixed probe beam intensity. The reflectivity roughly increased by a factor of four for a two-fold increase in pump power. This scaling is faster than the rate given by equation B-27, which predicts a proportional increase in R.

A summary of the experimental investigation into the dependence of reflectivity on the relative intensity of the backward pump beam is given in Figure 48. The plots summarize the data shown in Figure 45 (b), (c) and (d) in a manner similar to the previous figure. The line fits exclude the weakest probe intensity data points for each curve, which are outside the pump depletion regime where $R \propto 1/I_3$.

From the plots, it may be observed that the reflectivity increases with I_2/I_1, contrary to the trend predicted by equation B-27. This disagreement with the theory is to be expected in the limit of small I_2. While the theory predicts a diverging reflectivity in the absense of the backward pump as $I_2 \rightarrow 0$, the elimination of the backward pump would extinguish the interaction.

The diminution of the reflectivity with the backward pump may be understood as a transition from a well defined backward pump to a diffuse backward pump. As the backward pump intensity approaches the intensity level of randomly scattered pump beam in the cell, the scattered light could begin to play the role of backward pump. This noise in the backward pump would be imprinted by the four wave mixing on the outgoing signal. The fidelity of the phase conjugate reflection could be reduced to the extent that the signal is displaced from the probe beam path, diminishing the reflectivity measurement.

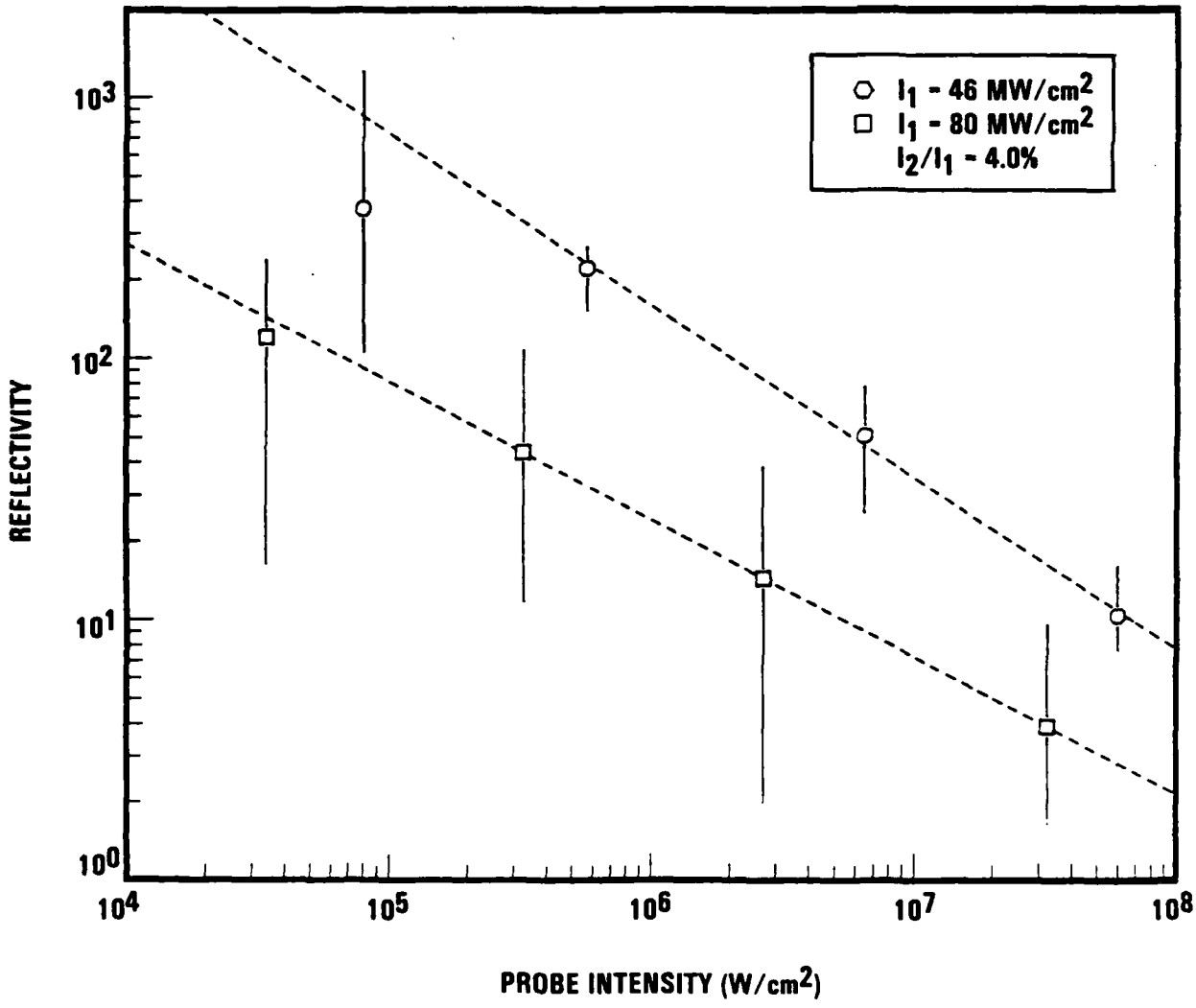

Figure 47. Reflectivity versus probe intensity for two pump powers.

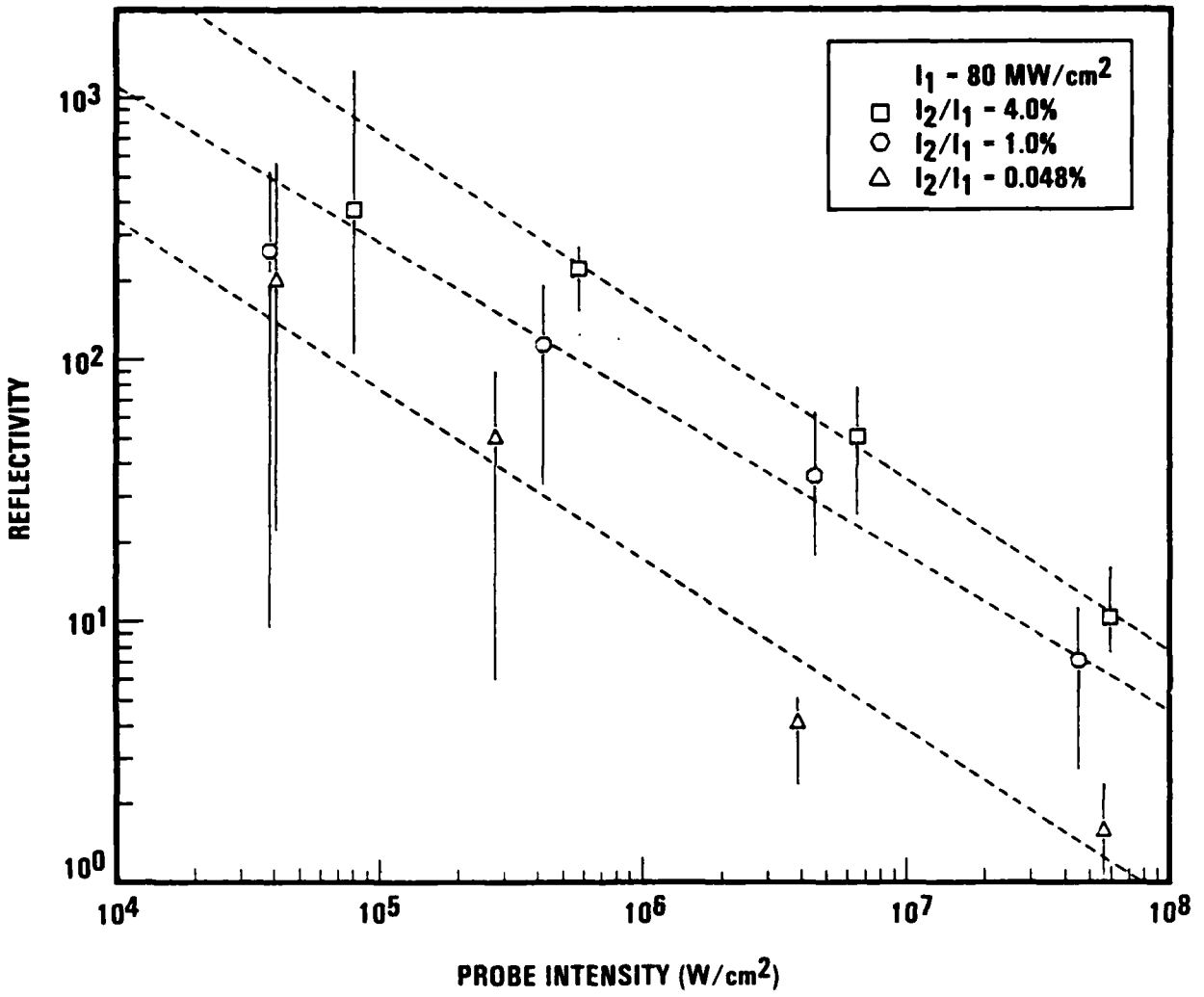

Figure 48. Reflectivity variation with relative backward pump intensity. The dashed lines are fits to the three most intense probe beam data points for each backward pump intensity.

4.4.3 FWSBS Efficiency Experiment

An experiment was performed to maximize the transfer of forward pump energy into the phase conjugate return beam. In this experiment, the lenses used to focus the pump and probe beams in the four wave mixing cell were intercharged such that the probe beam completely enveloped the pumped volume in the cell. With this reconfiguration, the pump spot cross section was reduced to a 0.43 mm x 0.74 mm ellipse, while the probe cross section was increased to a 1.48 mm x 2.3 mm elipse.

Figure 49 presents the variation of the four wave mixing efficiency with probe beam where the efficiency is defined as the fraction of the forward pump beam energy transferred into the signal beam. A maximum efficiency of 16% was demonstrated.

The data is seen to follow the predicted efficiency, shown as a dashed line in the figure. The efficiency is given by

$$\eta = \frac{I_3}{I_2 + I_3} , \qquad \text{(B-27)}$$

where the I_2 and I_3 are the backward pump and probe beam intensities, respectively. Note that the experiment was performed in the weak probe regime with no pump depletion. As with the reflectivity measurements, the experimental measurements outperformed the predictions in this regime.

4.4.4 Conclusion

Four wave stimulated Brillouin scattering phase conjugation has been demonstrated to given reflectivities as high as 100,000% and efficiencies as high as 16%. The dependence of the reflectivity on pump intensities, relative backward pump intensity and probe intensity was measured and compared to simple theoretical predictions.

The theory gave good estimates of reflectivity in the regime where $I_3 > I_2$. However, in two instances, the theory underestimated the reflectivity. First, the theory did not predict the large reflectivities we measured $I_3/I_2 \ll 1$. In addition, the theory underestimated the increase in the reflectivity with pump intensity, as shown in Section 4.4.2. In these experiments, the reflectivity was observed to grow with increasing I_2/I_1.

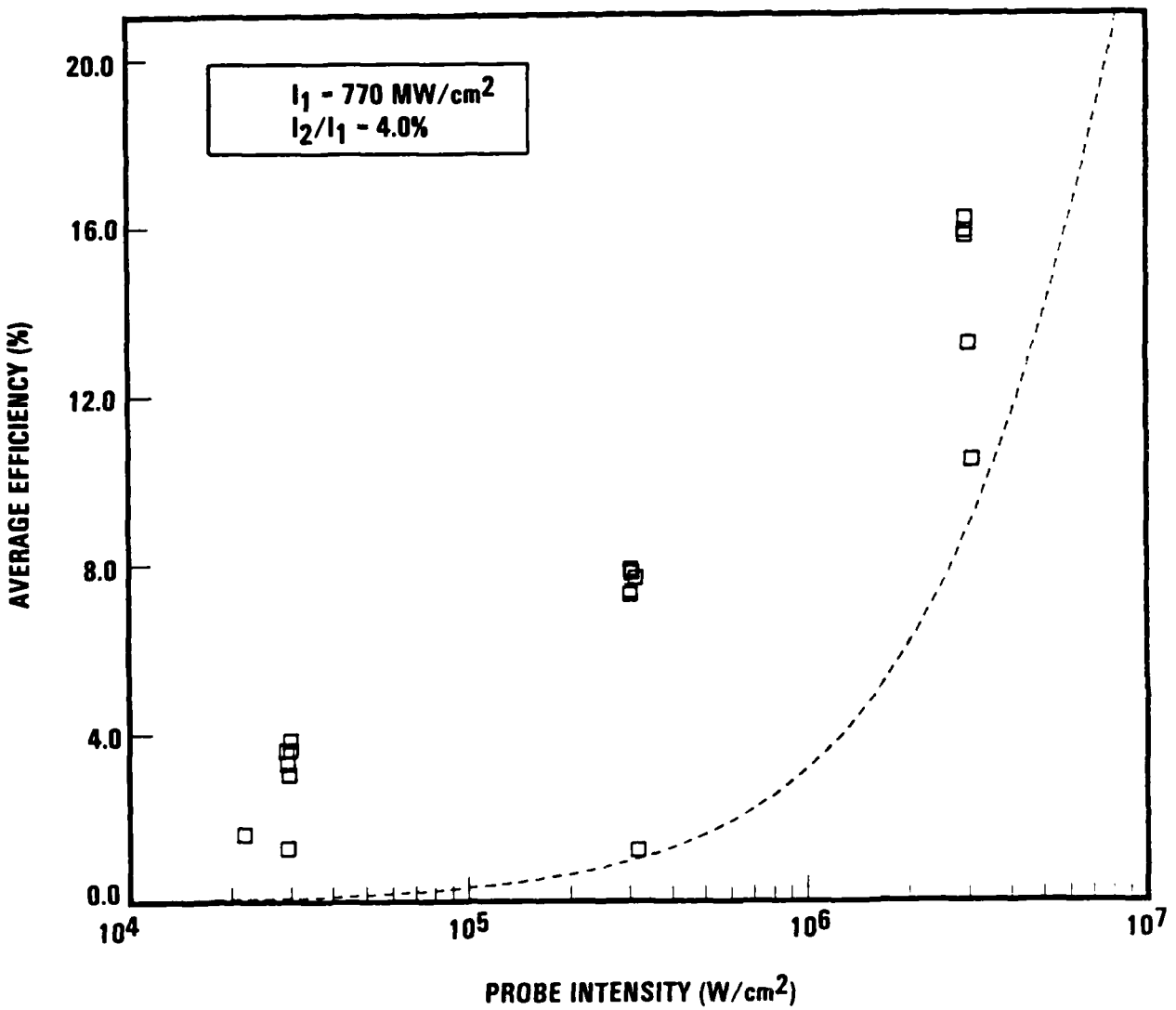

Figure 49. Average efficiency versus probe intensity. Efficiency was measured using a probe beam which enveloped the pumped volume in the four wave mixing cell. The theoretically predicted efficiency is given by the dashed line.

contrary to the prediction. .This disagreement between the theory and the experiment could be eliminated by the inclusion of backward pump intensity noise is the modelling. The experiment could recover the expected $R \alpha I_1/I_2$ for I_2 well in excess of the background noise.

Our attainment of reflectivities limited to 1000x was probably due to our limited forward pump power. Higher pump powers would allow the investigation of reflectivity scaling at giant reflectivites in the regime where $R \sim I_1/I_2$, with I_2 far greater than the background roise. Investigations by Russian and British researches [23,36] have obtained much larger reflectivities (one-million fold) using much lower I_2/I_1 with much larger forward pump intensities ($\sim$ 1 GW/cm^2).

V. CONCLUSION

In this program, three major concepts of phase conjugate FEL resonators were defined: the phase conjugate mirror, phase conjugate outcoupling and phase conjugate beam conversion. Each concept was developed to solve one or more problems that are pertinent to the conventional FEL resonator designs. Together, the new novel resonator designs are capable to satisfied the requirements for a ground-based high power FEL system.

For each concept, a new novel unconventional adaptive optics technique is identified. The new nonlinear optics technology includes the effects of multiple-pulse stimulated Brillouin scattering, short-pulse four wave mixing and four-wave stimulated Brillouin scattering. Each technique was found to well satisfy the requirements of the corresponding resonator concept.

Very few theoretical or experimental studies of these three effects have been reported before. A series of analytical theories, simulation codes and analyses are thus development to enhance our understanding of the effects and determine their feasibility to meet the system requirements.

For verification and scaling purpose, proof-of-principle experiments have been conducted for the short-pulse four wave mixing and the four-wave stimulated Brillouin scattering phenomena using the picosecond and nanosecond FEL simulators, respectively. A reflectivity of 10^3 has been observed for the latter phenomenon that demonstrated the feasibility of uplinking a high power conjugate beam from a ground-based FEL system.

The research in this program provides a first step (a promising first step) toward the realization of a simple, reliable and powerful FEL system. The physical bases of the technology involved are mostly understood from the theoretical and experimental efforts under this program. The system concepts were evaluated and proven to be viable from a number of system analyses.

The research has been carried out by a team of excellent elite scientists in TRW. Therefore, it is not surprised that a number of invention

disclosures, publications, and conference presentations are associated exclusively with this program. We are proud to present the following list.

Invention Disclosures

1. "Phase Conjugate Free Electron Laser Resonator", Docket number 11-0440

2. "Free Electron Laser Resonator With Phase Conjugate Outcoupling", Docket number 11-0439

3. "Discriminative Scattering Scheme For Four Wave Mixing", Docket number 11-0438

4. "Efficient Phase Conjugate Conversion of High Power Laser Beam", Docket number 11-0437

Publications

1. "Modeling of Transient Four-Wave Mixing", Proceeding Of SPIE Conference On Optics And Optoelectronic System. Volume 642, 1986.

2. "Theory Of Short-Pulse Four Wave Mixing", submitted to Optics Letters, May, 1986

3. "Analytical Theory Of Four Wave Stimulated Brillouin Scattering In The Saturation Regime", in process of clearance for publication in Physical Reviews.

Conference Presentations

1. "Modeling Of Transient Four-Wave Mixing", presented at SPIE Conference on Optics and Optoelectronic Systems, Orlando, April 2, 1986

2. "Phase Conjugate Free Electron Laser Resonators", presented at International Quantum Electronics Conference, San Francisco, June 12, 1986.

3. "Reflectivity Scaling With Fluence In Picosecond Four-Wave Mixing", presented at International Quantum Electronics Conference, San Francisco, June 13, 1986.

REFERENCE

1. D.A.G. Beacon et. al, Phys, Rev. Lett., 38, 892 (1977)

2. M. Billardon et. al., Phys. Rev. Lett., 51, 1652 (1983)

3. J.A. Edighoffer et. al., Phys. Rev. Lett., 52, 344 (1984)

4. B.E. Newman et. al., IEEE, J. Quant. Electr., QE-21, 860, 867 882, 889, 895, 904 (1985)

5. S.A. Maini and J.H. Hammond, Proc. Int. Conf. Lasers, pp. 586, 1981

6. P.B. Memola and D.C. Jordan, Los Alamos Conf. Opt., SPIE Vol. 228, pp. 54, 1981

7. A. Bhowmik, "Analysis of An Advanced Free Electron Laser Resonator Concept", Final Report, RI/RD 85-254, August, 1985

8. C. Shih and D.L. Bullock, "Effect of Mode Rotation and Intracavity Beam Divergence on The Alignment Sensitivity of FEL Ring Resonators" Nuclear Instruments and Methods in Physics Research-A, 1986

9. J.F. Ward and S.A. Von Laven, IEEE J. Quant. Electr., QE-21 1108 (1985)

10. V. Wang and A. Yariv, "Laser Having a Nonlinear Phase Conjugating Reflector", U.S. Patent 4,233,571

11. W.M. Grossman and D.C. Quimby, "Scaling of Alignment Tolerances for Free-Electron Laser Oscillators", Proceeding of Free Electron Generators of Coherence Radiation, SPIE Vol. 453, pp 86 (1983)

12. A. Yariv, "Compensation for Atmospheric Degradation of Optical Beam Transmission by Nonlinear Optical Mixing", Opt. Commun., 21, 49 (1977)

13. C. R. Giuliano, "Applications of Optical Phase Conjugation," Physics Today, pp. 27, April, 1981

14. J.B. Shellan, "FEL Phase Array Configurations", SPIE Conference on Optics and Optoelectronic Systems, Vol. 642, Orlando, April 1986

15. A.D. Kudriavtseva and A.I. Sokolvskaia, Opt. Commun., 26, 446 (1978).

16. G.L. Brekhovskikh and A.I. Sokolovskaya, Sov. J. Quant., Electr, 13, 372 (1983)

17. H.H. Barett and S.F. Jacobs, Opt. Lett, 4, 190 (1979)

18. P. Mathieu and P.A. Belanger, Appli. Opt., 19, 2262 (1980)

19. T.R. O'Meara, Opt. Eng. 21, 271 (1982)

20. D. Fink, Appl. Opt., 18, 581 (1979)

21. K.J. Witte and M.A. Greiner-Mathes, "Stimulated Brillouin Scattering with 100% Reflectivity Using 1-nsec Pulses at 1.32 μm," CLEO'85 Baltmore, 1985

22. D.M. Pepper and A. Yariv, in Optical Phase Conjugation, edited by R.S. Fisher, Chapter 2, (Academic Press, New York, 1983)

23. N.F. Andreev et. al., JETP letters, 32, 625 (1980)

24. N.M. Kroll, P.L. Morton and M.N. Rosenbluth, IEEE, J. Quant., Elect., QE-17, 1436 (1981)

25. Y.R. Shen, The Principles of Nonlinear Optics, Chapter 27, (John Wiley & Sons, New York 1984)

26. A. Yariv and D.M. Pepper, Opt. Lett., 1, 16 (1977)

27. A.E. Siegman, P.A. Belanger and A. Hardy, in Optical Phase Conjugation, edited by R.A. Fisher, Chapter 13, (Academic Press, New York, 1983)

28. I.M. Bel'dyugin et. al., Sov. J. Quant. Elec., 15, 1583 (1985)

29. C. Shih and D.L. Bullock, SPIE Conference on Optics and Optoelectronic Systems, Vol. 642, Orlando, April 1986

30. G.C. Valley, IEEE, J. Quant. Elect., QE-22, 704 (1986)

31. M.J. Damzen and H. Hutchinson, IEEE J. Quant. Elect., QE-19, 7 (1983)

32. B.R. Suydam and R.A. Fisher, in Optical Phase Conjugation, edited by R.A. Fisher, Chapter 3, (Academic Press, New York 1983)

33. W.P. Brown, J. Opt. Soc. Am., 73 629 (1983)

34. M.T. Grueneisen, A.L. Gaeta and R.W. Boyd, J. Opt. Soc. Am., B2, 1117 (1985)

35. A. Hardy and Y. Silberberg, J. Opt. Soc. Am., 73 594 (1983)

36. A.M. Scott and M. Hazell, OSA annual meeting, Washington, D.C., October 1985

37. A.M. Scott, Opt. Commun., 45, 127 (1983)

38. H. Peter Kortz, "Characterization of Pulsed Nd:YAG Active/Passive Mode-Locked Laser," IEEE J. Quantum Electron. QE-19 (4), 578 (1983).

39. Michele A. Lewis and J. Thomas Knudtson, "Active Passive Mode-Locked Nd:YAG Oscillator," Appl. Opt. 21 (6), 2897 (1982).

40. S. L. Shapiro and M. A. Duguay, "Observation of Subpicosecond Components in the Mode-Locked Nd:glass Laser," Phys. Lett. 28A (10) 698 (1969).

41. J. Reintjes, R. L. Carman, and F. Shimizu, "Study of Self Focusing and Self Phase Modulation in the Picosecond Time Regime," Phys. Rev. A, 8 (3), 1486 (1973).

42. Dietrich von der Linde, "Experimental Study of Single Picosecond Light Sources," IEEE J. Quantum Electron. QE-8 (3), 328 (1972).

43. Michel A. Duguay, J. W. Hanson, Stanley L. Shapiro "Study of the Nd:Glass Laser Radiation, IEEE J. Quantum Electron. QE-6 (11), 725 (1970).

44. Howard Nathel, dissertation to be published, Chapter 3, University of California, 1986.

45. See, for example, John F. Reintjes, Nonlinear Optical Parametric Processes in Liquids and Gases, Academic Press, Orlando, 1984 or W. Koechner, Solid Static Laser Engineering, Springer Verlag, 1976.

46. J. L. Ferrier, Z. Wu, X. Nguyen Phu and G. Rivoire, "Four Wave Mixing in the Picosecond Range: Intensities, Durations, Wavefront Reconstruction," Opt. Commun. 41 (3), 207 (1982).

APPENDIX A

Theory of Short-pulse Four Wave Mixing

Chun-Ching Shih
TRW, 01/1070
One Space Park
Redondo Beach, CA 90278

Abstract

An analytical solution of the transient four wave mixing phenomenon in a Kerr medium that is long compared to the pulse length is presented.

Optical phase conjugation via backward four wave mixing in a nonlinear medium can be described by two coupled-mode equations for the probe and the conjugated field.[1] By neglecting temporal derivatives in the equations, a steady-state solution has been found which gives the well-known reflectivity expression $|\tan(\kappa L)|^2$, where κ is the field coupling strength and L is the interaction length.[2] This expression is the result of solving the coupled equations with time-independent boundary conditions and cannot be applied to the transient four wave mixing involving time-varying pulses.[3]

Several attempts to solve the time-dependent coupled equations in the transient regime have been reported in recent years.[4-7] These solutions are based on the assumption of using either CW pump beams (constant κ) or slowly-varying pump pulses that are much longer than the interaction length (time-dependent κ). Consequently, the result cannot be applied to the picosecond four wave mixing experiments that have received extensive attention recently.[8,9] In these experiments, the probe and the pump pulses are supplied from the same picosecond laser source. The lengths of the interacting pulses are thus comparable with each other and, in many cases of interest, are shorter than the length of the nonlinear medium cell. The analysis of such experiments requires a fully transient theory of the short-pulse four wave mixing.

In this letter, we present the first complete solution, ever reported in the literature, of the time-dependent coupled equations. the coupling strength, which is proportional to the product of the pump fields, is a function of position as well as of time. We found that, for most experimental situations in the laboratory, the reflectivity can be obtained in closed form, which is convenient for parametric studies of the phenomenon. The result can also be generalized to account for the bandwidth effect in the limit when the coherence length is much shorter than the pulse length.

For convenience and simplicity, we will assume the slowly varying envelope approximation (SVEA) for the fields throughout this letter. We also assume weak probe and conjugated waves to avoid the complexity of pump depletion, self-focusing, and self-phase-modulation. Finally, we consider isotropic and instantaneous response of the Kerr effect in the non-absorbing medium. These are the typical assumptions involved in the coupled-mode theory of the four wave mixing effect.[3]

Consider the system consisting of four waves propagating in either

positive or negative z direction (Figure 1):

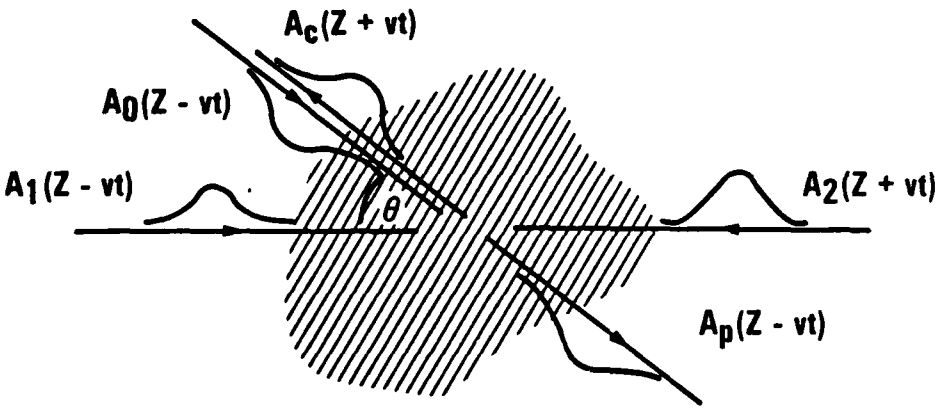

Initial Conditions

$A_p(-\infty, -\infty) = A_0(Z - vt)$

$A_c(\infty, -\infty) = 0$

Final States

$A_p(\infty, \infty) = A_p(Z - vt)$

$A_c(-\infty, \infty) = A_c(Z + vt)$

Figure 1. Schematic of short-pulse four wave mixing. The pulse interaction is assumed to be well within the medium cell so that the boundaries can be placed at $z = -\infty, \infty$ with initial and final states defined at $t = -\infty$ and ∞, respectively.

$$
\begin{aligned}
E_1(z,t) &= 1/2\ A_1(z - vt)\ \exp[i\omega_1 t - k_1 z] + c.c.,\\
E_2(z,t) &= 1/2\ A_2(z + vt)\ \exp[i\omega_2 t + k_2 z] + c.c.,\\
E_p(z,t) &= 1/2\ A_p(z,t)\ \exp[i\omega_p t - k_p z] + c.c.,\\
E_c(z,t) &= 1/2\ A_c(z,t)\ \exp[i\omega_c t + k_c z] + c.c.,
\end{aligned}
\qquad \text{(A-1)}
$$

where $A_1(z-vt)$ and $A_2(z+vt)$ represent the moving and non-depleting pump pulse profile, A_p and A_c are the slowly varying amplitude of the probe and the conjugated waves. By substituting Equation (1) into the inhomogeneous wave equation with nonlinear polarization and performing the following coordinate transformation:

$$
\begin{aligned}
x &= z - vt\\
y &= z + vt,
\end{aligned}
\qquad \text{(A-2)}
$$

we obtain the time-dependent coupled equations for A_p and A_c:

$$\frac{\partial}{\partial x} A_c = i\beta A_1(x) A_2(y) A_p^* \exp[i(k_p - k_1)x + i(k_2 - k_c)y]$$

$$\frac{\partial}{\partial y} A_p^* = i\beta^* A_1^*(x) A_2^*(y) A_c \exp[i(k_1 - k_p)x + i(k_c - k_2)y], \qquad \text{(A-3)}$$

where

$$\beta = \frac{\omega}{4}\sqrt{\frac{\mu}{\varepsilon}}\,\chi^{(3)} \qquad \text{(SI)}$$

$$= \frac{\pi\omega}{cn}\chi^{(3)} \qquad \text{(Gaussian)}. \qquad \text{(A-4)}$$

The pump field amplitudes A_1 and A_2, which are included in the constant κ, are now written out explicitly. The exponential factors in Equation (3) represent the phase mismatch for the nondegenerate case. These factors, containing x and y, can be absorbed into the profiles, $A_1(x)$ and $A_2(y)$, and do not affect the following derivations. For simplicity, the factors are dropped from now on.

The coupled equations can be further simplified by defining the normalized pulse profiles,

$$\tilde{A}_c(x,y) = A_c(x,y)/A_2(y)$$
$$\tilde{A}_p(x,y) = A_p(x,y)/A_1(x). \qquad \text{(A-5)}$$

and two fluence variables,

$$p = \int_{\infty}^{x} |A_1(x')|^2 dx'$$
$$q = \int_{-\infty}^{y} |A_2(y')|^2 dy'. \qquad \text{(A-6)}$$

In Equation (5), we note that the amplitude profile is normalized with respect

to only the pump pulse moving in the same direction. In Equation (6), p and q are the accumulated intensity (or fluence) from the front of the pump pulse to the point x or y defined by Equation (2). Since the interaction occurs well within the actual medium range, we can extend the medium boundaries to infinity in both directions without affecting the result. Under this boundary condition, the initial and final values of p and q are,

$$t = -\infty \; : \; p = o$$

$$q = o, \tag{A-7}$$

$$t = \infty \; : \; p = \int_{\infty}^{-\infty} |A_1(x)|^2 \, dx = P_1 \tag{A-8}$$

$$q = \int_{-\infty}^{\infty} |A_2(y)|^2 \, dy = P_2,$$

where P_1 and P_2 are the pulse energy density of the pump beam 1 and 2.

The equations now become

$$\frac{\partial}{\partial p} \tilde{A}_c(p,q) = -i \beta \tilde{A}_p^*(p,q)$$

$$\frac{\partial}{\partial q} \tilde{A}_p s(p,q) = i \beta^* \tilde{A}_c(p,q), \tag{A-9}$$

with the initial conditions

$$\tilde{A}_p(p,o) = \tilde{A}_o(p)$$

$$\tilde{A}_c(o,q) = o. \tag{A-10}$$

Equation (9) can be solved by using successive Laplace transforms with respect to p and q,

$$S_p \mathcal{L}_p(\tilde{A}_c) = -i\beta \mathcal{L}_p(\tilde{A}_p^*)$$

$$S_q \mathcal{L}_q(\tilde{A}_p^*) - \tilde{A}_o^* = i\beta^* \mathcal{L}_q(\tilde{A}_c). \tag{A-11}$$

From Equation (11), we have

$$\mathcal{L}_p\mathcal{L}_q(\tilde{A}_c) = \frac{-i\beta}{S_pS_q - \beta^2}\mathcal{L}_p(\tilde{A}_0^*)$$

$$\mathcal{L}_p\mathcal{L}_q(\tilde{A}_p) = \frac{S_p}{S_pS_q - \beta^2}\mathcal{L}_p(\tilde{A}_o), \tag{A-12}$$

and finally,

$$\tilde{A}_c(p,q) = -i\beta \int_o^p \tilde{A}_o^*(p-p')\ I_o\ (2|\beta|\sqrt{p'q})dp'$$

$$\tilde{A}_p(p,q) = |\beta| \int_o^p \tilde{A}_o(p-p')\ \frac{I_1(2|\beta|\sqrt{p'q})}{\sqrt{p'}}\ dp', \tag{A-13}$$

where I_o and I_1 are the modified Bessel functions of zeroth and first order. Equation (13) shows how the final pulse profiles can be calculated from the initial probe pulse profile.

Consider the case that the probe and the codirectional pump pulses have the same profile except for a proportional constant, i.e.,

$$\tilde{A}_o(p) = \sqrt{\frac{P_p}{P_1}}, \tag{A-14}$$

where P_p is the initial energy density of the probe pulse. This condition is most commonly seen in the laboratory when a single laser source is used. The final profile of the conjugated pulse can be readily found from Equation (13),

$$\tilde{A}_c(P_1,q) = i\ \frac{\beta}{|\beta|}\ \sqrt{\frac{P_p}{q}}\ I,(2|\beta|\sqrt{P_1q}). \tag{A-15}$$

$\tilde{A}_c\ (p_1,q)$ can be interpreted as the energy transfer rate from the beam 2 to

the conjugated beam. This rate is not uniform but depends on the fluence, q, of the beam 2. The nonuniformity can be seen by comparing the rate at the front and the rear end of the pulse,

$$\frac{\tilde{A}_c(P_1,P_2)(\text{Rear})}{\tilde{A}_c(P_1,o)(\text{Front})} = \frac{I_1(2|\beta|\sqrt{P_1P_2})}{|\beta|\sqrt{P_1P_2}}. \tag{A-16}$$

This ratio depends on the coupling strength and the product of pump energy densities.

From Equation (15) we can find the reflectivity, defined as the ratio of the energy densities in the conjugated and the probe pulses:

$$R \equiv \frac{P_c}{P_p} = \frac{1}{P_p}\int_{-\infty}^{\infty} dy\,|A_c(-\infty,y)|^2$$

$$= \frac{1}{P_p}\int_{o}^{P_2} dq\,|\tilde{A}_c(P_1,q)|^2$$

$$= I_o^2(n) + I_1^2(n) - 1, \tag{A-17}$$

where $$n = 2|\beta|\sqrt{P_1P_2}. \tag{A-18}$$

From the result in Equation (17), we found that the reflectivity depends directly on the product of pump pulse energy densities, but not on the detailed structure of any pulses, as long as the pulses in the probe and the pump beam 1 have the same profiles. Choose a nonlinear medium, e.g. CS_2, the dependent variable, n, for the case of equal pumps can be calculated as

$$n\ (CS_2) = 63\ P_{1,2}\ (\text{Joules/cm}^2). \tag{A-19}$$

The dependence of R on this variable is shown in Figures 2 and 3. It has a quadratic dependence at small n and exponential dependence at large n.

Furthermore, no oscillation condition can be found at any level of energy density in contrast to the solution of CW four wave mixing. In Figure (3), we also show the good agreement between this analytical result (solid line) and the simulation (dots) using the two-dimensional four wave mixing code developed at TRW.[10]

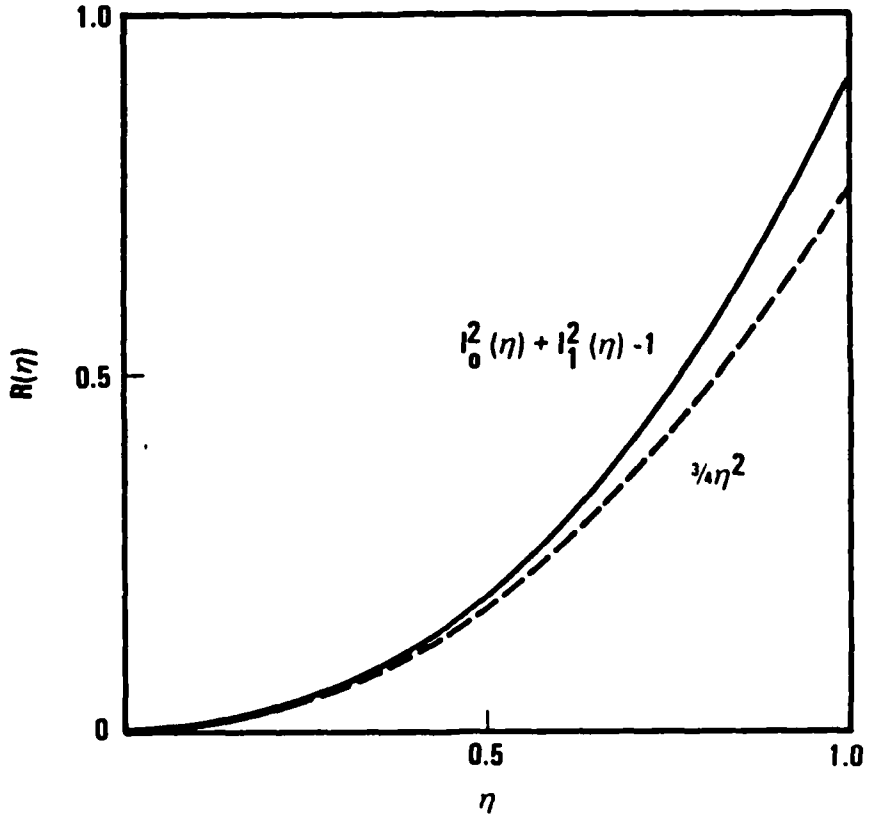

Figure 2. Reflectivity verse η in linear scale (Equation (17)).

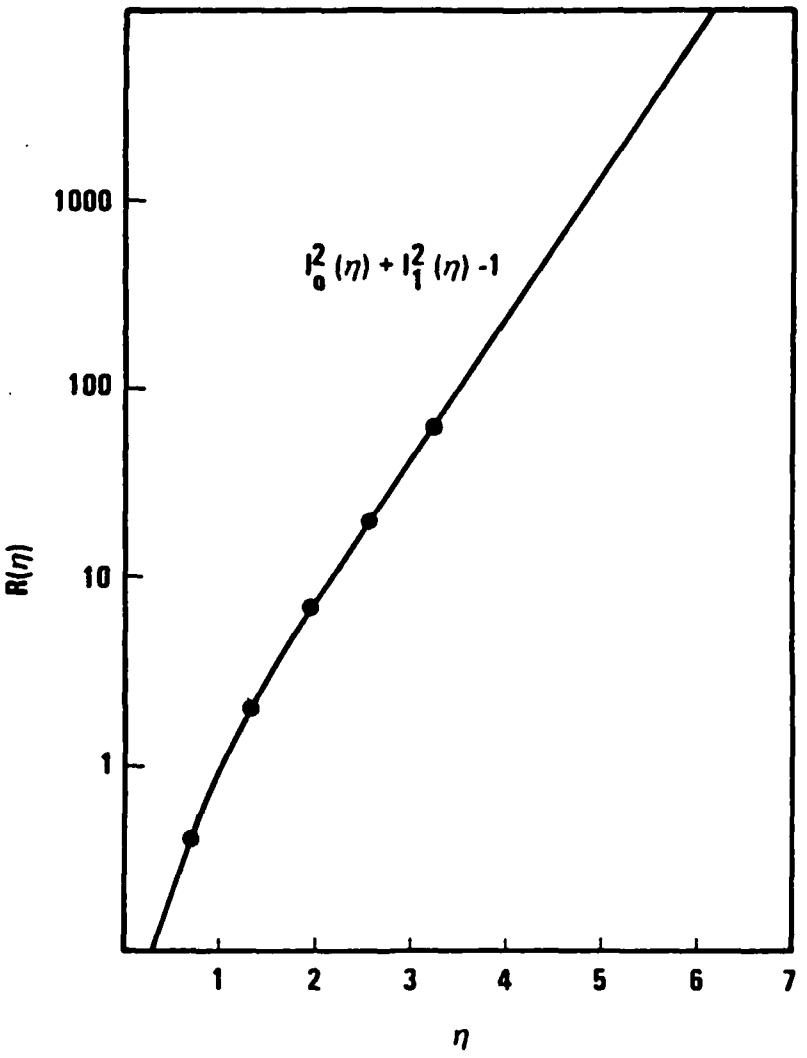

Figure 3. Reflectivity verse η is logarithm scale (Equation (17)). The dots are the simulation result from a two-dimensional four wave mixing code (Reference 10).

So far, we have neglected bandwidth effects and assumed only Fourier-transform limited pulses. It is of interest to generalize the solution to the cases where the coherence length is shorter than the pulse length. For this purpose, we consider a square pulse profile and divide the pulse into slots. The slot is equal to the coherent length. The fields in different slots are completely uncorrelated. Since the result in Equation

(17) is applied to arbitrarily short pulses, we can sum up the interactions between slots of different pulses to obtain the total reflectivity,

$$R(r) = \frac{1}{r}\left[I_0^2(r\eta) + I_1^2(r\eta) - 1\right], \qquad \text{(A-20)}$$

where r is the ratio of the coherence length to the pulse length. The reduction in reflectivity due to this bandwidth effect is shown in Figure 4 for r = 0.1, 0.2, 0.4, 0.6, 0.8, and 1.0. The decrease is substantial at high η. At small η, R(r) is proportional to the ratio r.

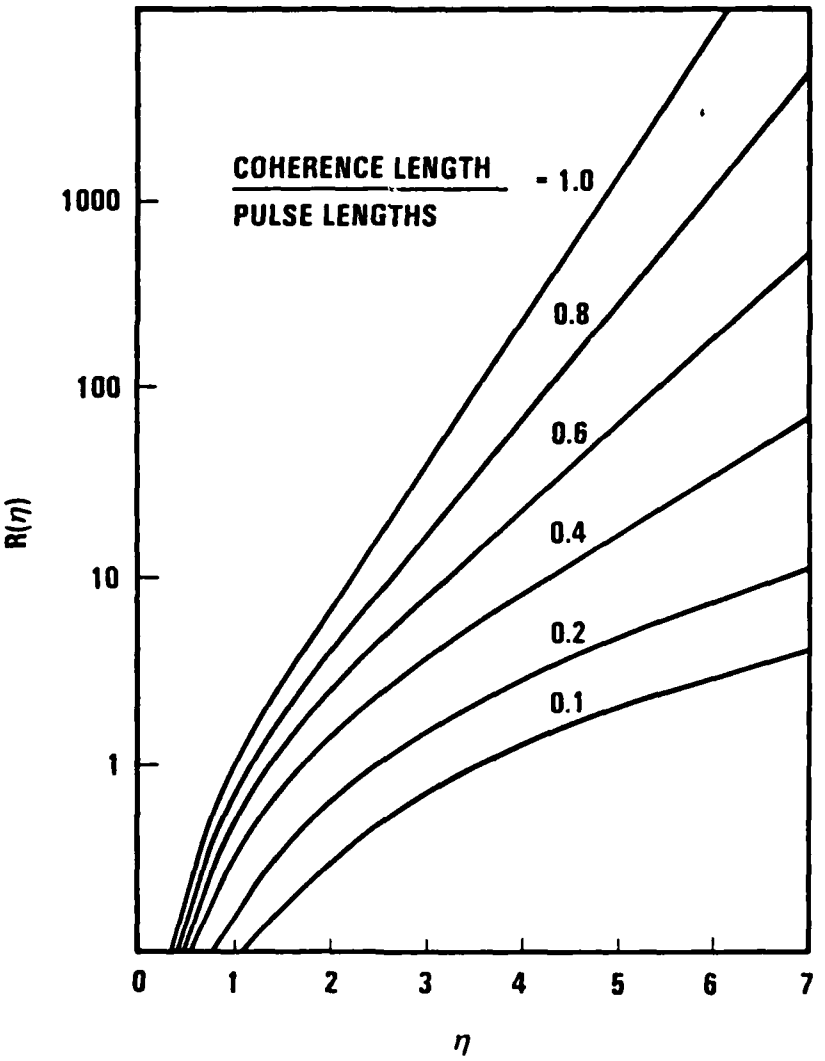

Figure 4. Reflectivity verse η for different ratios of coherence length and pulse length (Equation (20)).

In conclusion, we have successfully solved the time-dependent coupled equations for short-pulse four wave mixing. The theory has no restriction on the pulse profile of all participating beams. By using double Laplace transforms and a series of variable transformations, we are able to obtain the conjugate reflectivity in closed form. The result is then generalized to include the bandwidth effect.

The author acknowledges many stimulating discussions with Drs. D. L. Bullock and J. Menders in TRW.

References

1. D. M. Pepper and A. Yariv, "Optical phase conjugation using three-wave and four-wave mixing via elastic photon scattering in transparent media", in Optical Phase Conjugation, edi. by R. A. Fisher, Chapter 2, Academic press, N.Y. 1983.
2. A. Yariv and D. M. Pepper, "Amplified reflection, phase conjugation and oscillation in degenerate four-wave mixing", Opt. Lett. 1, 16, (1977).
3. B. R. Suydam and R. A. Fisher, "Transient response of Kerr-like phase conjugators", in Optical Phase Conjugation, edi. by R. A. Fisher, Chapter 3, Academic press, N.Y. 1983.
4. J. H. Marburger, "Optical-pulse integration and chirp reversal in degenerate four-wave mixing", Appl. Phys. Lett., 32, 372 (1978).
5. W. W. Rigrod, R. A. Fisher, and B. J. Feldman, "Transient analysis of nearly degenerate four-wave mixing", Opt. Lett., 5, 105 (1980).
6. R. C. Shockley, "Simplified theory of the impulse response of an optical degenerate four-wave mixing cell", Opt. Commun., 38, 221 (1981).
7. D. A. B. Miller, "Time reversal of optical pulses by four-wave mixing", Opt. Lett., 5, 300 (1980).
8. I. C. McMichael, "Degenerate four-wave mixing of short and ultrashort light pulses", Ph.D. Thesis, 1984.
9. J. Menders and C. Shih, "Reflectivity scaling with fluence in picosecond four-wave mixing", paper FBB5, IQEC, San Francisco, 1986.
10. C. Shih, "Modeling of transient four-wave mixing", Proceeding of SPIE Conference on Optics and Optoelectronic Systems, vol. 642, Orlando, 1986.

APPENDIX B

Analytical Theory of Four Wave Stimulated Brillouin Scattering in the Saturation Regime

Chun-Ching Shih
TRW, 01/1070
One Space Park
Redondo Beach, CA 90278

Abstract

An analytical solution of the enhanced stimulated Brillouin scattering arranged in four wave mixing configuration is presented. The theory includes the effect of pump depletion and is able to demonstrate the reflectivity, efficiency and field variations in the saturation regime.

I. Introduction

Four wave mixing (FWM) via third-order optical susceptibilities in a nonlinear medium has been recognized as an attractive optical phase conjugation technique for its simple configuration, low power requirement and high reflectivity.[1] Although early theory of FWM predicted an infinitely large reflection coefficient under certain pump conditions,[2] the highest reflectivity ever observed has not exceeded 100.[3] This is due to its stringent requirements which are difficult to meet in most experiments. Later analyses showed that this reflective singularity is highly unstable with respect to the change of pump intensity.[4,5] A small amount of pump depletion can drive the interaction out of the resonance regime and thus reduce the reflectivity significantly.

Recently, conjugate reflectivities in the range of 10^4 to 10^6 have been observed with the technique involving the combination of two major optical phase conjugation concepts: four wave mixing configuration and stimulated Brillouin scattering (SBS) process.[6,7] Together, we shall call it four wave stimulated Brillouin scattering (FWSBS). In this effect, two beams of the same frequency, ω, propagate toward each other (Figure 1). A probe beam of

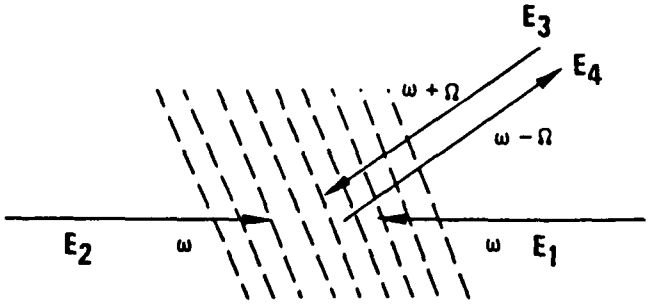

Figure 1. Schematic of FWSBS

slightly higher frequency is incident at a small angle into the interaction region. The frequency difference should be close to the acoustic wave frequency, Ω, of the backward SBS effect. This arrangement is identical to the ordinary nondegenerate FWM. However, the interaction mechanism is completely different. The SBS interaction between the backward pump (beam 2) and the probe signal (beam 3) creates an acoustic grating. This grating is further enhanced by the stimulated scattering of the forward pump (beam 1)

into the return field (beam 4). The result is a substantial energy flow from beam 1 to beam 4 which is a phase conjugation of the probe field.

To date, the theoretical studies of this effect have been limited to the constant pump approximation.[8,9] The results showed that the FWSBS reflectivity has no singularity in the normal operational regime. Therefore, the energy transfer from the pump beams can be as complete as possible without affecting the scattering process significantly. It was also found that the relectivity depends only on the ratio, but not the product as in FWM, of the pump intensities. The reflectivity can be brought to an extremely high level, say 10^6, by lowering the intensity in one of the pump beams. In order to demonstrate that the FWSBS can be a high reflectivity as well as a high efficiency process, the effect has to be studied in the saturation regime.

In this paper, we report an analytical solution of the four coupled equations describing the wave interaction in FWSBS.

In Section II, we derive the coupled equations and discuss the physical significance of each term. In Section III, we solve the equations with constant-pump approximation and check the conditions for high reflectivity. In Section IV, we give the analytical solutions of the four equations including the pump depletion effect and show the saturation phenomenon. Finally, a conclusion is drawn in Section V.

II. Coupled Equations

Consider the system consisting of four optical waves propagating in either positive or negative z direction and an acoustic wave with frequency, Ω,

$$\begin{aligned}
\mathcal{E}_1 &= E_1 \exp[i\omega_1 t + ik_1 z] + c.c. \\
\mathcal{E}_2 &= E_2 \exp[i\omega_2 t - ik_2 z] + c.c. \\
\mathcal{E}_3 &= E_3 \exp[i\omega_3 t + ik_3 z] + c.c. \\
\mathcal{E}_4 &= E_4 \exp[i\omega_4 t - ik_4 z] + c.c.,
\end{aligned} \tag{B-1}$$

$$\mathcal{A} = Q \exp\left[i\Omega t + i \frac{k_1 + k_2 + k_3 + k_4}{4} z\right] + c.c., \tag{B-2}$$

where E_j and Q are the slowly varying amplitude and the wave number of the acoustic wave is taken to be the average wave number of the four optical waves. For simplicity, the frequency difference between the pump beams and

other beams is assumed to be in resonance with the phonon field,

$$\Omega = \omega - \omega_4 = \omega_3 - \omega, \tag{B-3}$$

where

$$\omega = \omega_1 = \omega_2. \tag{B-4}$$

Using Equations (1) and (2), the basic equations for the slowly varying amplitudes can be written as [10]

$$\left(\frac{1}{v}\frac{\partial}{\partial t} - \frac{\partial}{\partial z}\right)E_1 = -ig_1 Q^* E_4 \exp\left[-i\frac{\Delta k}{2} z\right]$$

$$\left(\frac{1}{v}\frac{\partial}{\partial t} + \frac{\partial}{\partial z}\right)E_2 = -ig_1 Q E_3 \exp\left[-i\frac{\Delta k}{2} z\right] \tag{B-5}$$

$$\left(\frac{1}{v}\frac{\partial}{\partial t} - \frac{\partial}{\partial z}\right)E_3 = -ig_1 Q^* E_2 \exp\left[i\frac{\Delta k}{2} z\right]$$

$$\left(\frac{1}{v}\frac{\partial}{\partial t} + \frac{\partial}{\partial z}\right)E_4 = -ig_1 Q E_1 \exp\left[i\frac{\Delta k}{2} z\right],$$

$$\left(\frac{\partial}{\partial t} + \Gamma\right)Q = ig_2\left\{E_1^* E_4 \exp\left[-i\frac{\Delta k}{2} z\right] + E_2 E_3^* \exp\left[i\frac{\Delta k}{2} z\right]\right\}, \tag{B-6}$$

where v is the light velocity in medium, g_1 and g_2 are the coupling coefficients, Γ is the phonon relaxation rate, and the phase-mismatch, Δk, is (Figure 2)

$$\Delta k = k_1 + k_4 - k_2 - k_3.$$

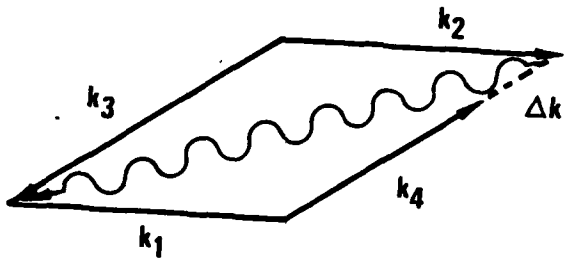

Figure 2. k-vector mismatch for the four waves

In Equations (5) and (6), we have assumed that the optical waves are coupled to each other through the same phonon field with slightly different phase-mismatch conditions. For steady-state analyses, the time derivatives can be neglected and the equations become

$$\frac{\partial E_1}{\partial z} = \frac{g}{2} I_4 E_1 + \frac{g}{2} E_3 E_4 E_2^* \exp[-i\Delta kz]$$

$$\frac{\partial E_2}{\partial z} = \frac{g}{2} I_3 E_2 + \frac{g}{2} E_3 E_4 E_1^* \exp[-i\Delta kz] \qquad \text{(B-7)}$$

$$\frac{\partial E_3}{\partial z} = \frac{g}{2} I_2 E_3 + \frac{g}{2} E_1 E_2 E_4^* \exp[i\Delta kz]$$

$$\frac{\partial E_4}{\partial z} = \frac{g}{2} I_1 E_4 + \frac{g}{2} E_1 E_2 E_3^* \exp[i\Delta kz]$$

where

$$I_j = |E_j|^2$$

$$g = \frac{2g_1 g_2}{\Gamma}. \qquad \text{(B-8)}$$

The two terms on the right hand side of Equation (7) have similar

expressions with the SBS and the nondegenerate FWM. The interaction process of FWSBS can be explained from Equation (7). Assume the power of beam 1 is much higher than the other two input beams, but is still below the threshold of the ordinary SBS effect. Although beam 1 does not have sufficient power to induce a Stokes wave from the noise, it can be reflected from the acoustic grating, created already by the SBS interaction between beam 2 and beam 3. This part of the field is represented by the second term in Equation (7). The reflected wave accumulates along its path in the opposite direction of beam 3. At low interaction strengths, this parametric superposition process will go through the whole medium, which is similar to the FWM process in a $\chi^{(3)}$ medium except that the coupling coefficient is real, not imaginary.

However, if the reflected wave becomes strong enough, the acoustic grating will be enhanced by the SBS interaction between beam 1 and beam 4. The reflected field is thus further amplified like in an ordinary SBS process that is represented by the first term in Equation (7). Due to the transition between different interaction processes, FWSBS has the combined advantages of the FWM and SBS effects: good conjugation fidelity because the reflected wave is generated from the field mixing ($E_4 \sim E_1 E_2 E_3^*$), not from noises; and high scattering efficiency because the amplification is a stimulated process that avoids the phase-mismatch problem. However, it is noted that FWSBS is a threshold phenomenon because of the stimulated amplification. For the conjugation process to be dominant, the second term in Equation (7) should be larger than the first term where E_4 starts from the noise level. This condition defines the threshold level for I_3,

$$I_3 > \frac{I_1 I_4}{I_2}. \tag{B-9}$$

Consider the noise level is roughly thirteen orders of magnitude lower than the pump intensity. The threshold condition for the three input beams becomes

$$I_2 I_3 > 10^{-13} I_1^2. \tag{B-10}$$

III Constant-Pump Approximation

If the probe intensity, I_3, is much lower than the pump intensities, I_1

and I_2, the first two equations in (7) can be neglected. The remaining two coupled equations for E_3 and E_4 can be solved exactly assuming constant I_1 and I_2.[8,9] Consider the nonlinear medium extends from 0 to L in the z direction. Using the boundary condition, $E_4(0) = 0$, the reflectivity was found

$$R = \frac{I_4(L)}{I_3(L)} = \frac{J_1 J_2}{|\alpha - \beta \coth \beta|^2}, \tag{B-11}$$

where

$$\begin{aligned} J_j &= gLI_j \\ \beta &= (\alpha^2 + J_1 J_2)^{1/2} \\ \alpha &= \frac{J_1 - J_2}{2} + i\Delta kL. \end{aligned} \tag{B-12}$$

The dimensionless variable, J_j, is a measure of the intensity, I_j, scaled by a factor gL. For a typical medium, acetone, at 1μm wavelength, we calculate $\Delta k = 2\ cm^{-1}$. In the limit of short interaction length, $\Delta kL << 1$, the reflectivity can be further simplified,

$$R = \frac{I_1 I_2 [\exp(J_1 + J_2) - 1]^2}{[I_1 + I_2 \exp(J_1 + J_2)]^2}. \tag{B-13}$$

It can be seen that the reflectivity is finite for all possible I_1 and I_2 and does not rely on unstable singularities. Now, from Equation (13), we can determine the condition of pump intensities to obtain high reflectivities. To avoid the ordinary SBS effect, it is required that $J_{1,2} < 30$, a threshold constant.[11] For example, we can choose $J_1 = 20$. At this power level, the exponential factor is $\exp(J_1) \sim 5 \times 10^8$ which is still much larger than the ratio (I_1/I_2) in most experimental conditions. Therefore, it is a very good

approximation to let the exponential factor approach infinity and we obtain the reflectivity

$$R = \frac{I_1}{I_2}. \tag{B-14}$$

Equation (14) shows that the constant-pump reflectivity is simply equal to the ratio of the two pump beam intensities. High reflectivity can thus be obtained by just lowering the backward pump intensity. This dependence is interesting comparing to the behavior in FWM, where the reflectivity increases with both pump intensities. We should also point out that the intensities have the following relation

$$\frac{I_4}{I_1} = \frac{I_3}{I_2}, \tag{B-15}$$

which is similar to the equality of reflectivities for the SBS effect of two pump beams sharing the same interaction region.[12] From Equation (15), we can see that if I_3 approaches I_2, a substantial energy transfer from pump beam 1 should result. In this pump depletion regime, the reflectivity will saturate with increasing probe intensity and the result in this section cannot apply.

IV Saturation Phenomenon

The saturation effect of FWSBS should be studied from the complete set of coupled equations in (7). To simplify the problem, we neglect the exponential factor of phase-mismatch. This factor is important only when the four wave mixing dominates the process for a long distance. In the saturation regime, the FWM-dominant region is confined to a small area near the rear end of the medium. Within this region, the exponential factor is nearly a constant and can be dropped from the equations. With this approximation, the coupled equations become

$$\frac{\partial E_1}{\partial z} = \frac{g}{2} I_4 E_1 + \frac{g}{2} E_3 E_4 E_2^*$$

$$\frac{\partial E_2}{\partial z} = \frac{g}{2} I_3 E_2 + \frac{g}{2} E_3 E_4 E_1^*$$

$$\frac{\partial E_3}{\partial z} = \frac{g}{2} I_2 E_3 + \frac{g}{2} E_1 E_2 E_4^* \qquad \text{(B-16)}$$

$$\frac{\partial E_4}{\partial z} = \frac{g}{2} I_1 E_4 + \frac{g}{2} E_1 E_2 E_3^*.$$

Equation (16) has the following constants,

$$p = I_1 - I_4$$

$$q = I_2 - I_3 \qquad \text{(B-17)}$$

$$r = E_1 E_2 - E_3 E_4$$

$$s = E_1 E_3^* - E_2^* E_4.$$

These four constants are not independent. They are related to each other by

$$|r|^2 - |s|^2 = pq. \qquad \text{(B-18)}$$

The four coupled equations are thus reduced to three independent constants plus an equation for any of the four intensities, for example,

$$\frac{\partial I_4}{\partial z} = g I_1 I_4 + g E_1 E_2 E_3 E_4. \qquad \text{(B-19)}$$

Define the average intensities I_{14} and I_{23},

$$I_{14} = \frac{1}{2}(I_1 + I_4)$$

$$I_{23} = \frac{1}{2}(I_2 + I_3). \tag{B-20}$$

From Equations (17), (19) and (20), we found the eqution for I_{14} and I_{23}.

$$\frac{\partial I_{14}}{\partial z} = \frac{g}{p^2}\{(r^2 + s^2 + p^2)(I_{14}^2 - \frac{p^2}{4}) + 2rs\, I_{14}(I_{14}^2 - \frac{p^2}{4})^{1/2}\}$$

$$\frac{\partial I_{23}}{\partial z} = \frac{g}{q^2}\{(r^2 + s^2 + q^2)(I_{23}^2 - \frac{q^2}{4}) - 2rs\, I_{23}(I_{23}^2 - \frac{q^2}{4})^{1/2}\}. \tag{B-21}$$

These two nonlinear equations can be further simplified by using the following transformation,

$$I_{14} = \frac{|p|}{4}(x + \frac{1}{x})$$

$$I_{23} = \frac{|q|}{4}(y + \frac{1}{y}). \tag{B-22}$$

The equations for x and y are

$$\frac{\partial x}{\partial z} = \frac{1}{4|p|}\{[(r + s)^2 + p^2]\, x^2 - [(r - s)^2 + p^2]\}$$

$$\frac{\partial y}{\partial z} = \frac{1}{4|q|}\{[(r - s)^2 + q^2]\, y^2 - [(r + s)^2 + q^2]\}. \tag{B-23}$$

These two equations can be integrated readily. The results are

$$\frac{x - A}{x + A} = \frac{x_o - A}{x_o + A} e^{\gamma z}$$

$$\frac{y - B}{y + B} = \frac{y_o - B}{y_o + B} e^{\gamma z}, \tag{B-24}$$

where

$$A^2 = \frac{(r - s)^2 + p^2}{(r + s)^2 + p^2}$$

$$B^2 = \frac{(r + s)^2 + q^2}{(r - s)^2 + q^2} \tag{B-25}$$

$$\gamma^2 = \frac{g^2}{4} [p^2 + q^2 + 2(r^2 + s^2)],$$

and x_o and y_o are the values of x and y evaluated at z = 0. The solutions in Equation (24), x(z) and y(z), can be substituted into Equation (22) to obtain the average intensities, $I_{14}(z)$ and $I_{23}(z)$. The intensity of each beam can thus be calculated

$$I_1 = I_{14} + \frac{p}{2}$$

$$I_2 = I_{23} + \frac{q}{2} \tag{B-26}$$

$$I_3 = I_{23} - \frac{q}{2}$$

$$I_4 = I_{14} - \frac{p}{2}.$$

Equations (22), (24) and (26) represent the complete analytical solution for the FWSBS effect. The result is expressed in terms of the boundary condition at one end of the medium. In reality, however, the boundary values are $I_1(L)$, $I_2(0)$, $I_3(L)$ and $I_4(0)$, which are defined at either $z = 0$ or $z = L$. It is very difficult to express the constants, p, q, r, s, in terms of these known quantities.

For the purpose of demonstration, we write Equations (22), (24) and (26) in a code which calculates $I_j(0)$ from the input values $I_j(L)$. By fixing $I_1(L)$ and $I_3(L)$, we can adjust the inputs $I_2(L)$ and $I_4(L)$ such that the output values of beam 2 and beam 4 equal the boundary condition $I_2(0)$ and $I_4(0)$. This process is quite stable and converges very quickly.

To demonstrate the saturation effect, we choose the forward pump intensity to be 500 MW/cm^2 and the backward pump intensity 0.5 MW/cm^2. In a 2 cm long acetone medium (g = 0.02 cm/MW), these correspond to $J_1 = 20$ and $J_2 = 0.02$, respectively. The probe intensity is varied over three orders of magnitude from 2.5 kw/cm^2 to 2.5 MW/cm^2 (Figure 3). As anticipated, the

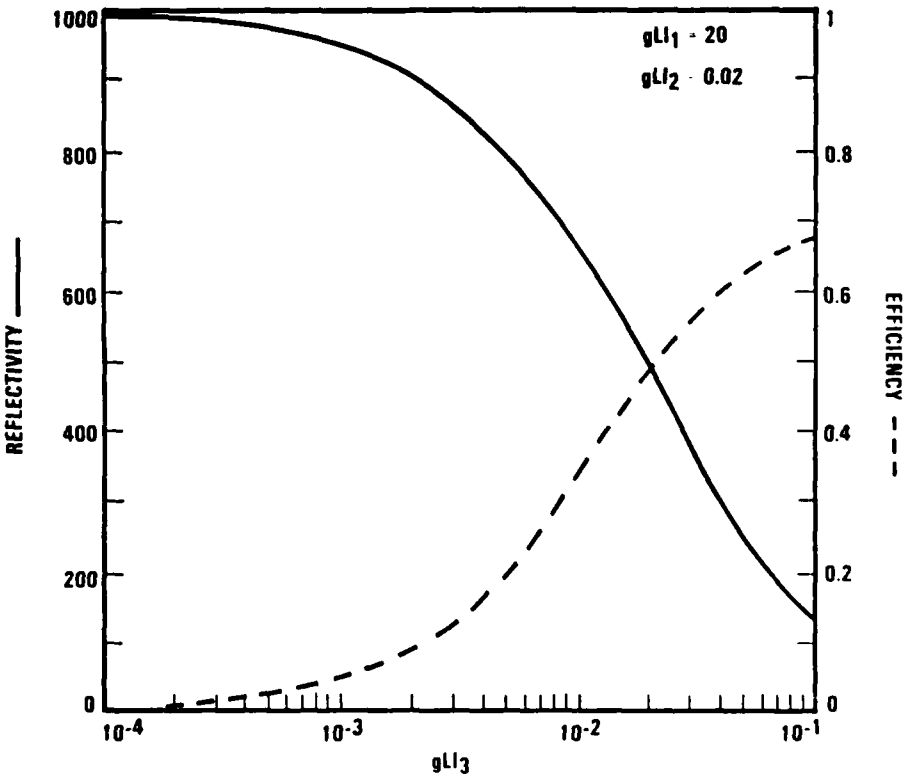

Figure 3. Saturation effect of FWSBS. The curves are found to be well described by $R = I_1/(I_2 + I_3)$ and $\eta = I_3/(I_2 + I_3)$.

reflectivity in the non-depletion regime approaches 10^3 which is the ratio of the pump intensities, I_1/I_2. The saturation is observed as the reflectivity decreases from 90 percent to 10 percent in the range of $I_3 = 0.1\ I_2$ to $I_3 = 10\ I_2$. The dependence seems to be well described by the following formulas

$$R = \frac{I_1}{I_2 + I_3}$$
$$\eta = \frac{I_3}{I_2 + I_3}, \tag{B-27}$$

where the efficiency, η, is defined as the fraction of the forward pump intensity transferred to the reflected wave.

Equation (27) can also be derived without actually solving the coupled equations. Since s is a constant and $E_4(0) = 0$, the fields at both boundaries have the relation

$$E_1(0)E_3(0) = E_1(L)E_3(L) - E_2(L)E_4(L). \tag{B-28}$$

In most cases of interest, $E_3(0)$ is several orders of magnitude lower than other quantities and the lefthand side of Equation (28) can be neglected. The reflectivity is then found to be

$$R \equiv \frac{I_4(L)}{I_3(L)} = \frac{I_1(L)}{I_2(L)}. \tag{B-29}$$

Since $I_3(0)$ is very small, $I_2(L)$ is approximately equal to $[I_2(0) + I_3(L)]$ which gives the formula in Equation (27). Again, Equation (29) is an example of equal reflectivities discussed in Reference 12, where $E_3(0)$ is at the noise level.

Equation (27) shows that high reflectivity and high efficiency can be obtained by properly choosing the input intensities. For example, if I_2 and I_3 are lower by two orders of magnitude from the case in Figure 3, the reflectivity will be approaching 10^5 and the efficiency is still the same. At

these intensity levels, the phase conjugation threshold condition in Equation (10) is still satisfied.

The intensity variation in the medium is demonstrated for the case of $I_2 = I_3$ where the reflectivity is half of its non-depletion value and the efficiency is near 50 percent (Figure 4). It is observed that $I_1(z)$ and $I_2(z)$

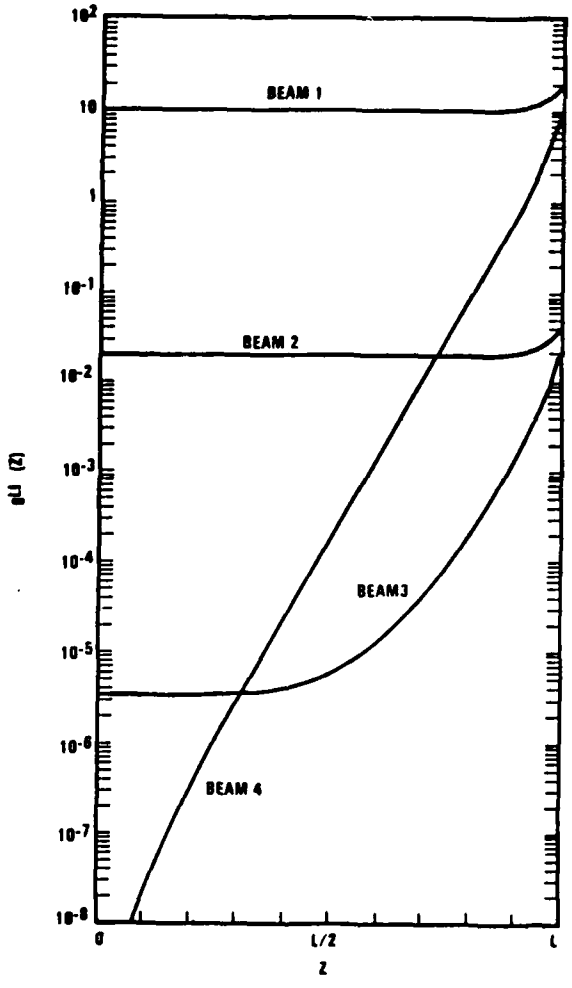

Figure 4. Intensity variation in the interaction region for the case of $I_2 = I_3$ in figure 3. The four wave mix process dominates only in the first one-fifth of the region. After that, the reflected wave grpwm exponentially.

have similar dependences except for a constant factor. this can be understood because x(z) and y(z) in Equation (24) have an identical structure. For most of the interaction region, the reflected wave intensity, $I_4(z)$, is subject to an exponential growth. This is the SBS-dominant region. Near the rear end of the interaction region (about one-fifth of the total length), the FWM process dominates the field growth. This further justifies the drop of the phase-mismatch exponential factor at the beginning of this section because the actual interaction length for FWM is much shorter than the medium length.

So far, we have assumed that the optical waves are coupled to each other through the phonon field only and neglected the involvement of other nonlinear effects, such as $\chi^{(3)}$. Since the second term in Equation (7) is similar to the structure of the coupled equations for FWM in a Kerr medium, we expect that the coupling through $\chi^{(3)}$ should take place. For completeness, the coefficient of the second term in Equation (7) should be replaced by

$$g \rightarrow g \pm i\, 8\, n_2\, k, \tag{B-30}$$

where n_2 is defined in the effective index of refraction

$$n = n_o + n_2 \langle I \rangle, \tag{B-31}$$

and <I> is the time average of the total intensity. In Equation (30), we add an imaginary part to the coupling coefficient. The positive sign is for beams 1 and 3, and negative sign for beams 2 and 4. Consider the medium CS_2, where n_2 is 2×10^{-8} (cm^2/MW) and g is 0.2 (cm/MW). We found that the imaginary part is one order of magnitude smaller than the real part in Equation (30). Therefore, it seems appropriate to neglect the contribution of FWM through the third-order nonlinear susceptibility in the FWSBS effect.

V. Conclusion

We have derived an analytical theory for the four wave stimulated Brillouin scattering effect in the saturation regime. The analytical solution shows a moderate saturation effect due to the pump depletion. Because of its high conjugation reflectivity and good energy transfer efficiency, the FWSBS is of interest to many applications which are the subject of further investigation.

The author appreciates many delightful discussions with Dr. J. Menders. This research is supported by the Office of Naval Research, Pasadena.

References

1. D. M. Pepper and A. Yariv, "Optical phase conjugation using three-wave and four-wave mixing via elastic photon scattering in transparent media", in Optical Phase Conjugation, edi. by R. A. Fisher, Chapter 2, Academic press, N.Y. 1983.
2. A. Yariv and D. M. Pepper, "Amplified reflection, phase conjugation and oscillation in degenerate four-wave mixing", Opt. Lett. 1, 16 (1977).
3. D. M. Bloom, P. T. Liao and N. P. Economou, "Observation of amplified reflection by degenerate four-wave mixing in atomic sodium vapor", Opt. Lett., 2, 58 (1978).
4. W. P. Brown, "Absorption and depletion effects on degenerate four-wave mixing in homogeneously broadened absorbers", J. Opt. Soc. Am., 73, 629-634 (1983).
5. M. T. Gruneisen, A. L. Gaeta, and R. W. Boyd, "Exact theory of pump wave propagation and its effect on degenerate four-wave mixing in saturable-absorbing media", J. Opt. Soc. Am., B2, 1117-1121 (1985).
6. N. F. Andreev, V. I. Bespalov, A. M. Kiselev, A. Z. Matveev, G. A. Pasmanik and A. A. Shilov, "Wave-front inversion of weak optical signals with a large reflection coefficient", JETP Lett., 32, 625-629 (1980).
7. A. M. Scott and M. Hazell, "Efficient phase conjugation by Brillouin enhanced four-wave mixing", OSA annual meeting, Washington, D.C., October 17, 1985.
8. N. F. Andreev, V. I. Bespalov, A. M. Kiselev, G. A. Pasmanik and A. A. Shilov, "Raman interaction in the field of opposing light waves", Sov. Phys. JETP, 55, 612-617 (1982).
9. A. M. Scott, "Efficient Phase conjugation by Brillouin enhanced four wave mixing", Opt. Commun., 45, 127-132 (1983).
10. G. C. Valley, "A review of stimulated Brillouin scattering excited with a broad-band pump laser", IEEE J. Quant. Elect., QE-22, 704-712 (1986).
11. I. D. Carr and D. C. Hanna, "Performance of a Nd:YAG oscillator/amplifier with phase conjugation via stimulated Brillouin scattering", Appl. Phys., B36, 83-92 (1985).

12. R. L. Abrams, C. R. Giuliano and J. F. Lam, "On the equality of stimulated Brillouin scattering reflectivity to conjugate reflectivity of a weak probe beam", Opt. Lett., 6, 131-132 (1981).
13. A Hardy and Y. Silberberg, "Saturation effects in phase-conjugate lasers", J. Opt. Soc. Am., 73, 594-599 (1983).

END

DTIC

7-86